EMG Signal Decomposition

Using

Motor Unit Potential Train Validity

by

Hossein Parsaei

A thesis
presented to the University of Waterloo
in fulfillment of the
thesis requirement for the degree of
Doctor of Philosophy
in
Systems Design Engineering

Waterloo, Ontario, Canada, 2011

I hereby declare that I am the sole author of this thesis. This is a true copy of the thesis, including any required final revisions, as accepted by my examiners.

I understand that my thesis may be made electronically available to the public.

Hossein Parsaei

Abstract

Electromyographic (EMG) signal decomposition is the process of resolving an EMG signal into its component motor unit potential trains (MUPTs). The extracted MUPTs can aid in the diagnosis of neuromuscular disorders and the study of the neural control of movement, but only if they are valid trains. Before using decomposition results and the motor unit potential (MUP) shape and motor unit (MU) firing pattern information related to each active MU for either clinical or research purposes the fact that the extracted MUPTs are valid needs to be confirmed.

The existing MUPT validation methods are either time consuming or related to operator experience and skill. More importantly, they cannot be executed during automatic decomposition of EMG signals to assist with improving decomposition results. To overcome these issues, in this thesis the possibility of developing automatic MUPT validation algorithms has been explored. Several methods based on a combination of feature extraction techniques, cluster validation methods, supervised classification algorithms, and multiple classifier fusion techniques were developed. The developed methods, in general, use either the MU firing pattern or MUP-shape consistency of a MUPT, or both, to estimate its overall validity.

The performance of the developed systems was evaluated using a variety of MUPTs obtained from the decomposition of several simulated and real intramuscular EMG signals. Based on the results achieved, the methods that use only shape or only firing pattern information had higher generalization error than the systems that use both types of information. For the classifiers that use MU firing pattern information of a MUPT to determine its validity, the accuracy for invalid trains decreases as the number of missed-classification errors in trains increases. Likewise, for the methods that use MUP-shape information of a MUPT to determine its validity, the classification accuracy for invalid trains decreases as the within-train similarity of the invalid trains increase. Of the systems that use both shape and firing pattern information, those that separately estimate MU firing pattern validity and MUP-shape validity and then estimate the overall validity of a train by fusing these two indices using trainable fusion methods performed better than the single classifier scheme that estimates MUPT validity using a single classifier, especially for the real data used. Overall, the multi-classifier constructed using trainable logistic regression to aggregate base classifier outputs had the best performance with overall accuracy of 99.4% and 98.8% for simulated and real data, respectively.

The possibility of formulating an algorithm for automated editing MUPTs contaminated with a high number of false-classification errors (FCEs) during decomposition was also investigated. Ultimately, a robust method was developed for this purpose. Using a supervised classifier and MU firing pattern information provided by each MUPT, the developed algorithm first determines whether a given train is contaminated by a high number of FCEs and needs to be edited. For contaminated MUPTs, the method uses both MU firing pattern and MUP shape information to detect MUPs that were erroneously assigned to the train. Evaluation based on simulated and real MU firing patterns, shows that contaminated MUPTs could be detected with 84% and 81% accuracy for simulated and real data, respectively. For a given contaminated MUPT, the algorithm on average correctly classified around 92.1% of the MUPs of the MUPT.

The effectiveness of using the developed MUPT validation systems and the MUPT editing methods during EMG signal decomposition was investigated by integrating these algorithms into a certainty-based EMG signal decomposition algorithm. Overall, the decomposition accuracy for 32 simulated and 30 real EMG signals was improved by 7.5% (from 86.7% to 94.2%) and 3.4% (from 95.7% to 99.1%), respectively. A significant improvement was also achieved in correctly estimating the number of MUPTs represented in a set of detected MUPs. The simulated and real EMG signals used were comprised of 3–11 and 3–15 MUPTs, respectively.

Acknowledgements

I have become indebted to many people throughout this work for their support, advice, encouragement, and patience. There is no way to acknowledge them all or even any of them properly. I owe very special thanks to all of them.

In the first place, I would like to thank my supervisor Dr. Daniel W. Stashuk. Dan, as he always does to assist his graduate students succeed, did his best to provide feedback, comments, suggestions, and enlightening discussions throughout this four–year research. In addition, his diverse experience and knowledge about the subject of this thesis led to many worthwhile discussions that were influential in completing this thesis. Dan has been more than just an advisor. He has been and continues to be a good friend as well. I am truly fortunate to have been able to join his research group and work with him.

Special thanks go to Dr. Miki Nikolic for sharing several clinical EMG signals, reading and evaluating this thesis as external examiner, and for his valuable comments. The discussions that I had with Dr. Nikolic while attending ISEK 2010 in Denmark were helpful in improving this work.

I would like to gratefully thank Dr. Kevin McGill, Dr. Zoia C. Lateva, Dr. J.R. Florestal, Dr. P.A. Mathieu, and Mr. Hamid Reza Marateb for sharing several EMG signals and the decomposition results of these signals. The knowledge that I gained by attending two EMG signal decomposition workshops presented by Dr. McGill and his co–workers in ISEK 2008 and ISEK 2010 along with the discussions that we had in these two conferences were worthwhile and helped with improving this thesis.

Dr. Ali Ghodsi and Dr. Paul Fieguth deserve significant thanks. Dr. Ghodsi has provided helpful discussions on the cluster validation methods upon which part of this work is based. Dr. Figuth, as a member of my committee, has provided motivating comments and suggestions by reading both my proposal and thesis. The valuable knowledge that I gained by taking or attending in the undergraduate and graduate level courses that Dr. Ghodsi and Dr. Fieguth have been offering on the subject of pattern recognition, data mining, and classification contributed greatly in enriching the content of this thesis.

I would like to thank the other member of my committee: Dr. Kumaraswamy Ponnambalam and Dr. Shoja'eddin Chenouri for the valuable time they spent reading both my proposal and my thesis and for their stimulating conversations, intriguing ideas and suggestions. Without these ideas, the work would be significantly poorer.

My deepest gratitude goes to my family for their love, support, and encouragement. Perhaps most significantly thanks to my wife Rafat. Without her love, support, and patience, I would not be able to finish this work. To help me with writing this thesis, in Spring 2011 Rafat paused writing her thesis and took all the responsibility of our daily life especially taking care of our newborn baby, Sana, which I know seemed like a crazy job to many people. Thank you, Rafat, for everything.

Dedication

This thesis is dedicated to

    my parents,

       my wife Rafat,

          my daughter Sana,

             and my sisters and brothers.

Table of Contents

List of Figures

xii

List of Tables

List of Symbols and Abbreviations

A_c	Accuracy for a decomposition algorithm
A_{CT}	Accuracy in classifying contaminated MUPTs
A_{IV}	Accuracy in classifying invalid MUPTs
A_{NCT}	Accuracy in classifying non–contaminated MUPTs
A_r	Assignment rate for a decomposition algorithm
A_T	Total accuracy in classifying valid and invalid MUPTs , or
A_V	Accuracy in classifying valid MUPTs
AcS	Active segment
A/D	Analog-to-digital
AFNNC	Adaptive fuzzy k-nearest neighbor classifiers
AGB	Adaptive gap-based MUPT validation method using Beal criterion
AGDH	Adaptive gap-based MUPT validation method using Duda and Hart criterion
AMTFC	Adaptive matched template filter classifiers
ANDMC	AND multi-classifier used for MUPT validation
APB	Adaptive PCA-based MUPT validation method using Beal criterion
APDH	Adaptive PCA-based MUPT validation method using Duda and Hart
AVGMC	Average multi-classifier used for MUPT validation
C_{AT}	Certainty assignment threshold
CC_r	Correct classification rate for a decomposition algorithm
CV	Coefficient of variation of IDIs of a MUPT
CV_L	Lower CV
CV_U	Upper CV
E_{NMUPTS}	Error in finding the correct number of MUPTs
EFE	Error-Filtered Estimation
EMD	Empirical mode decomposition
EMG	Electromyographic
FCE	False-classification errors
FDA	Fisher discriminate analysis
FR-MCD	Firing rate mean consecutive difference
FPVC	Firing pattern validity classifier
GS	Gap statistic
gv	Gap value
IDI	Inter-Discharge Interval
ID rate	Identification rate
IDI-MCD	IDI mean consecutive difference
$LIDI_R$	Lower IDI ratio
LRMC	Logistic regression multi-classifier

MAPC	Maximum *a posterior* classifier
MCE	Missed-classification errors
MFP	Muscle fibre potential
MN	Monopolar needle
MVC	Maximum voluntary contraction
MU	Motor unit
MUP	Motor unit potential
MUPT	Motor unit potential train
MVB	MUPT validation system using AGB and FPVC
MVDH	MUPT validation system using AGDH and FPVC
NMJ	Neuromuscular junction
NNERVE	Neural network extraction of repetitive vectors for electromyography
PCA	Principal component analysis
PC	Pseudo-correlation
PD	Pattern discovery
PDF	Probability density function
PGS	PCA-based gap statistic method
PI	Percentage of inconsistency
PJ	PCA-based jump method
PRMC	Product multi-classifiers used for MUPT validation
PSI	Percentage of shape inconsistency
QEMG	Quantitative electromyography
RMS	Root mean square
r_1	First Coefficient of Serial Correlation
s_i	80-dimensional vectors representing the MUP template of a MUPT
SFN	Single fiber needle
SMUP	Superimposed MUP
SNR	Signal-to-noise ratio
STBC	Shape and temporal based clustering
SVC	MUP-shape validity classifier
SVM	Support vector machine
SVMMC	SVM multi-classifier
SVMVC	SVM validity classifier
W_K	Within-cluster dispersion for K cluster
$\widehat{K}$	Optimum number of clusters in a data set
μ	The mean of IDIs of a MUPT
μ_{Loc}	Local mean of IDIs of a MUPT
σ	The standard deviation of the IDIs of a MUPT

Chapter 1

Introduction
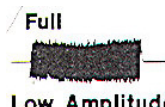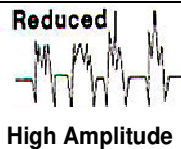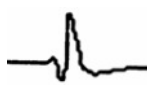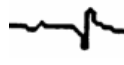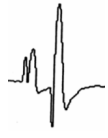
1.1 Preface

An electromyographic (EMG) signal, detected during a muscle contraction, is the superposition of the motor unit potential trains (MUPTs) created by the active motor units (MUs) and background noise. The characteristics of a detected EMG signal depend on several factors such as the level of contraction, the shape and size of the electrode used, and the position and orientation of the electrode relative to the muscle fibers of the active MUs [1-4]. In addition, the characteristics of an EMG signal detected from a contacting muscle are related to the anatomical and physiological features of the muscle and therefore to its age and state of health or fatigue. Some parameters of EMG signals for normal and abnormal muscles are compared in Table 1.1. Consequently, analyzing EMG signals provides information that can be used clinically or for physiological investigation. The technique of detecting, evaluating and analyzing EMG signals is known as electromyography.

Recent advances in computer technology, signal processing, and pattern recognition techniques have lead to the development of new techniques for extracting valuable information from the EMG signals detected from a muscle. Therefore, electromyography now plays a major role in physiological investigations and clinical examinations for either the study of motor control or the diagnosis of neuromuscular disorders. One such technique is EMG signal decomposition.

EMG signal decomposition is a process by which MUPTs are extracted from an EMG signal such that each extracted MUPT estimates the actual MUPT generated by a single MU. The purpose of EMG signal decomposition is to provide an estimate of the firing pattern and MUP template of each active MU that

Table 1.1: Some parameters of EMG signals for normal and abnormal muscles [4].

EMG parameter	Normal	Myogenic	Neurogenic
Interference pattern	Full	Full / Low Amplitude	Reduced / High Amplitude
Motor unit potential		Small Unit	Large Unit

contributed significant MUPs to the composite EMG signal. EMG signal decomposition involves the application of digital signal processing and pattern recognition techniques and was first reported by De Luca and co-workers [5], [6] . Since then, various different methods have been developed to decompose an EMG signal, to estimate MU firing pattern statistics and MUP features, and to analyze decomposition results quantitatively. Figure 1.1 summarizes the decomposition results for a needle EMG signal obtained using DQEMG [7], a system developed at the University of Waterloo for the decomposition and quantitative analysis of EMG signals. The individual MUPs assigned to each MUPT are plotted on top of each other in a shimmer plot. In this example, the MUP template and several morphological feature values, along with the MU discharge patterns, instantaneous firing rates, and several MU firing pattern feature values for each extracted MUPT are illustrated. The obtained MUP templates and MU firing patterns and their estimated feature values can assist with the diagnosis of neuromuscular disorders [8-13], the understanding of motor control [14-16], and the characterization of MU architecture[17]. Specifically, the shape characteristics of needle-detected MUPs can be used to aid in the diagnosis of some neuromuscular disorders such as myopathic and neuropathic diseases [8], [12], [13], [18]. Diagnosis is then facilitated by decomposing a needle detected EMG signal into its constituent MUPTs, measuring the features of the extracted MUPTs and finally analyzing the measured features [7], but only if the obtained MUPTs are valid. Before using extracted MUPTs for further investigation (either clinically or for physiological investigation), their validity must be determined.

An extracted MUPT is considered valid when it accurately represents the activity of a single MU and is contaminated by low numbers of false-classification errors (FCEs). Alternatively, an invalid MUPT either

MUP Template	MUP Stability		IDI Histogram	Firing Graph	MURE: 3 RR: 3.6
1. N=51	CoV: 0.38	Vpp: 524.0 µV Duration: 16.2 ms Area: 859.5 uVms AAR: 1.6 ms Phs: 4 Turns: 5 Fibre Count: 3 A.Jiggle: 22.7 %	mean 94 ms sd 14.9 ms cov 0.16 94 ms		FR: mean 10.6 H FR: MCD 0.18 H ID Rate 95.5% # of Mups: 112
2. N=51	CoV: 0.47	Vpp: 255.0 µV Duration: 7.8 ms Area: 398.4 uVms AAR: 1.6 ms Phs: 3 Turns: 5 Fibre Count: 2 A.Jiggle: 18.5 %	mean 92 ms sd 19.0 ms cov 0.21 92 ms		FR: mean 10.9 H FR: MCD 0.14 H ID Rate 66.8% # of Mups: 75
3. N=51	CoV: 0.54	Vpp: 261.0 µV Duration: 20.7 ms Area: 607.3 uVms AAR: 2.3 ms Phs: 5 Turns: 5 Fibre Count: 2 A.Jiggle: 11.7 %	mean 94 ms sd 17.5 ms cov 0.19 94 ms		FR: mean 10.7 H FR: MCD 0.26 H ID Rate 63.5% # of Mups: 72

Horz: 5 ms/div Vert: 200 µV/div Sweep: 25 ms	Horz: 2 ms/div Vert: 200 µV/div Sweep: 10 ms	Horz: 50 ms/div Sweep: 250 ms	Horz: 2 s/div Vert: 5 Hz/div Sweep: 20 s

Figure 1.1: Decomposition results of an EMG signal. From left to right, the first three columns show the MUP template, the shimmer plot of the assigned MUPs, and the features of the MUP template of each extracted MUPT. The last three columns (4–6) show the MU firing pattern information for the extracted MUPTs. The fourth column shows the IDI histogram and corresponding statistics for each extracted MUPT. Finally, the last two columns show the discharge patterns, instantaneous firing rates, and firing pattern features for each MU.

represents the activity of more than one MU (i.e., it is a merged MUPT) or contains a high percentage of FCEs (i.e., it is a contaminated MUPT). The class label of an extracted MUPT (single, merged, or contaminated) can be determined using the MU firing pattern and MUP shape information provided by the train.

Unfortunately, the MUP template shapes and MU firing patterns of invalid MUPTs cannot be easily distinguished from those of valid trains. Often, the MUP template shape of an invalid train looks similar to that of a valid train; nevertheless, the train does not represent the MUPs of a single MU. As such, the variability of MUP shapes and possibly the MU firing pattern are greater for invalid trains compared to valid trains. If such inaccurate information is not detected and excluded from further analysis, it could improperly suggest an abnormal muscle when interpreted clinically or it may contribute to scientific misstatements. Consequently, the first and most critical step in the quantitative analysis of MUPTs is assessing their validity.

Detecting invalid trains during decomposition can assist with improving the performance of these decomposition methods in terms of estimating the correct number of MUPTs constituting an EMG signal as well as reducing the number of missed-classification errors (MCEs) and FCEs in the extracted trains. At the end of each pass during decomposition, invalid MUPTs are detected and then either have their FCEs corrected or are split into valid trains. Such corrections can help find the correct number of constituent MUPTs, lead to better estimates of the MUP template and MU firing pattern statistics of each train, and also allow more MUPs to be correctly assigned to the obtained trains (i.e., reduce MCEs) during the next steps of decomposition. Consequently, MUPT validation can improve decomposition accuracy.

To date, MUPT validation is conducted qualitatively by an expert operator. An expert assesses the raster/shimmer plots of the MUPs assigned into a MUPT to decide on the MUP shape validity of the given MUPT [1], [7], [19-21]. The accuracy of such manual MUPT evaluations, as with other methods that need operator supervision, depends on operator experience and skill. In addition, such evaluations are time consuming and cannot be practically completed in a busy clinical environment. More importantly, manual MUPT validation methods cannot be executed during automatic decomposition of EMG signals. To overcome these issues, methods need to be developed to automatically estimate the validity of a given MUPT. This thesis presents several methods developed to automatically estimate the validity of MUPTs extracted by a decomposition algorithm.

1.2 Objectives and Approach

This thesis concentrates on automatic validation of a given MUPT using both its MUP shape and MU firing pattern information. Motivation for developing automated methods to estimate the validity of MUPTs are to: 1) facilitate the use of EMG signal decomposition results for clinical applications of quantitative electromyography by providing the overall validity of MUPTs and excluding or highlighting invalid MUPTs; 2) assist with improving the accuracy and completeness of decomposition results. For this purpose, several methods based on a combination of feature extraction, data mining, cluster validation techniques, and supervised classification algorithms were developed and evaluated. The goal was to develop a fast and accurate MUPT validation system that can be used both during the decomposition process and after decomposition is completed.

The effectiveness of using the developed MUPT validation algorithm to improve EMG signal decomposition was explored as well. During the decomposition process, the validity of extracted MUPTs

4

are determined; invalid trains are corrected and the assignment threshold for each train is adjusted based on the estimated validity (i.e., adaptive classification) with a goal to obtain a decomposition results such that the number of extracted MUPTs is correct and the extracted MUPTs have low MCE and FCE rates.

1.3 Overview of the Thesis

This thesis explores a verity of techniques to detect merged and contaminated MUPTs obtained by decomposing an EMG signal. Identifying merged MUPTs using only either MU firing pattern information or MUP shape information was investigated. The effectiveness of using both these two sets of information to determine the class label of a MUPT (merged or single) was also explored. Identifying contaminated MUPTs and then editing these trains automatically was another subject that was investigated in this thesis. Finally, it is shown that using the presented MUPT validation and MUPT editing algorithms during EMG decomposition will improve the decomposition results.

The thesis is organized as follows. Chapter 2 explains the concepts of EMG signals and EMG signal decomposition techniques. The steps involved with decomposition of an EMG signal, the methods developed for each step along with their strengths and limitations are discussed and compared. Chapter 3 explains the concept of MUPT validation. Single, merged, and contaminated MUPTs are described in detail.

The main contribution of this thesis begins with Chapter 4, where a supervised classifier developed to identify merged MUPTs using only MU firing patterns is described. The details of developing, training and testing this classifier are explained.

Chapter 5 presents several methods constructed to determine the validity of a MUPT using only its MUP shape information. Detailed descriptions of the developed methods along with their evaluation process using simulated and real data are provided. The advantages, disadvantages, and limitations of each method are discussed as well.

In Chapter 6 several algorithms that fuse the MU firing pattern and MUP shape information of a MUPT to estimate its validity are described. The structure of the methods and how they were evaluated using both simulated and real data are presented in detail.

In Chapter 7 a method for detecting MUPTs contaminated by a high number of FCEs and then a method for removing the FCEs from a contaminated train are presented.

Chapter 8 presents a novel EMG signal decomposition system. In this chapter, the structure of a newly developed EMG signal decomposition system that employs the methods presented in Chapters 4-7 with the goal of obtaining robust performance across a variety of EMG signals is presented. The performance of the developed EMG decomposition system was evaluated using several simulated and real EMG signals and was compared with that of the decomposition system used in DQEMG.

Finally, Chapter 9 presents conclusions and some recommendations for future work to enhance the performance of the system.

Chapter 2

EMG Signal Decomposition

2.1 Introduction

This chapter presents the fundamentals of EMG signal composition followed by a detailed discussion of EMG signal decomposition and its evaluation. A comprehensive survey of EMG signal decomposition algorithms is provided. Recent advances and an up-to-date evaluation of current research and developments in the field of EMG signal decomposition are provided. The steps required to decompose an EMG signal and to evaluate the obtained MUPTs are discussed comprehensively. The methods developed for each step, and the evolution, strengths and limitations of these methods are discussed.

2.2 EMG Signals

In order to appreciate the concepts of EMG signal decomposition and its application in quantitative electromyography, it is important to be familiar with the composition of an EMG signal.

An EMG signal is the sequence of voltages detected from a contracting muscle over time. The potentials are detected in the voltage field generated by active muscle cells or fibers of a contracting muscle. Each muscle is composed of muscle fibers that are innervated in groups by α-motor neurons. Formally, a single α-motor neuron, its axon and the muscle fibers it innervates are called a MU [2], [22]. Figure 2.1 shows a schematic of a MU.

The wave of depolarization and repolarization propagating along the membrane of a muscle fibre can be detected as a temporally changing voltage called a muscle fiber potential (MFP) [23]. The summation
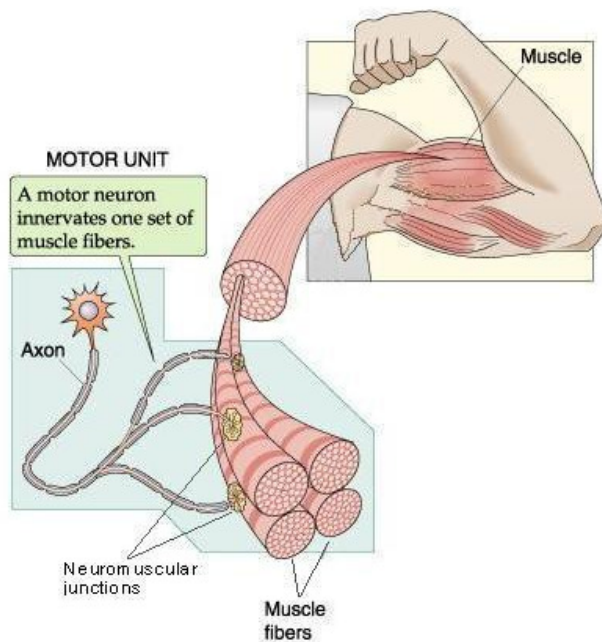
Figure 2.1: Motor unit (copied from [22]). Note: in reality the muscle fibers of a MU are randomly distributed within a muscle.

of the MFPs created by the spatially and temporally dispersed depolarizations and repolarizations of all of the fibers of a single MU is called a MUP and is given by

$$MUP_j(t) = \sum_{i=1}^{n} MFP_i (t - \tau_i) s_i$$

(2.1)

where n is the number of muscle fibers in the jth MU of a contracting muscle, τ_i is the temporal delay of $MFP_i(t)$ and s_i is a binary variable which is "1" if fiber i fires and is "0" if it does not fire.

The initiation delay τ_i depends on the location of the neuromuscular junction of fiber i relative to the detection electrode and the muscle fiber conduction velocity. This parameter varies from MU discharge to discharge because of the variability in the time required at the neuromuscular junction of this fiber to depolarize its membrane and hence initiate a new MFP. This variability results in variable times of initiation of the MFPs of a MUP which in turn causes the shapes of the MUPs of a MU to vary from MU discharge to discharge [24]. The shapes of MUPs may also change due to electrode movement because this changes the position of the electrode relative to the fibers of the active MUs. MUP shapes will also vary if some fibers of the corresponding MU do not fire (known as blocking [24]). These sources of

inherent MUP shape variability, can be the cause of the most challenging problems in EMG signal decomposition [1], [19], [25], [26].

In order to maintain the force of a muscle contraction, MUs fire repetitively and generate trains of MUPs. The train of MUPs created by a single MU, positioned at their times of occurrence, is called a MUPT and is described as:

$$MUPT_j(t) = \sum_{i=1}^{M} MUP_{ji}(t - \delta_{ji})$$

(2.2)

where M is the number of times that the jth MU fires, δ_{ji} is the ith firing time of MU_j and $MUP_{ji}(t)$ is the ith MUP generated by MU_j during its ith firing.

A detected EMG signal is simply the algebraic summation of the generated MUPTs and background interference which includes instrumentation noise and artifacts:

$$EMG(t) = \sum_{j=1}^{N} MUPT_j(t) + n(t)$$

(2.3)

where N is the number of active MUs, $MUPT_j(t)$ is the MUPT generated by the jth MU, and $n(t)$ is background noise.

Figure 2.2 shows both an anatomical and physiological model for an EMG signal. In this figure, $h_i(t)$ is a filter with impulse response MUP_i, and the impulses represent action potentials emerging from an α-motor neuron to innervate the connected muscle fibers.

Based on Equations 2.1 to 2.3, all active muscle fibers in a contracting muscle contribute to an EMG signal detected from a muscle; however, the amplitude of the MFPs of the fibers located far from the electrode detection surface may be attenuated below the level of the background noise. This is because of the distance-dependent attenuation and low pass filtering characteristics of the volume conductor external to the muscle fibers. Attenuation increases and the cutoff frequency of the volume conductor filter decreases as the distance between the electrode detection surface and the active fibers increases [2], [3]. Therefore, the amplitude of MUPs of active MUs with fibers located far from the electrode detection surface will be attenuated below the level of the background noise and consistently discriminating them from the noise will be difficult.
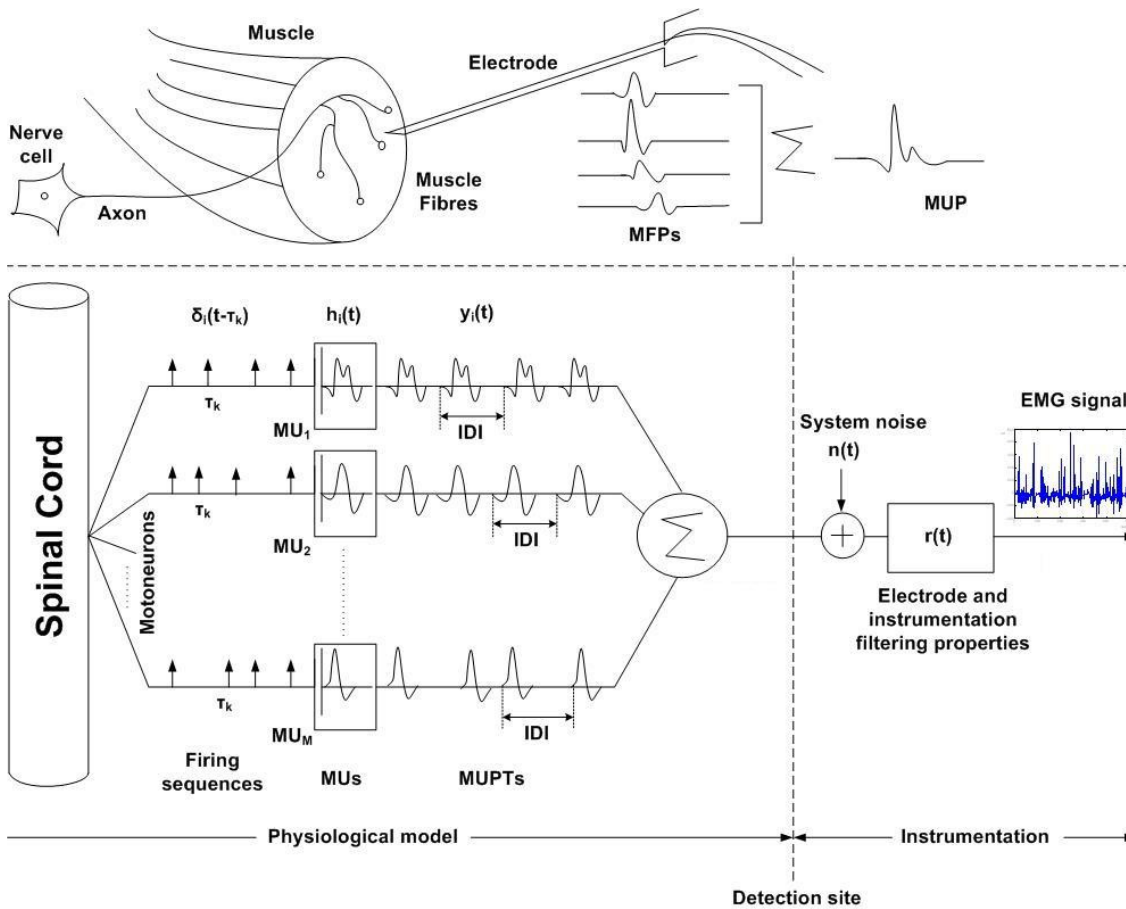
Figure 2.2: Anatomical and physiological model for an EMG signal (copied from [27] and [28]).

Two main types of electrodes are used to detect EMG signals: surface and needle electrodes. Surface electrodes are applied to the skin overlying a muscle. They are noninvasive, convenient to use, and do not cause pain. Signals detected using surface electrodes are known as surface EMG signals. Surface EMG signals are easy to detect, but they do not provide much information about deep muscles due to the filtering characteristics of the volume conduction properties of the overlying muscles and other subcutaneous tissues. Moreover, due to the generally large pick-up area of surface electrodes, surface detected signals are often contaminated by the activity of adjacent muscles (cross talk) [23], [29]. For diagnostic purposes it is useful to get detailed temporal and spatial information about the fibers of a MU. Therefore, to detect EMG signals for clinical use, indwelling electrodes such as concentric needle, monopolar needle, and single fiber needle electrodes inserted directly into a muscle, are used. Schematic representations of the various clinical electrodes are shown in Figure 2.3. Indwelling electrodes are able
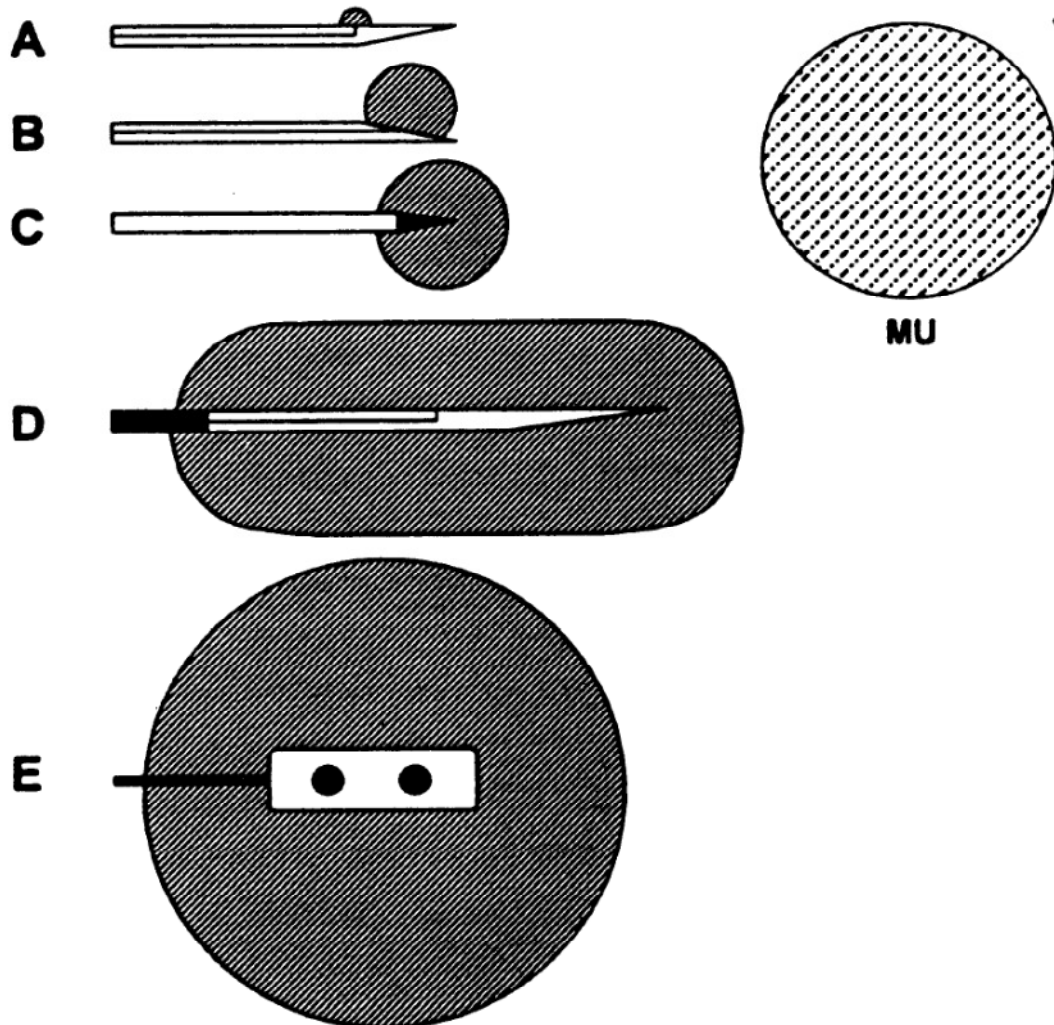
Figure 2.3: Schematic representations of the different clinical electrodes that are used for detecting EMG signals. A) single fiber needle, B) concentric needle, C) monopolar needle, D) macro needle, and E) a bipolar surface electrode configuration. The shaded regions illustrate the approximate uptake area of each electrode relative to a typical MU territory (from [9]).

to detect EMG activity in deep muscles. However, there are several disadvantages associated with their use. They cause some pain when inserted, they can be difficult to suitably position within a muscle, and the needle and/or detection surface may move during muscle contraction. In general, signals detected using indwelling electrodes are known as intramuscular EMG signals. More specifically, signals detected using needle electrodes are known as needle EMG signals.

The characteristics of an EMG signal are largely affected by the level of contraction, the anatomical and physiological properties of the muscle, the physical characteristics of the electrode used to detect the signal as well as the position of this electrode relative to the active muscle fibers [1-3], [30], [31]. Surface electrodes have a larger detection surface than indwelling electrodes such that they detect MUPs created by many MUs with fibers similarly close to the detection surface. Therefore, EMG signals detected using surface electrodes are generally more complex than those detected using indwelling electrodes. EMG signals become more complex and larger in amplitude with increasing force of contraction (or level of activation) as the number of active MUs and the rate at which they fire increases and as larger MUs that generally produce larger MUPs are activated.

EMG signals may contain valuable information regarding activity, state of health, and characterization of the muscle from which they were detected [1], [7-13], [20], [21], [32-37]. As an example, the duration and size of the MUP waveform of a MU can be used to study and investigate the size of the MU and/or the conduction velocity of its fibers [9]. The complexity of the MUP shapes of active MUs of a contracting muscle reflects the healthiness of the muscle being studied. Hence, feature values (shape characteristics) of needle-detected MUPs can be used to aid in the diagnosis of some neuromuscular disorders such as myopathic and neurogenic disorders [8], [10], [12], [13]. The firing patterns of individual MUs can be used to investigate and understand how MUs are controlled during muscle contraction [14], [15]. They can also be used to explore the level of abnormality in some motor neuron diseases. Therefore, EMG signals can provide valuable information for physiological investigation and clinical examinations. One effective way to extract such information is via EMG signal decomposition.

2.3 EMG Signal Decomposition

2.3.1 Concepts

EMG signal decomposition resolves a composite EMG signal into its component MUPTs. This is shown conceptually in Figure 2.4. EMG signal decomposition is based on two assumptions. First, all of the MUPs of the active MUs contributing significant MUPs to a detected EMG signal can be detected. Second, the MUPs created by a single MU exhibit more similarity to each other than to those produced by different MUs. While these two basic assumptions apply to the decomposition of both surface and intramuscular EMG signals, the methods used to accomplish decomposition can be quite different for intramuscular versus surface signals. And although the decomposition of multi-channel surface EMG
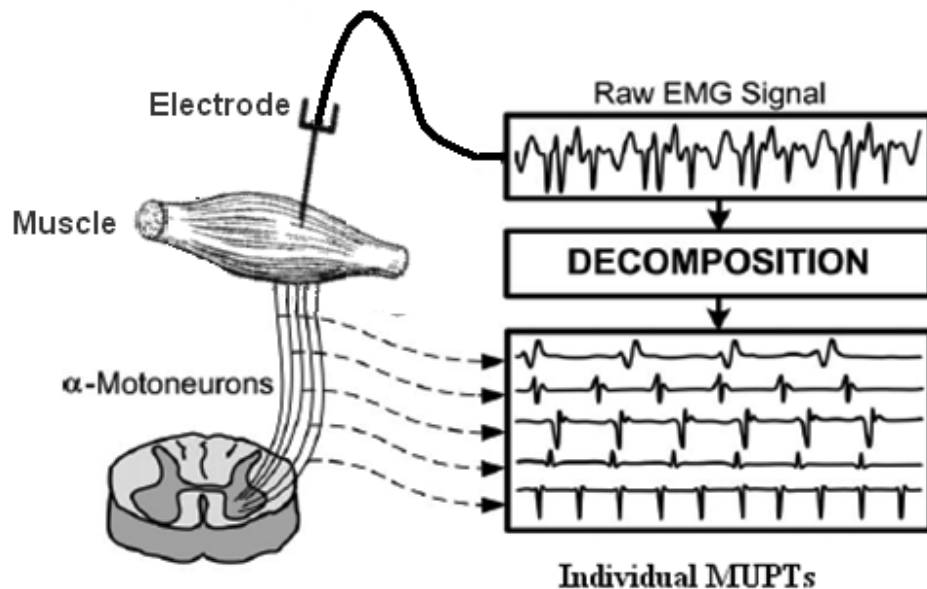
Figure 2.4: A schematic representation of EMG signal decomposition (adapted from De Luca et. al. [14], [38])

signals is of interest and progress is being made towards being able to decompose such signals [38-42], this chapter focuses on the decomposition of intramuscular EMG signals because the main objective of this thesis is to improve the of intramuscular EMG signal decomposition results and facilitate using such results for clinical applications of quantitative electromyography.

Decomposition techniques applied to intramuscular signals can be categorized as manual, semi-automatic or automatic. The initial manual methods used visual inspection of an EMG signal shown on an oscilloscope or plotted on a grid paper to identify MUPTs [43], [44]. Such methods were quite tedious, time consuming, and inaccurate. They were only suitable for the analysis of EMG signals collected during low-level contractions and could not resolve superimposed MUPs. Semi-automatic methods are much more powerful than the manual methods and utilize many of the same techniques used in automatic methods [5], [6], [45]. Nonetheless, the accuracy of the results obtained by manual methods depend greatly on the skills and experience of the operator. With automatic methods, the process of extracting MUPs and sorting them into MUPTs is implemented by employing digital signal processing and pattern recognition techniques. In general, an automatic intramuscular EMG signal decomposition process includes seven steps: (1) signal acquisition, (2) signal preprocessing, (3) signal segmentation and MUP detection, (4) feature extraction, (5) clustering and supervised classification of detected MUPs, (6)

resolving superimposed MUPs, and (7) estimating MU firing pattern statistics and MUP templates. Details of each of these steps are given below.

2.3.2 Signal Acquisition

An inadequately detected EMG signal cannot be decomposed accurately even by using complex methods. The type and positioning of the electrode as well as the level of muscle contraction are parameters that affect the decomposability of a detected signal. Controlling and reducing artifacts such as electrode movement can also help with decomposition accuracy. In addition to these technical conditions, the subject/patient should be prepared both mentally and physically for the study.

In general, monopolar or concentric needle or fine wire electrodes are used to acquire selectively detected (i.e., micro) EMG signals. If information regarding MU size and fiber spatial distribution is required, an indwelling macro or overlying surface electrode is used to also simultaneously acquire a more broadly detected (i.e., macro) EMG signal. Decomposing the micro signal into its constituent MUPTs and extracting the firing pattern information of the active MUs provides information that allows a simultaneously acquired macro signal to be analyzed using triggered averaging techniques [1], [19], [31], [46].

The detection of a micro signal with adequate sharpness and signal-to-noise ratio (SNR) for accurate decomposition requires that the electrode is positioned close to the fibers of the active MUs. Adequate sharpness and SNR facilitate decomposition by making it easier to discriminate between the MUPs and the background noise as well as between the different MUPs created by distinct MUs. One method to obtain a suitable electrode position is to adjust the electrode position in a minimally contracting muscle until the amplitude and sharpness of the detected MUPs are maximized. Once a suitable electrode position is found, if the decomposition algorithm to be used can process signals acquired during force varying contractions, signal acquisition is initiated. Otherwise, the subject is asked to increase the level of contraction, as isometrically as possible, to a desired level before signal acquisition is started. The desired level of contraction maintained during signal acquisition depends on the ability of the decomposition methods to be used. In general, signals detected at higher force levels will be more complex and more difficult to decompose. For most of the currently available decomposition methods contraction levels should be below 50% of maximum voluntary contraction (MVC).

The detected continuous EMG signal acquired from a muscle using a selective indwelling electrode is then fed to an analog preprocessing stage to be amplified and band-pass filtered (typically10 Hz to 10

kHz). The signal is then sampled at a certain rate (10–50 kHz), digitized using an analog-to-digital converter (A/D), and stored. The sampling rate and resolution of the A/D converter are two other parameters that should be considered in this step. EMG signals are band limited with a maximum frequency of around 5 kHz, hence based on the Nyquist-Shannon sampling theorem [47], [48] the minimal sampling rate should be twice this frequency (i.e., 10 kHz). However, if the signal is sampled at this rate, an extra processing step such as interpolation will be required to obtain good temporal resolution for graphical display and also for comparing MUP shapes and grouping them into MUPTs. High sampling rates increase memory requirements, may need special hardware, and also increase decomposition processing time. Both literature and our own experience suggest that a sampling rate of 25 kHz can reduce the artifacts of undersampling and also manage issues of oversampling [1], [7].

2.3.3 Signal Preprocessing

The signal-preprocessing step is involved with filtering the signal to remove background noise and low-frequency information. Filtering, in addition to improving SNR, shortens MUP durations and decreases MUP temporal overlap. Filtering also sharpens MUPs, increases the differences between MUPs and the background noise, and accentuates the differences between MUPs created by different MUs. Therefore, filtering improves MUP detection and classification. In general, band-pass filters or low-pass difference (LPD) filters are used [49-52]. The lower cut-off frequency of the filter should be set at a value that makes the signal baseline more stable by suppressing low frequency noise but without seriously attenuating the MUP amplitudes. Likewise, the upper cut– off frequency of the filter should be set at a value that removes the high frequency noise and accentuates the MUP spikes but without seriously attenuating the MUP amplitudes. LPD filters are easy to implement and fast; hence they are suitable for real-time and clinical applications. However, LPD filters are not ideal and therefore some high frequency noise components will pass through. Figure 2.5 shows the effect of first-order and second-order LPD filtering on MUP shape and discrimination. As shown, the amplitudes of the filtered MUPs are preserved, but the filtered MUPs have shortened durations and reduced baseline noise compared to the unfiltered ones.

Recently, complex wavelets and empirical mode decomposition (EMD) methods have been applied to remove noise from EMG signals [53-57]. These methods, in general, include a signal decomposition step, a soft thresholding step, and a signal reconstruction step. These techniques may work better than LPD filtering for removing noise from the signal and preserving signal information. However, their processing
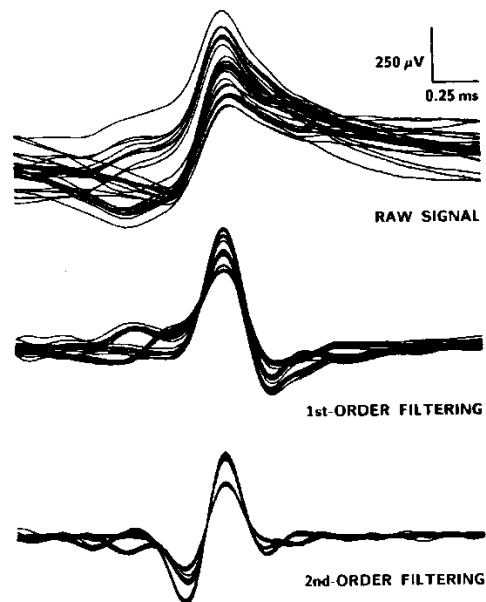
Figure 2.5: The effect of 1st -order and 2nd -order low pass difference filtering on MUPs (copied from McGill et al. [50]).

time is longer than that of LPD filtering and their results depend on several user-defined parameters such as the mother wavelet for the wavelet-based methods [53-56] and the denoising threshold for both the wavelet-based and EMD-based methods. Although for the EMD-based methods [57] the threshold is defined based on an estimate of the level of noise in the signal, finding a suitable region from which this parameter can be accurately estimated may not be easy or may need operator input.

2.3.4 Signal Segmentation and MUP Detection

Signal segmentation divides an EMG signal into segments containing possible MUPs that were generated by active MUs that contributed significantly to the detected EMG signal. Theoretically, the goal is to detect all MUPs generated by active MUs. However, in practice MUs with no muscle fibers close to the detection surface of the electrode will contribute low amplitude MUPs to the detected EMG signal. These low amplitude MUPs are also composed of low frequency components and are very similar in shape. Therefore, it is very difficult to assign such MUPs to their correct MUPTs and only MUPs of MUs that have a good chance of being correctly assigned should be detected in this step. Generally, this is done using a threshold crossing technique [1], [5-7], [25], [26], [45], [49], [50], [53-55], [58-74]. Scanning the raw or filtered signal for peaks that exceed a threshold produces a set of peaks that indicate candidate

16

MUP positions. A window centered at each identified peak is then applied to the signal and the data points that fall in the window are stored as a MUP.

The detection threshold can be a user-pre-defined absolute value [5-7], [53], [62-68], or it can be determined based on the characteristics of the signal and the noise contaminating it [7], [49], [50], [59], [60], [65-68], [75]. In practice, maximum absolute value, mean absolute value, and root mean square (RMS) value of the signal are three characteristics that may be used to set a detection threshold value. The former reduces the probability of small MUPs being lost in larger MUPs, but also introduces a possible bias against small MUPs. In using the signal RMS value, the detection threshold is calculated as either a constant (typically 1.5) times the RMS value of the filtered signal[7] or a constant (typically 3) times the RMS value of the baseline noise of the filtered signal [49], [50], [59], [60], [65-68], [75]. It is obvious that higher threshold values reduce the chance of small MUPs being detected. Using low threshold values helps in detecting MUPs created by almost all MUs active during signal acquisition, but as mentioned above, assigning MUPs with small amplitude and/or only low frequency components to their correct MUPTs is difficult.

The length of the window applied to the signal for selecting MUPs can be variable [54], [55], [59], [65], [69-71], or it can be fixed [1], [7], [19], [26], [45], [49], [50], [53], [54], [58], [66], [67], [72], [74-82]. If a variable-length window is chosen for analysis, the length of the window is adjusted based on the duration of the MUPs, for which the beginning and end of the MUPs are detected by thresholding. A MUP begins when its sample values exceed a threshold and ends when they fall below this threshold [54], [55], [59], [70], [71]. If a fixed-length window is chosen for analysis, the length of the window is set to include a fixed duration, typically 2.5 ms [1], [7], [19], [26], [27], [72], [74], [76-78], [81-83] or 6 ms [58], [66], [67]. Longer windows improve MUP representation, but will increase decomposition time. Using a short fixed window can cause multiple detection of complex or long-duration MUPs. Although using a short-window simplifies clustering and classification of the detected MUPs, further analysis such as discovering temporal relationships between MUPTs is required to identify and merge trains that represent portions of multiply detected MUPs [1], [7], [19].

Once MUPs are detected they must be aligned for subsequent analysis. Such alignment can be achieved by simply using local peak values of either the raw or filtered signal or by using methods based on discrete Fourier transforms (DFTs) [84]. Using peak values is simple and fast, but may not perform well especially for MUPs with sharp peaks due to time-quantization errors [49], [84]. These time quantization errors can be reduced by using higher sampling rates or avoided by using DFTs to

interpolate between samples. Using DFTs and a Nyquist sampling rate may or may not be more computationally expensive than using peak values depending on the increased sampling rate used to reduce time quantization errors.

2.3.5 Feature Extraction

Typically, for pattern recognition problems, each of the given patterns is represented by a feature vector, which contains a number of features that are descriptive of the pattern. The number of features should not be too large, because of the curse of dimensionality[1] [85] but should be large enough to accurately characterize and classify the input pattern. Generally, a parsimonious set of features that has high discriminant ability among the different classes is desired. The multi-dimensional space that contains all possible values of these features is called the feature space.

For EMG signal decomposition, to measure the similarity of detected MUPs and sort them into MUPTs, the MUPs are represented by a vector of feature values. In representing a MUP using a feature vector, the following factors should be taken into consideration.

- The length of the feature vector (i.e., the number of features used).
- The processing time required to compute the feature vector values.
- The amount of correlation between the feature values.
- The discriminative power of the features used.
- The effect of MUP superpositions and shape variability on the feature values.

Ideally, a feature vector should be comprised of a low number of uncorrelated features that are computationally easy to compute, have high ability to discriminate between classes, and are minimally sensitive to the shape variability of the MUPs created by a MU.

Until now, different features have been used to represent detected MUPs and improve decomposition processing time and accuracy. Raw-data (time samples) and first- or second -derivative of time samples [1], [5-7], [19], [25], [27], [72], [74], [76-80], [82], [86], [87], power spectrum and Fourier transform coefficients [45], [49], [50], [62], wavelet coefficients [53-55], [59], [59], [79], [81], [83], [88-94], and

---

[1] The phrase "curse of dimensionality" describes the fact that the time and number of samples required to compute an approximate solution to a pattern recognition problem grows exponentially with the dimension of the feature space.

principal components of wavelet coefficients [95] are features that have been used to represent and assign MUPs to MUPTs. Using power spectrum coefficients [62] or wavelet coefficients of MUPs decreases the dimensionality of the feature space and hence may improve the processing time. Frequency-domain or wavelet-domain features can be more effective than time-domain features (i.e., raw-data and first-derivative time samples), especially when detected MUPs are contaminated by low-frequency baseline drift or high frequency noise [53], [59], [96]. However, power spectrum coefficients may not be able to properly discriminate between similar MUPs created by different MUs because phase information is lost during computation of the power spectrum. Using wavelet coefficients can decrease the effect of time-quantization errors [49], [49] and MUP shape variability [1], if the wavelet coefficients of lower scales are skipped [53], [59]. However, these low scale coefficients reflect high frequency information and are useful in discriminating similar MUPs created by different MUs [95]. To utilize all of the wavelet coefficient frequency information and to also have a low dimensional feature space, Yamada et al. [95] applied principal component analysis (PCA) to all of the wavelet coefficients in order to extract features that discriminate between the MUPs created by the MUs. Their experimental results, using five EMG signals composed of up to five MUPTs, showed that using PCA-based wavelet feature selection could improve decomposition performance with average accuracy of 90.4% versus 89.4% for the wavelet-based methods.

To speed up decomposition, a number of algorithms use a small number of easy -to- calculate features [65], [70], [97], instead of time-domain, frequency-domain or wavelet-domain features. Loudon et al. [65] represent MUPs by their morphological characteristics such as maximum peak-to-peak amplitude, maximum positive peak amplitude, total positive area, MUP duration, number of turns, and number of phases. Florestal et al. [70], [97] use a set of symbolical features to represent MUPs. These symbolical features are: the sequence of extrema separated by a baseline crossing, the rounded ratio of the magnitude of each extremum over the baseline, and the time separating each consecutive extrema pair.

2.3.6 Clustering and Supervised Classification of Detected MUPs

Clustering is the task of partitioning a set of unlabelled objects into several meaningful groups or clusters based on a measure of similarity such that objects assigned to a cluster are as similar as possible and objects assigned to different clusters are as different as possible. A wide variety of clustering algorithms have been proposed in the pattern recognition literature. Jain et al. [98], Xu and Wunsch [99], Berkhin [100], and Jain [101] have conducted exhaustive surveys of current clustering algorithms. Examples of popular clustering algorithms are K-means [101], [102], fuzzy c-means [103], [104], and the hierarchical

algorithm [98], [99]. In general, clustering is a difficult problem. There is no prior knowledge about the labels of the objects and depending on the similarity measure or algorithm used different clustering results are obtained for the same set of data. Moreover, finding the optimum number of clusters is a major challenge in clustering an unlabelled data set.

In supervised classification [105-107], however, the clusters and some information about them are available. Typically, collections of pre-classified (labeled) objects are provided and the problem is then to label given unlabeled objects. The labeled objects, which are known as training samples, are used to train a classification algorithm that in turn is used to label a new unclassified object.

The objective of the clustering and supervised classification of the MUPs detected during signal segmentation is to group these MUPs into sets of MUPTs such that each MUPT represents the activity of a MU that contributed significant MUPs to the composite signal. Therefore, each MUPT should have a consistent MU firing pattern and the MUPs assigned to a MUPT should be more similar to each other than they are to those assigned to a different MUPT. Several existing decomposition procedures are based solely on clustering [53], [58], [65-67], [69], [74], [91], [93], [94], [108-111]. However, generally, a clustering technique is followed by supervised classification [1], [2], [7], [19], [27], [54], [55], [62], [72], [73], [76-80], [80-82], [86-89], [112], [113] and both clustering and supervised classification tasks are repeated across a number of iterations. Throughout multiple iterations, the detected MUPs are assigned to the corresponding MUPTs until either the extracted MUPTs are stable or some termination criteria are met. MUP assignment is based on some measure of similarity or dissimilarity between MUP shapes and/or MU firing pattern consistency.

When clustering is to be followed by supervised classification, the goal of clustering is to provide the necessary initial information required for supervised classification such as estimates of the number of MUPTs, their prototypical MUP shapes (or templates), and their MU firing pattern statistics. To extract such information, a part of the signal (perhaps the initial t seconds or an interval with the highest intensity of MUPs) can be selected and MUPs contributing to this part partitioned into a number of MUPTs. However, neither the number of MUPTs nor their MUP templates are known beforehand. This information must be estimated using MUPs detected in the interval of the signal selected for clustering. Stashuk and Qu [74] proposed to use the MUPs detected in a 30 ms interval of maximum intensity to estimate the number of clusters and to set the cluster centers (MUP templates). When clustering is to be followed by supervised classification, the validity of the estimated number of MUPTs and their MUP templates extracted during clustering is more critical than assigning all of the MUPs detected in the

20

interval of the signal used for clustering. In fact, each incorrectly assigned MUP increases the probability of more errors during supervised classification. Therefore, superimposed MUPs can be ignored during clustering and the algorithm can be conservative when deciding to assign MUPs to a train.

When supervised classification follows clustering, MUPs are assigned to their associated trains based on the information about the possible MUPTs provided by the clustering results. In general, these assignments are based on the same information as during clustering (i.e., MUP shapes and/or MU firing patterns). Possible steps for a supervised classification algorithm used for classification of individual MUPs are summarized below [1], [19], [26]:

Step 1:   Examine the results of clustering to identify false classification errors (FCEs) and remove these incorrectly assigned MUPs from the resulting MUPTs.

Step 2:   Estimate the MUP template and MU firing pattern statistics of each MUPT.

Step 3:   Derive MUP shape similarity assignment thresholds for each MUPT.

Step 4:   Classify unassigned MUPs to the extracted MUPTs given their MUP shape and MU firing pattern statistics.

Step 5:   Update the MUP template and MU firing pattern statistics of each MUPT.

Step 6:   Merge MUPTs if they represent the activity of the same MU.

Step 7:   Split MUPTs if they do not represent the activity of a single MU.

Step 8:   Repeat Steps 3 to 7 until the compositions of the MUPTs do not change.

A supervised classification algorithm used for EMG signal decomposition should be computationally efficient, accurate, and perform well even with a small number of training patterns (i.e., MUPs) provided. The training data (i.e., MUPs) is usually provided by decomposing a portion of the given signal either manually or by using a clustering algorithm. Additional important attributes of a supervised classification algorithm are: (1) minimal use of predefined parameters; (2) the ability to merge trains with similar shaped MUPs; (3) the ability to assess the validity of the extracted trains; (4) the ability to detect MUPTs corresponding to the activity of more than one MU and to split them into valid trains; and (5) minimal sensitivity to any inherent MUP shape variability that may exist in the extracted trains.

MUP shape variability is caused by interfering contributions from the MUPs of other active MUs (i.e., superposition), by the variability of muscle fiber conduction velocities, or by neuromuscular junction (NMJ) jitter. NMJ jitter is the variability in the time required at the neuromuscular junctions of a MU to depolarize its muscle fiber membranes [1], [19], [114], [115]. This variability results in variable arrival times of the constituent MFPs of a MUP at the electrode and causes the shape of the MUPs to vary from

MU discharge to discharge. In addition, if the electrode moves during EMG signal acquisition, the amplitudes and/or shapes of the MUPs may drift (i.e., become non-stationary) because this movement changes the position of the electrode relative to the fibers of the active MUs. MUP shape variability and non-stationarity can reduce decomposition accuracy and may result in the creation of trains with a large number of MCEs, i.e., incomplete trains.

In addition to MUP shape variability and non-stationarity, the similarity of the MUPs from different MUs may also affect performance of clustering and supervised classification algorithms. In fact, it can result in the creation of merged or contaminated trains. A merged train results when two or more trains, which each represents the activity of a MU, are placed in the same train. A contaminated train contains an unacceptable number of FCEs. A classification algorithm must be able to discriminate between similarly shaped MUPs generated by different MUs. MU firing pattern information can assist with discriminating between these types of MUPs.

MU firing pattern information can be used to test the validity of assignments made using MUP shape only, (i.e., passively) [19], [45], [49], [50], [58], [65], [74], [75], or it can be used together with shape information to measure the certainty in assigning a MUP to a MUPT (i.e., actively) [1], [2], [5-7], [19], [25-27], [68], [72], [76-79], [81], [82]. However, one should consider that MU firing pattern information may not be valid in all cases. It depends on the stationarity of the firing pattern and the accuracy of the algorithms used to estimate MU firing pattern statistics. MU firing pattern statistics may vary if the contraction force is varied drastically during signal acquisition. For example, during recruitment or abrupt changes in muscle activation, a MU may fire twice in a short period of time (10 to 20 ms) creating a so-called doublet of closely spaced in time MUPs. In addition, the MU firing pattern statistics of a MUPT estimated by the algorithm used for this purpose may not be acceptable if the level of MCEs is high or the inherent variability of the firing pattern of the generating MU is high. Therefore, when using MU firing pattern information to augment MUP shape information for assigning a MUP to a particular MUPT, all of these issues should be taken into consideration. To achieve desired decomposition accuracy, a decomposition algorithm should consider both the MUP shape and MU firing pattern sources of variability just discussed.

Most of the clustering techniques developed for EMG decomposition are based on adaptations of general clustering algorithms such as the nearest-neighbor [1], [26], [53], [115], single linkage [54], [55], [91], [93], [94], [116], [117], K-means [1], [7], [26], [68], [74], fuzzy c-means [66], [67], [118], minimal spanning tree [54-56], [59], [65], [69], [119], [120], leader-based clustering [6], [25], and self-organizing

neural nets algorithm [58]. In many of these algorithms MU firing pattern information is used passively or actively along with MUP shape information to assign an individual MUP to the correct train.

Regardless of the type of clustering algorithm used, three challenges face each algorithm: i) depending on the similarity measure used, different clustering results may be obtained; ii) the optimum number of clusters ($\widehat{K}$) is not known in advance; and iii) the clustering results may vary from run to run. Many of these algorithms use the standard Euclidian distance as a similarity measure. The calculated distance is then normalized by the energy of the MUP, MUP template, or a combination of both to reduce the sensitivity of the similarity measure to the size of the MUPs. To find $\widehat{K}$ (optimum number of MUPTs), different strategies are employed. The methods that are based on single linkage concepts use a threshold to cut dendograms and hence estimate the number of MUPTs. The threshold can be fixed or determined based on MUP shape similarity, MU firing pattern consistency, or both. In K-means clustering based methods, $\widehat{K}$ is estimated using either the Kothari and Pitts [121] method presented for estimating the number of clusters in a dataset; or by counting the number of MUPs that lie in a "high activity" section of the signal [7], [26], [74] and then using these MUPs as initial cluster centers (MUP templates). Having the number of clusters and also their centers (MUP templates) defined, the clustering results are stabilized and do not vary from run to run. Although various techniques have been used to address the three challenges mentioned above, decomposition results still depend on the threshold(s) used in these algorithms and accuracy may decrease for a signal having a high level of noise and/or highly variable MUP shapes. Therefore, the thresholds used should be somehow adjusted based on the level of noise in the signal. Thresholds should also be adapted to the characteristics of each extracted MUPT individually; a threshold for each MUPT should be derived. Moreover, the validity of any MU firing pattern information used should also be evaluated and then weighted based on the validation results.

There are several decomposition methods that combine clustering with a mathematical model of each active segment (AcS) of the detected EMG signal [60], [109-111]. Each AcS may contains one or more than one MUPs. Variable-length window technique (see Section 2.3.4) is general used to segment the given EMG signal into several active segments. The aim of the EMG decomposition methods presented in [60], [109-111] is to find the innervation sequences of the active motor units for each AcS. Gut and Moschytz [109] used communication techniques to resolve this optimization problem efficiently. They used MUP shape and MU firing pattern information provided by a clustering step and a sparse-sequence constrained Viterbi algorithm to find the best combination of motor units for each segment. Koch and Loeliger [110], [111] used a graphical model of each segment and then a sum-product algorithm (belief

propagation) to resolve each AcS efficiently. Ge and his et al. [60] used a Tabu search algorithm and MUP shape and MU firing pattern information to obtain a maximum *a posteriori* probability-based estimate of the innervation sequences of the MUs for each pair of consecutive active segments. They used two consecutive segments instead of one to avoid dependent errors caused by local solutions of individual segments. The drawbacks of these methods are that they are sensitive to variation in the shape of the MUPs created by each MU and their computation time increases exponentially as the number of active motor units contributing to a detected signal increases.

EMG signal decomposition methods that use supervised classification techniques to classify individual MUPs employ a variety of classification techniques such as maximum *a posterior* classifiers (MAPCs) [2], [5], [6], [108], artificial intelligence-based MAPCs [25], [122-124], artificial neural networks [86], [87], fuzzy logic-based classifiers [68], [77], [78], [82], [88], [89], [125], certainty-based classifiers [1], [7], [27], [72], [76], [79], [80], [82], [125], matched template filter classifiers [2], [5], [6], [45], [49], [50], [75], and multi-classifiers [27], [79], [82], [88], [89], [125] for this purpose. All supervised classification methods require training data to characterize properties of each MUPT (class). The training data, which are sets of labeled MUPs, is usually obtained from the clustering results of a section of the signal. Others however, use a specific algorithm to extract this information. For example, in the NNERVE (neural network extraction of repetitive vectors for electromyography) algorithm developed by Hassoun et al. [86], [87] an auto-associative algorithm is used to extract the number of possible MUPTs and their MUP templates.

Nawab et al. [25], [122-124] employed artificial intelligence techniques to improve the performance of the Precision Decomposition (PD) algorithm developed by LeFever and De Luca in 1982 (known as PD I) [5], [6]. This system which is called PD II is a new version of PD I. PD II uses a knowledge-based artificial intelligence framework called IPUS (integrated processing and understanding of signals) [126],[127] to set the parameters of PD I automatically based on the statistics and characteristics of a given EMG signal. The IPUS framework also assists PD I in efficiently resolving superimposed MUPs as well as finding the optimum number of MUPTs comprising a given signal. Given N extracted MUPTs, the algorithm merges these N MUPTs to get M $\leq$ N trains such that the sum of within-train dissimilarity and between-train similarity over the M resulting MUPTs is minimized. One solution to find these M MUPTs is to search all possible combinations of the N given MUPTs and then choose the best set, but this is computationally expensive. The IPUS framework assists the algorithm by decreasing the search space using template energy and inter-discharge interval (IDI) information extracted from the N MUPTs.

It was shown that the PD II system performed well even for EMG signals detected during force-varying contractions. Across the set of EMG signals used for evaluation, PD II performed better than PD I in terms of both computation time and accuracy. The average accuracy for PD II was 86.0 % compared to 65.2% for PD I. Both the PD I and PD II algorithms are specifically designed to analyze multichannel EMG signals detected using a custom quadrifilar needle electrode that provides an EMG signal comprised of three channels of differential voltage [43]. Due to different spatial orientations of the fibers of a MU relative to the detection surfaces of the quadrifilar electrode, each channel contains a different-shaped MUP generated by a MU. This additional MUP shape information can improve decomposition results. Florestal et al. [97] also showed that the additional information provided by the use of multichannel recordings could improve decomposition accuracy; nevertheless decomposing multiple channel signals takes more time than decomposing single channel signals.

A number of EMG signal decomposition methods that use fuzzy logic-based classifiers have been developed [68], [77], [78], [88], [128],[128]. Chauvet et al. [128] developed a fuzzy classifier to assign MUPs to extracted MUPTs based on their degree of satisfaction and degree of rejection. For each MUP, these two values are calculated via three trapezoidal fuzzy membership functions using MUP shape (peak-to-peak amplitude and MUP time samples) and MU firing pattern information. Rasheed et al. [77], [78], [88] used fuzzy k-nearest neighbor (k-NN) classifier to classify the detected MUPs to several MUPTs. Finally, Erim and Lin [68] developed a method in which MUPs are assigned by a fuzzy inference system that uses the raw distance, the normalized distance, and the firing time of the given MUP. The raw distance is the Euclidian distance between the given MUP and the MUP template of the considered MUPT. The normalized distance is the raw distance normalized by the energy of the MUP. Given these three inputs, the fuzzy inference system determines the certainty of assigning a given MUP to each extracted MUPT. This MUP is then assigned to the MUPT that has the highest membership value if this value is above a user defined threshold.

Certainty-based classifiers (CBC) [1], [7], [27], [72], [76], [79], [80], [82], [125] estimate a measure of confidence (certainty) in assigning a MUP to one of the extracted MUPTs. The certainty algorithm combines both MUP shape and MU firing-pattern information to calculate the confidence of assigning a candidate MUP to a particular train. The certainties of assigning a candidate MUP are evaluated for the two trains that have the most and the next most similar MUP templates. These two trains are found by calculating the Euclidian distance between the candidate MUP and the MUP template of each MUPT.

The candidate MUP is assigned to the MUPT which has the greatest certainty value, if this value is greater than the certainty assignment threshold. Otherwise, the MUP is left unassigned.

Recently, multiple classifier systems have been used to enhance classification accuracy and overcome limitations of individual classifiers. One approach to build such a system is through classifier fusion. Classifier fusion techniques applied for EMG signal decomposition [27], [79], [81], [82], [88], [89], [125] use a pool of base classifiers to assign MUPs. The pool of base classifiers consists of three kinds of classifiers: adaptive certainty-based classifiers (ACCs) [76], [80], [88] adaptive fuzzy k-nearest neighbor classifiers (AFNNCs) [77], [78], [88], and adaptive matched filter classifiers (AMFCs) [27], [88]. An ACC is a modified version of the certainty-based classifier [1], [7], [27], [72], [76], [79], [80], [82], [125] where the minimum certainty threshold for each MUPT is adjusted during the decomposition process depending on its level of FCE [76], [80], [88] using several heuristic rules. An AFNNC uses the same scenario as an ACC does, but here a fuzzy k-NN classifier is used instead of the certainty-based classifier [77], [78], [88]. An AMFC uses the same procedure as an ACC to adjust the minimal similarity threshold for each MUPT [27], [88]. The AMFC, also employs both MUP shape and MU firing pattern information to measure the similarity between a MUP and the MUP template of a MUPT, but here the shape similarity between the MUP template of a MUPT and a candidate MUP is calculated using either normalized cross correlation [27], [88], [129] or pseudo-correlation [70]. These base classifiers use different types of features such as time samples, first- or second-order discrete derivative, or wavelet coefficients of MUPs. The decisions made by each of these classifiers are combined by classifier fusion schemes to make the final assignment decision. Across the EMG signal data sets used for evaluation, the classifier fusion approach had better average classification performance overall, especially in terms of reducing classification errors.

Although results of these supervised classification techniques are promising, their performance depends on the parameters used and the validity of the training data provided by the clustering results. The shape of various classes can also affect the results of Euclidean distance-based methods such as those that use certainty-based classifiers; if the shapes of the classes are not hyperspheric these methods may not perform well. This issue can be resolved by using matched filter classifiers, k-NN classifiers, or classifier fusion techniques, but the processing time of the last two methods are high and hence impractical for clinical applications. The criteria used to merge MUPTs with similar MUPs also influence decomposition results. Using high threshold values results in duplication of some MUPTs while using low threshold values results in some invalid MUPTs. Data-driven thresholds or threshold-free methods should be

26

developed to assist with merging of MUPTs. Finally, the variability of MU firing patterns may decrease classification accuracy. For example, certainty-based classifiers that use both MUP shape and MU firing pattern information equally, may not perform well if MUs do not fire in a regular fashion or the contraction force changes drastically during signal acquisition. Therefore, both MUP shape and MU firing pattern information need to be evaluated and weighted based on their validity and variability. Figure 2.6 summarizes the decomposition results of a real EMG signal. In this example, the MUP template and several morphological feature values, along with the MU discharge patterns, instantaneous firing rates, and several MU firing pattern feature values for each extracted MUPT are illustrated. The individual MUPs assigned to each MUPT are plotted on top of each other in a shimmer plot.

2.3.7 Resolving Superimposed MUPs

During muscle contraction, a number of MUs are active. The number of active MUs and the rate at which they fire depend on the level of contraction and MU recruitment thresholds. Even though MUs fire independently and at similar but variable firing rates, two or more different MUs will, at some points in time, fire at the same time or within a sufficiently short time interval such that their MUPs will superimpose and overlap such that the detected potential is the algebraic summation of the individual MUPs from these MUs and is known as a superimposed MUP (SMUP) [7]. If a full or complete decomposition is required, SMUPs need to be resolved into their constituent MUPs. Resolving SMUPs is the process of identifying the MUPs that contributed to a SMUP and identifying the precise timing of these MUPs [1], [5], [130-136].

Methods proposed to resolve SMUPs can be classified into two categories: sequential and modeling based. Sequential approaches (also known as peel-off methods) are based on matching the MUP templates of the extracted MUPTs, one template at a time, with the SMUP or its residual [5], [53], [66], [67], [117], [117], [130], [131], [134]. By measuring the matches between a given SMUP and the MUP template of a MUPT, the most likely MUP template is identified and subtracted (peeled off) from the SMUP. The resulting waveform in then used to reveal the next MUP template by searching among the other remaining MUP templates. This process is usually repeated until a stopping criterion is reached.

Modeling based approaches are based on developing a mathematical model for a SMUP [61], [135-137]. This model is given by

MUP Template | MUP Stability | | IDI Histogram | Firing Graph | MURE: 5
RR: 3.7

1. N=45 | CoV: 0.85 | Vpp: 624.7 µV / Duration: 11.9 ms / Area:1166.5 uVms / AAR: 1.9 ms / Phs: 2 Turns: 2 | mean 90 ms / sd 5.8 ms / coy 0.07 / 90 ms | | FR: mean 11.2 Hz / FR: MCD 0.07 Hz / ID Rate 87.9% / # of Mups: 131

2. N=44 | CoV: 0.44 | Vpp: 316.3 µV / Duration: 11.5 ms / Area: 838.6 uVms / AAR: 2.7 ms / Phs: 2 Turns: 2 | mean 82 ms / sd 6.4 ms / coy 0.08 / 82 ms | | FR: mean 12.2 Hz / FR: MCD 0.08 Hz / ID Rate 67.1% / # of Mups: 123

3. N=30 | CoV: 0.54 | Vpp: 337.2 µV / Duration: 3.9 ms / Area: 206.5 uVms / AAR: 0.6 ms / Phs: 2 Turns: 2 | mean 55 ms / sd 19.1 ms / coy 0.35 / 55 ms | | FR: mean 18.3 Hz / FR: MCD 0.56 Hz / ID Rate 30.3% / # of Mups: 87

4. N=27 | CoV: 0.30 | Vpp: 262.9 µV / Duration: 10.7 ms / Area: 498.3 uVms / AAR: 1.9 ms / Phs: 2 Turns: 2 | mean 107 ms / sd 5.3 ms / coy 0.05 / 107 ms | | FR: mean 9.4 Hz / FR: MCD 0.04 Hz / ID Rate 51.3% / # of Mups: 71

5. N=25 | CoV: 0.75 | Vpp:1380.8 µV / Duration: 11.4 ms / Area:2862.1 uVms / AAR: 2.1 ms / Phs: 2 Turns: 4 | mean 85 ms / sd 6.6 ms / coy 0.08 / 85 ms | | FR: mean 11.8 Hz / FR: MCD 0.10 Hz / ID Rate 40.3% / # of Mups: 70

6. N=4 | CoV: 0.16 | Vpp: 483.5 µV / Duration: 8.6 ms / Area:1118.5 uVms / AAR: 2.3 ms / Phs: 2 Turns: 2 | | | # of Mups: 13

7. N=3 | CoV: 0.47 | Vpp: 566.7 µV / Duration: 4.7 ms / Area: 710.6 uVms / AAR: 1.3 ms / Phs: 1 Turns: 0 | | | # of Mups: 10

Horz: 5 ms/div / Vert: 500 µV/div / Sweep: 25 ms | Horz: 2 ms/div / Vert: 500 µV/div / Sweep: 10 ms | | Horz: 50 ms/div / Sweep: 250 ms | Horz: 2 s/div / Vert: 5 Hz/div / Sweep: 20 s |

Figure 2.6: Decomposition results of an EMG signal. From left to right, the first three columns show the MUP template, the shimmer plot of the assigned MUPs, and the features of the MUP template of each extracted MUPT. The last three columns show MU firing pattern information for the extracted MUPTs. The fourth column shows the IDI histogram and corresponding statistics for each extracted MUPT. Finally, the last two columns show the discharge patterns, instantaneous firing rates, and firing pattern features for each MU (from [19]).

$$\text{SMUP} = \sum_{i=1}^{n} w_i S_{i,t_i} + \text{noise} \tag{2.4}$$

where n is the number of extracted MUPTs, S_i is the MUP template of the ith MUPT, t_i is the firing time of the corresponding MU and can take non integer values, and w_i is a binary variable which is "1" if S_i contributed to the SMUP and is "0" if it did not. The goal is to find $T = \{t_1, t_2, \ldots, t_n\}$ and $W = \{w_1, w_2, \ldots, w_n\}$ such that

$$e(T, W) = \left\| \text{SMUP} - \sum_{i=1}^{n} w_i S_{i,t_i} \right\|^2 \tag{2.5}$$

is minimized. A number of algorithms have been proposed for solving this optimization problem in an efficient way [61], [117], [135-138]. Some of these methods limit the number of assumed contributing MUPs to 2 or 3, [61], [117], [131] while the newer algorithms [135-137] resolve SMUPs consisting of up to six MUPs with reasonable accuracy.

The peel-off methods are simple and fast, however they may fail to find the optimal solution because in each step alignment and subtraction is completed without considering the results of previous steps. Errors made during each step can affect subsequent steps and hence cause an incorrect or unsuccessful resolution of the SMUP. Moreover, these approaches do not perform well when MUPs are combined in such a way that their out-of-phase peaks are summed together and cancel each other (i.e., destructively superimposed). Alternatively, the modeling based approaches perform better than the peel-off methods in resolving SMUPs. However, their processing time is greater than the peel-off methods because they explore a large search space to find the best solution and the size of the search space increases with n. Therefore, when selecting a SMUP resolution algorithm, its processing time and accuracy for different types of SMUPs should be considered. For clinical use of EMG signal decomposition results, where only mean MU firing rate and MU firing rate variability are to be studied, resolving SMUPs is not necessary [1], [7] because the desired MU firing parameters can be estimated from incomplete discharge patterns [7], [139], [140]. However, for detailed studies of MU control and muscle architecture, SMUPs must be resolved. For such applications, accuracy and completeness is more important than the speed because an incomplete decomposition may provide a misleading representation of MU firing rates [25].

2.3.8 Estimating MUP Templates and MU Firing Pattern Statistics

Once the decomposition process is completed, the prototypical MUP shape (MUP template) and MU firing pattern statistics for each extracted MUPT needs to be estimated for future analysis (especially for quantitative electromyography). To reduce the effect of interference from the MUPs of other motor units and noise when estimating the MUP template for a MUPT, different methods such as mean, median [141], [142], median-trimmed-mean [143], statistical [64] and interference cancelling averaging techniques [49], [50], [75] have been proposed. When the number of MUPs assigned to a train is large, mean estimation can provide a better SNR than the other methods because the SNR improves with the square root of the number of available MUPs. It is also the simplest method. However, if the number of MUPs in a MUPT is small, interference from the MUPs of other MUs can significantly affect the estimated MUP template. Using the median or median trimmed mean averaging techniques can reduce the effect of interfering MUPs. These two methods also work better than the simple mean, if the background noise contaminating the MUPs has a non-Gaussian distribution, such as the Laplacian distribution (which has been suggested to be a good model for the background noise of EMG signals) [61], [143]. Given the MUP template of each extracted train, its features such as (duration, peak-to-peak voltage, number of phases and turns, area and area to amplitude ratio) are calculated for QEMG [7], [8]. In Figure 2.6, MUP templates were estimated using the median trimmed mean averaging technique and its features were calculated using standard methods [7], [144].

When estimating MU firing pattern statistics, to obtain accurate estimates of the mean and standard deviation of the IDIs of each MUPT, IDIs related to FCEs and MCEs must be excluded from the calculations. Stashuk and Qu [140], based on McGill's work [49], [50], [75], developed a method called error-filtered estimation (EFE) for this purpose. Xu and Xio [139] also proposed a method using a weighted matching between the IDI probability density function (PDF) and a multi Gaussian model for estimating IDI statistics of a train. The method proposed by Xu and Xio [139] performs better than the EFE algorithm, but it depends on the estimated PDF of the IDIs and is slower than the EFE algorithm. In Figure 2.6 the IDI statistics of each train were estimated using the EFE algorithm.

2.4 Summary of EMG Signal Decomposition Methods

A chronologically ordered summary of the EMG signal decomposition algorithms discussed is provided in Table 2.1. As shown, various types of electrodes (single channel or multichannel) and various signal processing, clustering, and supervised classification techniques have been employed in the hope of

developing fully automated and robust procedures for EMG signal decomposition. With the exception of a few methods, such as PD I [5], EMGLAB [45], and the method developed by Stashuk and DeBruin [62], which are semi-automatic and need operator input, all of the methods listed in Table 1 are automatic. In addition, most of the methods (68%) make either passive or active use of MU firing pattern information.

Many of these decomposition algorithms use single linkage clustering techniques. One key factor may be the ability of these clustering algorithms to correctly group MUPs generated by a MU even if the MUP shapes are non-stationary due to electrode movement. However, single linkage clustering techniques are computationally expensive and therefore several decomposition algorithms such as DQEMG and the multiple-classifier-based techniques use a customized K-means clustering method called Shape and temporal -based clustering (STBC) to group MUPs. STBC uses both MUP shape and MU firing pattern information to cluster MUPs. In fact, in these methods, the clustering objectives are to provide accurate training information for supervised classification and the issue of MUP shape non-stationary is dealt with during supervised classification.

Across the sets of EMG signals used for evaluation, the majority of these algorithms performed well. In general, the newer algorithms perform better than the older ones. For example, Yamada et al. [95] improved the accuracy of the wavelet-based decomposition algorithms by up to 5% by using the full set of MUP wavelet coefficients together with PCA. Rasheed et al. [27], [79], [82], [88], [89], [125] showed that multiple classifier fusion approaches using the ACC, AFNNC, AMFC, and the CBC had better performance in terms of both MCE rate and FCE rate than using these classifiers individually. The accuracies of the classifier fusion methods were 1% to 8% higher than for the classifiers used individually. In addition, both the AFNNC and ACC performed better than the CBC while the AFNNC was the best among these three classifiers. In addition, by employing artificial intelligence techniques, Nawab et al. [25], [122], [123] reduced the processing time and increased the accuracy of the PD I algorithm [5]; the average accuracy for PD II was 1.3 times of that of PD I.

Using multichannel signals can improve the accuracy with which MUPs are assigned to MUPTs. Florestal et al.[97] showed that the extra information provided by additional (5-7) channels enhances MUP assignment accuracy with a mean improvement of 6% for the majority (78%) of the MUPTs extracted. However, the decomposition of multichannel signals takes more time than that of single channel signals. Therefore, decomposing multichannel signals may not be practical for real-time

applications, but it may be suitable for applications in which decomposition accuracy is more important than decomposition speed.

Several methods such as PD I [5], EMGLAB [45], PD II [25], and the method developed by Stalberg and his co-workers [64] provide a convenient graphical interface as well as a number of automatic procedures for the operator to inspect and edit decomposition results. Such facilities are useful in improving the decomposition results of signals that are difficult to decompose. Specifically, it assists with decreasing FCE rates in MUPTs created by different motor units while having similarly shaped MUPs. Nevertheless, such improvement still depends on the skill and experience of the operator.

2.5 Evaluating EMG Signal Decomposition Algorithms

The performance of EMG signal decomposition algorithms should be evaluated using signals detected from normal and abnormal muscles during different levels of contraction and using different types of electrodes. Ideally, a decomposition system should be able to decompose signals composed of five or more MUPTs with: variable MUP shapes, frequent superpositions of MUPs, variable MU firing patterns, similar MUP shapes generated by two or more MUs, and MU recruitment and de-recruitment.

In general, a decomposition system is evaluated both qualitatively and quantitatively. For qualitative evaluation, each MUPT is assessed using the shapes and occurrence times of the MUPs assigned to it [1], [19-21]. MUP shape-based validation of a MUPT is made using the raster/shimmer plots of the MUPs assigned to it. If the shapes of MUPs assigned to a train are consistent, the MUPT is considered valid; otherwise, it is considered invalid.

Qualitative MU firing pattern-based validation of a MUPT is based on viewing its IDI histogram and the instantaneous firing rates of the corresponding MU versus time. MU discharges corresponding to a valid MUPT occur at regular intervals [1], [45], [97], [145] (for example see MU firing patterns of MUPTs 1, 2, and 4 shown in Figure 2.6) . However, MU discharges corresponding to an invalid MUPT will not have a Gaussian shaped IDI distribution and will have large variations in its instantaneous firing rate plot (see the MU firing patterns of MUPT #3 shown in Figure 2.6 as an example). For full decomposition algorithms, in addition to consistent MU firing patterns, the residual signal created after subtracting classified MUPs from the composite EMG signal is also investigated. A fully decomposed EMG signal should have a flat residual and regular MU discharges intervals [45], [97], [145].

Table 2.1: Summary of developed EMG signal decomposition methods. (Methods indicated by an '*' are developed for multichannel EMG signals.)

Investigators	Segmentation Technique	Features Used	Clustering Algorithm	Supervised Classification Algorithm	MU Firing patterns used Actively/Passively?	Resolve Superpositions?
De Luca et al. (PD-I)[5], [6] *	User defined & signal dependent threshold for MUP amplitude, variable - length window.	Time samples	—	MAP–based template matching	Actively	Yes
Gerber et al.[61]	Signal dependent threshold for MUP amplitude, variable-length window.	MUP morphological features,	Single linkage	Minimum distance-based template matching	—	Yes
McGill et al. (EMGLAB) [45], [49], [50], [75]	Signal dependent threshold for MUP amplitude, fixed-length window.	Discrete Fourier transform coefficients	—	Template matching	Passively	Yes
Stashuk and De Bruin[62]	User defined and signal dependent threshold for MUP amplitude, or fixed MUP slope and amplitude criteria, fixed-length window	Power spectrum coefficients	Initial information is provided by the user	Minimum distance	Actively	No
Haas and Meyer [116], [117]	Threshold for mean slope of the MUPs, variable -length window.	Time samples+ MUP morphological features	Single linkage	—	—	Yes
Loudon et al.[65]	Signal dependent threshold for MUP amplitude, fixed-length window.	MUP shape morphological features	Minimum spanning tree	—	Passively	Yes

33

Table 2.1: Continued

Investigators	Segmentation Technique	Features Used	Clustering Algorithm	Supervised Classification Algorithm	MU Firing Patterns Used Actively/Passively?	Resolve Superpositions?
Stashuk et al. (DQEMG) [7], [72], [74], [146]	Signal dependent threshold for MUP amplitude, or fixed MUP slope and amplitude criteria, fixed-length window.	Time samples	STBC	Certainty-based classifier	Passively during clustering and actively during supervised classification	No
Hassoun et al. [86], [87]	Fixed-length window	Time samples	Artificial Neural Network	Artificial Neural Network	Passively	No
Stålberg et al. [64] *	Fixed threshold for MUP amplitude and slope of the MUP.	MUP shape morphological features	—	Template matching	—	No
Nandedkar et al (MMA). [141]	Signal dependent threshold for MUP amplitude, variable–length window	Time samples	—	Template matching	Actively	No
Nikolic et al. (EMGPAD). [69], [147]	Signal dependent threshold for MUP amplitude, variable–length window	Time samples	Minimum spanning tree	—	—	Yes
Christodoulou et al. [58]	Signal dependent threshold for MUP amplitude, fixed-window	Time samples	Self-organizing Neural Nets	Minimum Euclidian distance	Passively	Yes
Wellig et al. [91], [93], [94]	Not specified	Wavelet coefficients	Single linkage	—	—	No

Table 2.1: Continued

Investigators	Segmentation Technique	Features Used	Clustering Algorithm	Supervised Classification Algorithm	MU Firing Patterns Used Actively/Passively?	Resolve Superpositions?
Fang et al.[53], [90]	User defend threshold for MUP amplitude, fixed-window	Wavelet coefficients from lower frequency bands	Nearest-neighbor	—	Passively	Yes
Gut and Moschytz1[109]	Signal dependent threshold for MUP amplitude, variable –length window	Time samples	Single linkage	MAP and mathematical model of each AcS	Actively	Yes
Zennaro et al.[59], [119], [120] *	Signal dependent threshold for MUP, variable–length window	Wavelet coefficients from lower frequency bands	Minimum spanning tree	—	Passively	No
Yamada et al.[95]	Not specified	PCA of wavelet coefficients	Complete linkage	—	—	No
Koch and Loeliger [110], [111], [148]	Not specified	Time samples	—	Belief propagation and mathematical model of each AcS	Actively	Yes
Katsis et al.[66], [67], [118]	Signal dependent threshold for MUP amplitude, fixed-length window	Time samples	Fuzzy c-means	—	—	Yes
Ren et al. [54-56]	Signal dependent threshold for MUP amplitude, variable -length window	Wavelet coefficients	Minimum spanning tree	Minimum distance classifier	—	No
Florestal et al.[70], [97], [137]	Signal dependent threshold for MUP, variable–length window	Symbolic features	Not specified	Template matching	Passively	Yes

Table 2.1: Continued

Investigators	Segmentation Technique	Features Used	Clustering Algorithm	Supervised Classification Algorithm	MU Firing Patterns Used Actively/Passively?	Resolve Superpositions?
Rasheed et al.[27], [76-80], [88], [89], [125]	Signal dependent threshold for MUP amplitude, fixed-length window	Time samples and wavelet coefficients	STBC	Adaptive Fuzzy k-NN, adaptive certainty based, Adaptive matched template filter classifiers multi classifiers	Actively	No
Nawab et al. (PD-II)[25], [122-124]*	Signal dependent threshold for MUP amplitude, Variable-length window	Time samples	—	MAP-based template matching	Actively	Yes
Erim and Winsean*[68]	User defined and signal dependent threshold for MUP amplitude, variable-length window	Time samples	K-means	Fuzzy Inference System	Actively	Yes
Ge et al. [60]	Signal dependent threshold for MUP amplitude, variable-length window	Discrete Fourier transform coefficients of MUPs	Not specified	MAPC and a mathematical model of each AcS	Actively	Yes

Quantitative evaluation of a decomposition system is based on the accuracy, extent, and speed with which it can decompose an EMG signal. Accuracy is the percentage of correctly assigned MUPs. Extent refers to the number of assigned MUPs represented as a percentage of the number of detected MUPs. Speed refers to the processing time, which includes the time required for decomposing the acquired signal and also measuring MUPT parameters. Accuracy is the most important metric when evaluating a decomposition system, but the weight of the other two criteria depends on the area of application. For clinical applications, accuracy and speed are most important. While for research applications, accuracy and extent may be more important than the speed. Up to now three methods have been proposed to estimate the accuracy of an EMG signal decomposition system [19], [145], [149], [150]: i) using simulated signals of known compositions as a reference; ii) using real signals decomposed manually as a reference; iii) decomposing two EMG signals detected from two locations in a muscle during the same contraction and comparing results obtained thereafter. Following are the implications of these three evaluation methods:

i)   Using simulated data for evaluation of an algorithm is relatively straightforward. It is similar to estimating the accuracy of a supervised classifier, in which a dataset with known labels are classified and then the results are compared with the known labels. In the present context, the dataset is a set of simulated EMG signals of known composition. To estimate the accuracy of a decomposition algorithm, these signals are decomposed by the algorithm and the resultant MUPTs are compared with the original MUPTs. This method may provide an inaccurate assessment of performance because all of the factors that affect decomposition accuracy cannot be included in simulated data. Many EMG signal simulators have been developed [151-153], but none of them include all variables that fully define an EMG signal. For example, detection surface movement which causes MUP shape non-stationarity has a significant effect on decomposition results, but it has not been included in the EMG simulators developed so far. Moreover, the mean and standard deviation of IDIs may change during the recording of a real EMG signal while it is assumed constant during simulation. Therefore, an EMG signal decomposition algorithm may perform well when applied to simulated EMG signals, but have poorer performance when applied to real signals.

ii) Using real data is analogous to using simulated data, but here the reference is being provided from real EMG signals decomposed manually. This technique is more practical than using

simulated data, but can only be executed for EMG signals detected during low-level contractions with good SNR. An algorithm may successfully decompose such simple EMG signals, but may fail to perform as well on more complex signals [149]. Moreover, the resulting MUPTs provided by manual decomposition depend on the similarity/dissimilarity of the MUPT templates, background noise, and operator skills [26]. Different decomposition results may be created by different operators, especially if MUs fire irregularly or MUPs of different MUs are relatively similar in shape.

iii) The simultaneously-but differently detected EMG signals technique (also known as cross-checking) [145] is currently the best method to evaluate the accuracy of an EMG signal decomposition algorithm. Two indwelling electrodes are placed lengthwise along the muscle fibres so that they detect the activity of the same pool of MUs as much as possible. Each detected signal is decomposed individually and then the results are compared. Usually, the time occurrences of all the MUPs of each MUPT common to both signals are compared. This approach is more realistic than the other two methods, but it needs a special electrode configuration and at least two channels of data acquisition. Precisely positioning the electrodes, if two distinct electrodes are used, is also another issue. As one electrode is positioned farther away from the other, it is obvious that the detected signals will be less likely to represent the activity of the same MUs. Moreover, it is not guaranteed that all of the MUPTs obtained by decomposing the two detected signals are valid. Therefore, before comparing the two decomposition results, qualitative validity of the resulting MUPTs needs to be confirmed.

Qualitative evaluation of an EMG signal decomposition does not depend on the decomposition algorithm and the signal used. Moreover, it is useful for detecting invalid MUPTs and excluding them from further analysis. However, it cannot be used for comparing two or more decomposition systems, or for studying the accuracy of a decomposition algorithm as a function of signal parameters such as its decomposability and complexity. Qualitative evaluation of a decomposition result depends on operator experience and skill. In addition, it is time consuming and hence cannot be practically completed in a busy clinical environment. To overcome the last two issues, methods needs to be developed to estimate validity of a given MUPT automatically.

Quantitative evaluation of the results of an EMG signal decomposition provide performance indices regarding the accuracy of a given algorithm in decomposing an EMG signal. Therefore, they can be used for comparing different decomposition systems and for exploring decomposition accuracy as a function

of signal parameters. However, high decomposition accuracy estimated using the three existing methods does not guarantee that the algorithm will work well for all detected EMG signals. Therefore, before using decomposition results for either clinical or research purposes, the validity of the extracted MUPTs need to be assessed both qualitatively and quantitatively.

2.6 Summary

EMG signal decomposition is the process by which a composite EMG signal is resolved into its constituent MUPTs. The basic concepts about the composition of an EMG signal have been presented. Further, the procedures for intramuscular EMG signal decomposition are outlined along with their advantages and disadvantages. Methods for extracting important MUP shape and MU firing pattern information from the MUPTs extracted from a composite EMG signal by a decomposition algorithm have also been described. Such information is used for research and clinical studies based on EMG signal decompositions. For a review of clinical QEMG methods that are greatly facilitated by EMG signal decomposition see Farkas et al. [8]. Finally, qualitative and quantitative methods for evaluating EMG signal decompositions have been reviewed.

EMG signal decomposition has been studied for many years. Several existing signal processing and pattern recognition techniques have been used to improve the decomposition accuracy of EMG signals detected using intramuscular electrodes. However, the performance of these methods still depends on user defined parameters and the complexity of the signal being decomposed. Performance therefore, can be improved and/or stabilized if these parameters are tuned based on both the characteristics of the signal being decomposed and the validity of the information extracted in previous steps/iterations of the decomposition. For this purpose, knowledge-based signal processing and pattern recognition methods should be integrated into the decomposition algorithms. Finally, methods need to be developed for estimating the decomposition accuracy of a decomposition algorithm applied to any given EMG signal.

Chapter 3

Problem Formulation

3.1 Introduction

The first and most critical step in the quantitative analysis of MUPTs is assessing the validity of these trains because as in other pattern recognition problems errors may happen during their creation. Depending on the complexity of the signal being decomposed as well as the parameters and criteria used by a decomposition algorithm, to either assign a MUP to a train or to merge or split trains, different classes of MUPTs may be obtained. This chapter discusses these classes in details. The features of each class of MUPT that can be used to distinguish one class from the others will be discussed as well. These features will be used in the next chapters to developed automatic methods to determine the class label of a MUPT.

3.2 MUPT Classes

MUPTs extracted during EMG signal decomposition can be categorized by the types and numbers of errors made during their creation. In general, four classes of MUPTs can be defined: single, merged, contaminated, and incomplete. Following are a detailed discussion of these MUPTs.

A single, or valid, train represents the firings of a single MU with an acceptable (low) number of FCEs. A merged train results when two or more trains, each of which represent the activity of a single MU, are placed together in the same train. A contaminated train is a single train that contains a high number of FCEs. FCEs are due to the fact that the exact shape of the MUP template of a MUPT and MU firing pattern statistics are not known. Therefore, when MUPs created by two or more MUs are similar they may be assigned to the wrong MUPTs. Finally, an incomplete train contains a high number of MCEs.

Incomplete trains are created due to unresolved superimposed MUPs, insufficient knowledge about the exact shape of the MUP template of a MUPT and its MU firing pattern statistics. The percentage of FCEs relative to the total number of MUPs in a train is called the FCE rate. The percentage of MCEs relative to the expected number of MUPs in a train is defined as the MCE rate.

Our own experience reveals that the MUP template and firing pattern of a single MUPT with a FCE rate <5% can be suitably estimated using the median-trimmed-mean [143] and the EFE [140] algorithms. Therefore, in this thesis FCE rates ≤5% and >5% were respectively considered acceptable and unacceptable.

In general, merged MUPTs and contaminated MUPTs are considered as invalid MUPTs and must be detected and excluded from further analysis of MUPTs obtained from decomposition of an EMG signal because invalid information extracted from invalid MUPTs may contribute to either clinical or scientific misstatements when used clinically or for physiological investigation. Moreover, identifying invalid MUPTs and then correcting them during EMG signal decomposition can improve decomposition accuracy.

To emphasize the importance of validity of a MUPT, an example is provided in Figure 3.1. The first two rows show two valid MUPTs and their MUP templates and MU firing patterns. The third row shows the same data for an invalid train. These valid trains were obtained from decomposing a simulated EMG signal into its constituent MUPTs using the DQEMG program [7]. The invalid train was created by merging these two valid MUPTs. As shown in the third column, the instantaneous MU firing rate versus time plots for the invalid train provides a confused representation of the firing rates of a MU. The invalid MUPT has higher firing rate variability than the two valid trains shown here. The mean firing rate for this train is 21.1 Hz while that for the two valid MUPTs shown in the first two rows are around 10 Hz. Moreover, the MUP template of this invalid train has lower area than the templates of the valid trains shown in this figure. Clearly, such invalid trains must be excluded when using the EMG signal decomposition results because the invalid information extracted from these trains may contribute to either clinical or scientific misstatements when used clinically or for physiological investigation. Therefore, the most critical step in the quantitative analysis of MUPTs, obtained using either a manual or automatic EMG signal decomposition process, is assessing their validity.

Several characteristics of merged, contaminated, and incomplete trains differ from that of single trains. Often the variability (inconsistency) of MUP shape and possibly the variability of MU firing patterns of merged trains are higher than that of single trains [49], [50], [75], [88], [154]. Figure 3.2, which shows a

Horz: 1.0 ms/div
Vert: 0.5 (V/S)/div

Horz: 1.0 ms/div
Vert: 0.5 (V/S)/div

Horz: 10.0 S/div
Vert: 5.0 Hz/div
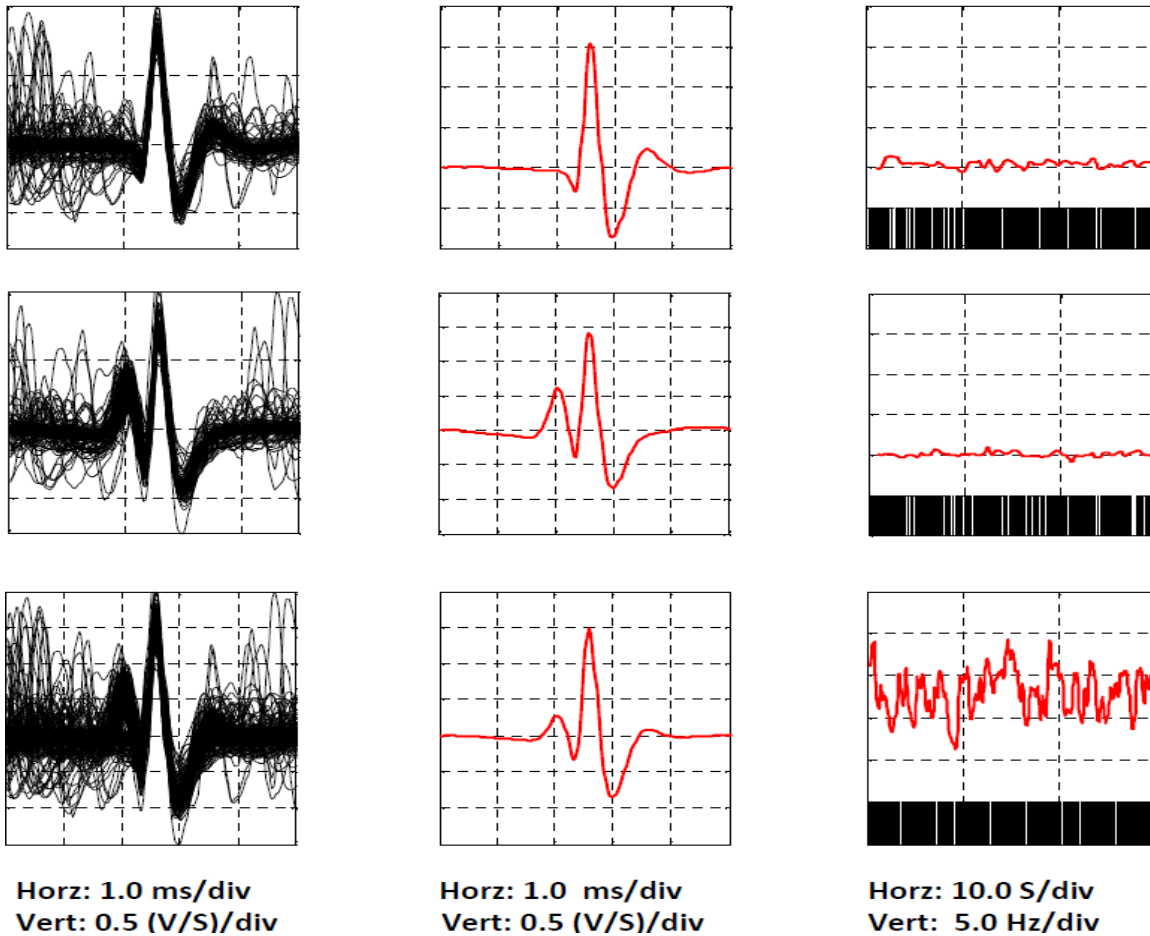
Figure 3.1: (top two rows) Two valid MUPTs, their MUP templates (second column) and firing patterns (third column). Bottom row an invalid MUPT, its MUP template and MU firing pattern. It is clear that the invalid MUPT has higher MUP shape and MU firing rate variability than the two valid trains. In addition, the MUP template of the invalid train has a higher number of phases and turns than those of the valid trains shown.

close-up of the shimmer plots for the MUPs of the valid and invalid MUPTs given in Figure 3.1 supports the statement that the shapes of MUPs assigned to a single MUPT are consistent while that of the merged (invalid) train are inconsistent. As shown, overall the MUPs of the valid MUPT are homogeneous in shape, but that of the merged MUPT have distinct shapes in the regions specified. Consequently, the within train MUP shape variability of the merged train shown in Figure 3.2 is 1.5 unit higher than that of the presented single train. The within train variability here is the mean squared distances between MUPs of the given train and its MUP template.

42
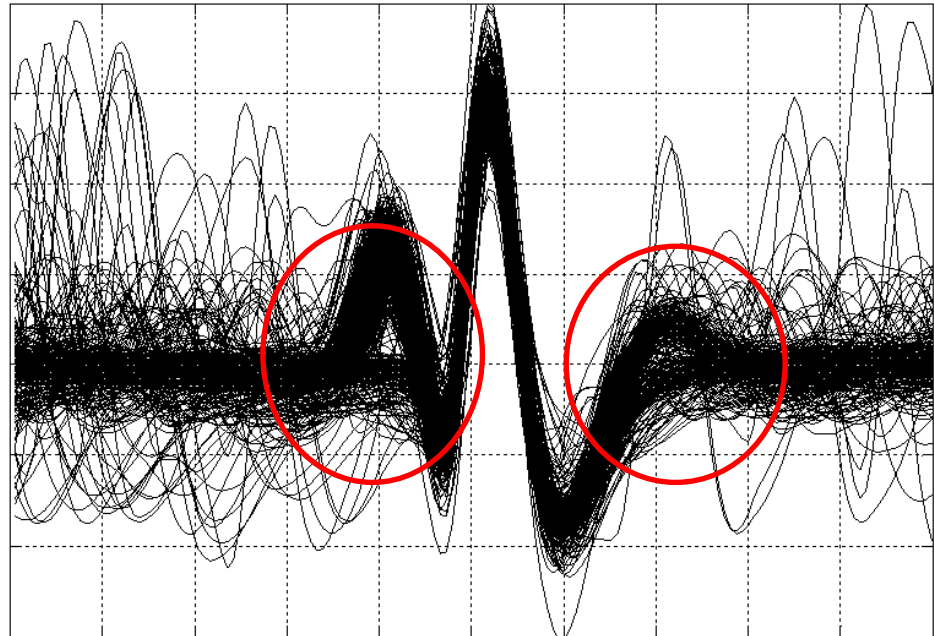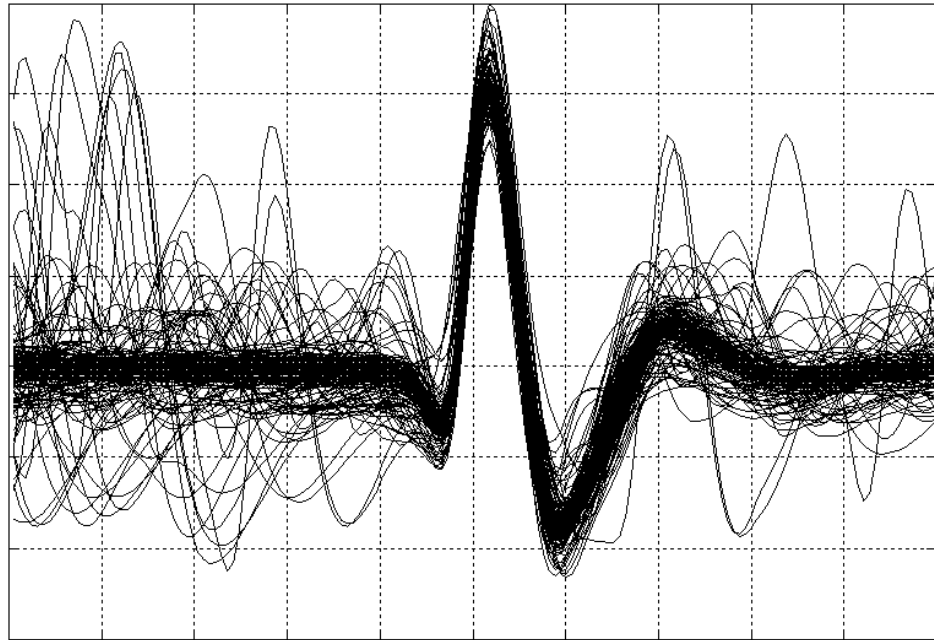
Horz: 0.5 ms/div   Vert: 0.5 (V/S)/div

Figure 3.2: The shimmer plots of the MUPs of the first valid MUPT (top row) and invalid MUPT (bottom row) presented in Figure 3.1. The circles on the plot for the invalid MUPT identify the two regions in which the shapes of the MUPs are inconsistent.
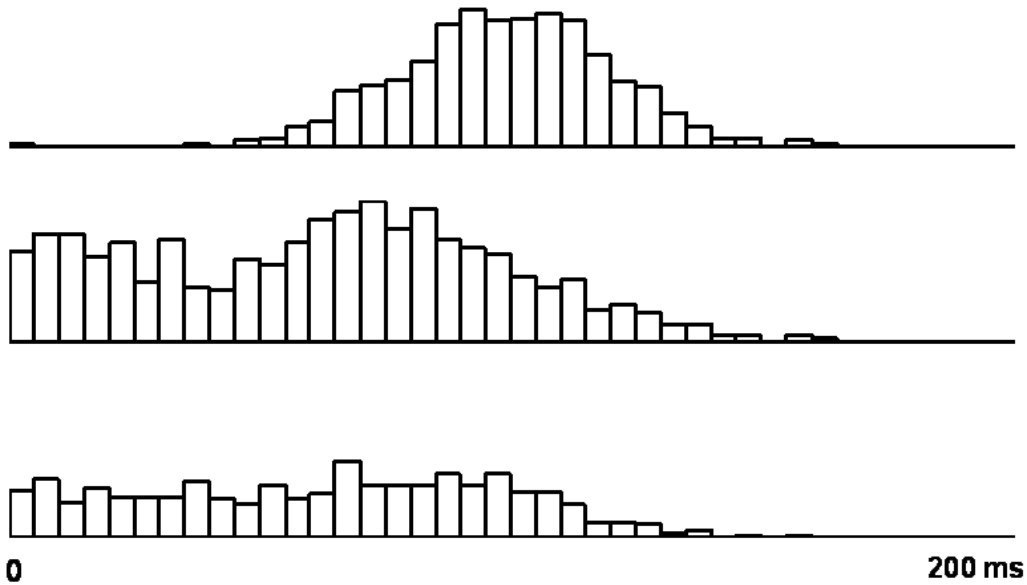
Figure 3.3: Examples of IDI distributions of a single train (top row) compared to that of merged trains (middle and bottom rows). As can be seen, the number of short IDIs in the merged trains are higher than that in the single train, consequently the IDI distributions of merged trains are left-skewed and do not follow a Gaussian distribution.

MU firing patterns of merged MUPTs also differ from those of single trains. The MU firing pattern of a MUPT is, in general, represented by the intervals between consecutive MUP occurrences (i.e., by its IDIs). Let $t_1, t_2, \ldots, t_N$ be the occurrence times of the N MUPs assigned to a MUPT, the corresponding IDIs are $IDI_1, IDI_2, \ldots, IDI_{N-1}$ where $IDI_i = t_{i+1} - t_i$ and $t_{i+1} > t_i$. The MU discharges corresponding to a single MUPT occur at regular intervals and in general, have a Gaussian-shaped IDI histogram while for a merged MUPT the IDIs have large variations and will not have a Gaussian-shaped IDI histogram (see Figure 3.3). Generally, merged MUPTs have a much lower mean relative to the mean IDI of single valid trains because invalid trains include more short IDIs than valid trains. Finally, merged trains have higher MU firing rate variability than valid trains (Figure 3.1).

For contaminated trains, their within train MUP shape variability may or may not be higher than that of single (valid) MUPTs, but their MU firing rate and IDI variability will be. Specifically, the IDI distribution of contaminated MUPTs will not be symmetric around the mean because FCEs cause the number of shortened IDIs in a train to increase. As shown in Figure 3.4, the IDI distributions of the two contaminated MUPTs presented are skewed to the left. The percentage of short IDIs in contaminated

44
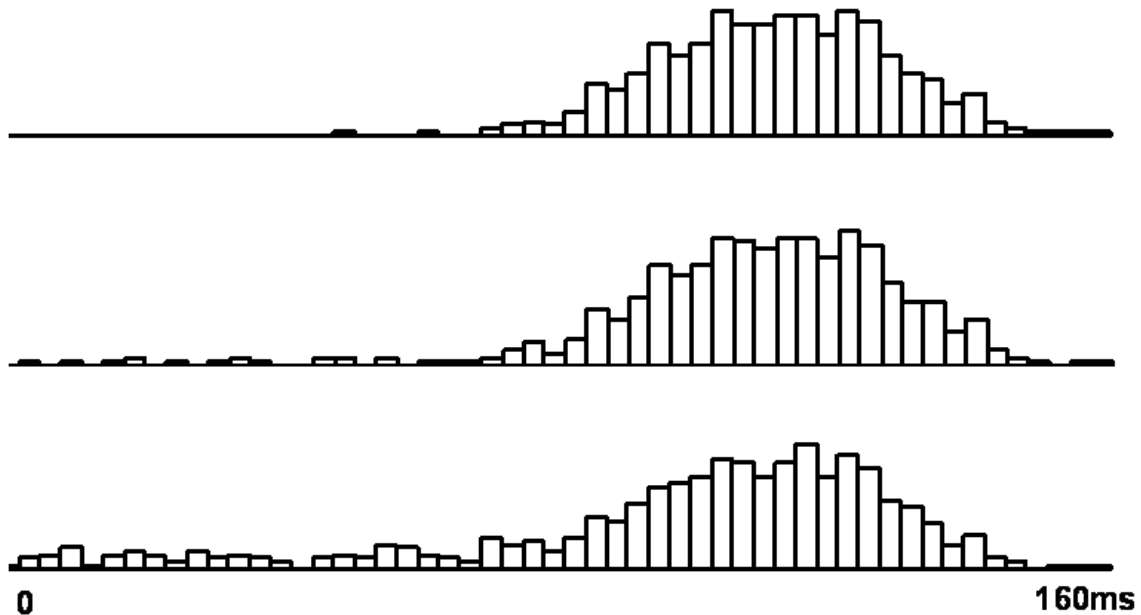
Figure 3.4: Effect of FCE on the IDI distribution of a MUPT. The IDI distribution of a correctly decomposed train (top row); a single train, i.e. one with acceptable (2.5%) FCE (middle row); a contaminated train, i.e. one with unacceptable (12.5%) FCE (bottom row). As shown, both the single and contaminated trains have some short IDIs and they also each has a left-skewed IDI distribution, but the left tail area of the IDI distribution of the contaminated train is greater than that of the correctly decomposed train and the single train.

MUPTs are, in general, higher than that in valid trains. The MU firing pattern variability of contaminated MUPTs may be higher than that of valid trains. For an example of a contaminated MUPT created by DQEMG applied to a real EMG signal, see MUPT# 3 in Figure 2.6. In this example, we can see that the FR−MCD (see Chapter 4), which presents the variability of the firing rate over time, for this invalid train is higher than that for the two first valid MUPTs.

As FCE rate in a contaminated train increases the percentage of short IDI in the train increase and ultimately causing the skewness of the IDI distribution to increase; comparing the examples shown in Figure 3.3 for three different FCE rates (0%, 2.5%, and 12.5%) supports this claim.

For incomplete MUPTs, the within train MUP shape variability is smaller than or equal to that of valid MUPTs, but the IDI distributions of the incomplete MUPTs are skewed to the right because the missing MUPs introduce long intervals between consecutive MUPs. Two examples of the effects of relatively

45
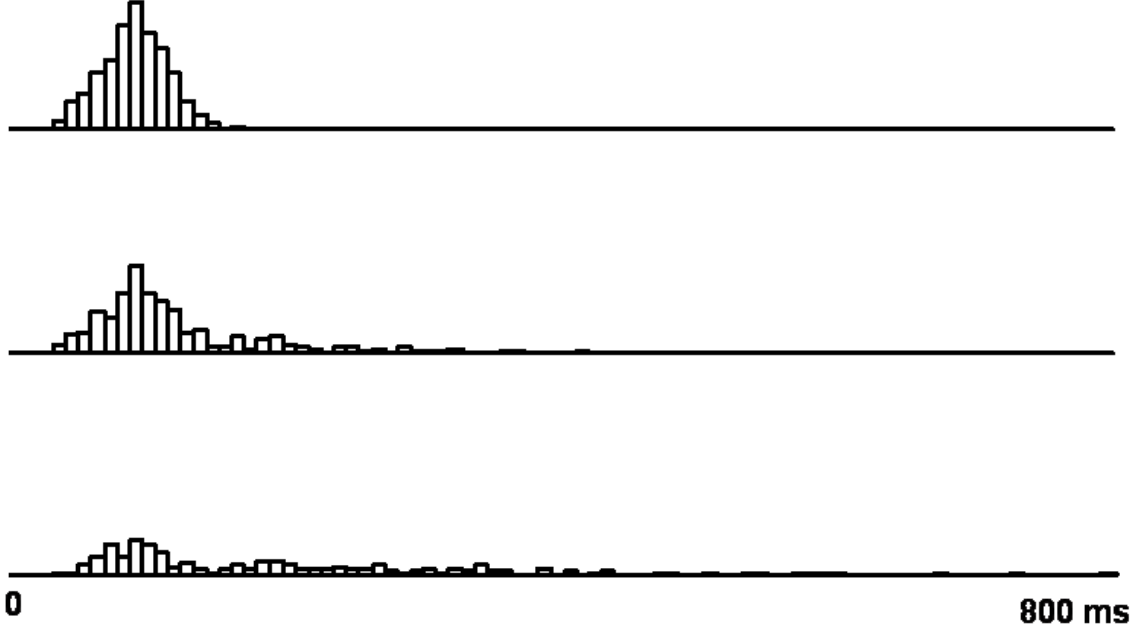
Figure 3.5: Effect of MCE on the IDI distribution. The IDI distribution of a full train (i.e., MCE rate = 0%) (top row); a train with MCE rate = 20% (middle row); a train with MCE rate = 50% (bottom row). It can be seen that MCEs skew the IDI distributions to the right. As MCE rate increases, the number of long IDIs in a train increases and ultimately the skewness (to the right) of the IDI distribution increases.

small and large MCE rates on IDI histograms are presented in Figure 3.5. As shown, the MCEs skew the IDI distribution to the right.

McGill [49] shows that the IDI distribution of a MUPT contaminated by some MCEs follows a multi-modal Gaussian model as

$$\hat{p}(\tau) = \sum_{n=1}^{\infty} p_d \, (1 - p_d)^{n-1} p^{(n)}(\tau) \tag{3.1}$$

where P_d is the detection probability (MCE rate=1-P_d) and $P^{(n)}(\tau) \cong N(n\mu, n\sigma^2)$, μ and σ are the mean and standard deviation of the IDIs, respectively. Based on this model, when the detection probability decreases the major peak will decrease and the height of the other peaks (one at each multiple of μ) will
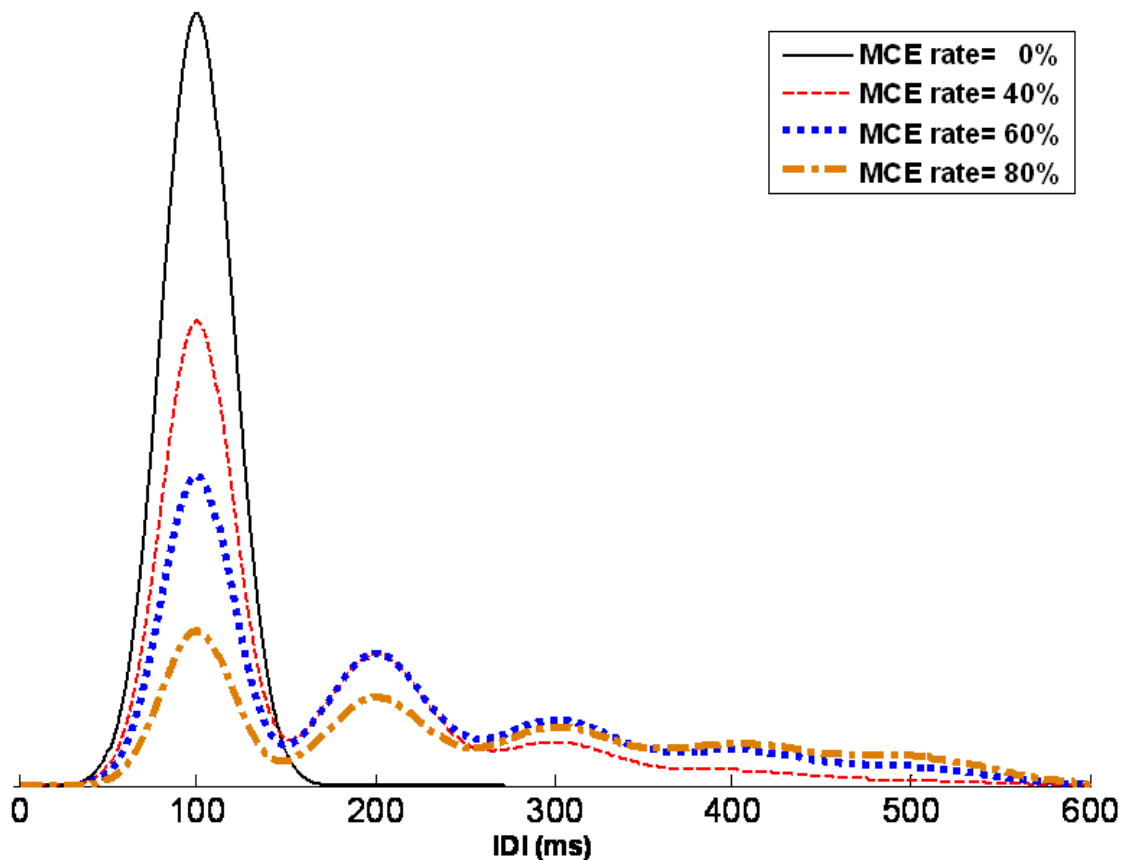
Figure 3.6: The effect of MCE on the IDI density distribution of a MUPT (with mean IDI =100ms) based on the McGill model (i.e. Equation 3.1). As shown, when MCE rate increases, the major peak of the IDI distribution (i.e. peak at mean of IDIs) will decrease and the height of the other peaks (appeared at each multiple of mean of IDIs) will increase.

decrease (see Figure 3.6). High levels of MCE make the measurement of MU firing pattern statistics and the MUP template for each active MU unreliable, because the sample size is small.

3.3 Validating a MUPT

In general, validating a MUPT is a process of determining whether a given MUPT accurately represents the activity of a single MU or not. The validity of a MUPT can be defined using two different criteria: MU firing pattern validity, and MUP shape validity. MU firing pattern validity of a MUPT is determined by assessing its IDI histogram (density function) and the instantaneous firing rate of the corresponding

MU versus time. The goal is to assess whether a given MUPT represents the firings of a single MU or the merged activity of more than one MU. If the firing pattern of the train represents the firings of a single MU, a further analysis is required to investigate whether the estimated level of FCEs in this train are acceptable or not. As discussed in the previous section, the MU discharges corresponding to a valid MUPT occur at regular intervals and in general, have a Gaussian-shaped IDI histogram while for merged and contaminated MUPTs the IDIs have large variations and will not have a Gaussian-shaped IDI histogram. Even though some researchers have demonstrated that the IDI distribution of a MU cannot actually be Gaussian [155], [156], for MUPTs of MUs that are consistently recruited, the Gaussian density is an appropriate approximation [7], [49], [50], [75], [88], [157-159]. If an extracted MUPT represents the firing of a single MU and has suitably low levels of classification errors, it has MU firing pattern validity. As an example, all three MUPTs shown in Figure 1.1 have MU firing pattern validity.

To determine MUP shape validity, a given train is assessed using the shapes of the MUPs assigned to this train. Assuming the MUPs generated by a single MU are homogeneous in shape, the MUPT under study can be assumed to have MUP-shape validity when its MUPs have consistent shapes. As an example, all three MUPTs shown in Figure 1.1 have MUP-shape validity.

Finally, a train can be considered valid based on a combination of its MU firing pattern and MUP shape validity. For example, all three MUPTs shown in Figure 1.1 and the first and second MUPTs presented in Figure 2.6 have both MU firing pattern and MUP shape validity.

To date, MUPT validation in conducted qualitatively by an expert operator. The MUP shape validity of a MUPT is assessed by an expert using raster/shimmer plots of its assigned MUPs [1], [19-21], [26], [32]. MU firing pattern validity of a MUPT is determined by viewing and qualitative evaluation of its IDI histogram and the plots of the firing rate as a function of time. The accuracy of such qualitative MUPT evaluations, as with other methods that need operator supervision, depends on operator experience and skill. In addition, such evaluations are time consuming and cannot be practically completed in a busy clinical environment. More importantly, manual MUPT validation methods cannot assist with improving the performance of automatic EMG signal decomposition algorithms. To overcome these issues, methods need to be developed to automatically estimate the validity of a given MUPT.

McGill and Marateb [160] developed a rigorous statistical method for assessing the validity of MUPTs extracted by decomposing an EMG signal. The evaluation results are promising, but due to the computational complexity of the procedures used in this method, the algorithm is only efficient for assessing the decomposition accuracy of 5–second–long, low-complexity signals composed of at most 6

MUPTs. In addition, full decomposition in required in this method. Therefore, this method neither can be used during decomposing nor in busy clinical environment.

This thesis presents several automatic and fast methods to estimate the overall validity of a MUPT. The objective of developing such methods was to: 1) facilitate the use of intramuscular EMG signal decomposition results for clinical applications of quantitative electromyography by providing the overall validity of MUPTs and excluding or highlighting invalid MUPTs; 2) assist with improving the accuracy and completeness of decomposition results. Using the characteristics of the IDI distribution, MU firing patterns, and within train MUP shape variability of merged, contaminated and single MUPTs discussed in the previous section several methods based on a combination of feature extraction, cluster validation techniques, supervised classification algorithms, and multiple classifier fusion techniques was developed, details are presented in the next four chapters.

3.4 Summary

The MUPTs obtained by decomposing a given EMG signal may accurately represent the activity of a MU (i.e., is valid) or may not (i.e., is invalid). Invalid MUPTs must be detected and either corrected or excluded before using the obtained MUPTs for QEMG because the information provided by invalid MUPTs could improperly suggest an abnormal muscle when interpreted clinically or it may contribute to scientific misstatements. Fortunately, some characteristics of invalid trains (merged and contaminated trains) differ from those of valid trains such that these characteristics can be used to automatically highlight and correct merged and contaminated MUPTs. The next four chapters present several methods developed for this purpose.

Chapter 4

Validating MUPTs using MU Firing Pattern Information

4.1 Introduction

As discussed in the previous chapter, the IDI characteristics and MU firing patterns of single trains differ from those of merged trains (see Figures 3.1 and 3.3). These facts motivate the development of supervised classifiers that use features of the IDIs and MU firing pattern of a MUPT to classify the MUPT.

This chapter presents a firing pattern validity classifier (FPVC) that determines whether a MUPT represents the firings of a single MU or the merged activity of more than one MU. The MU firing pattern of a given MUPT are represented by nine features and assessed using a supervised classifier. The classifier used was trained using simulated data and tested using simulated and real data. The accuracy of the FPVC in categorizing a train correctly is 99% and 96% for simulated and real data, respectively. Detailed definitions and calculation methods for the features used, the composition of the classifiers employed, how these classifiers were trained, and the evaluation of their performances using both simulated and real data are presented in detail**.**

4.2 Discriminative Features

Using the occurrence times of the N MUPs assigned to a MUPT, the corresponding IDIs are calculated and then are represented by nine features for classification. Features were selected based on their ability to discriminate between single or merged trains even for incomplete trains (i.e., MUPTs with high MCE

rate). In calculating these features, the mean (μ) and standard deviation (σ) of the IDIs of the given MUPT were estimated using the error-filtering algorithm (EFE) presented by Stashuk and Qu [140].

In the EFE algorithm, through adjusting low and high boundaries in the IDI histogram, the IDI distribution is divided into three regions such that the second region, which contributes to the main peak in the histogram, contains valid IDIs and the two other regions contain erroneous IDIs caused by FCEs and MCEs. The IDIs which lie in the second region are considered for estimating the mean and standard deviation of the IDIs of the considered MUPT. If the algorithm is able to find such a region in the histogram of the IDIs of a given MUPT, the train is called full. Otherwise, the train is called sparse. When the MCE rate is high, causing the number of MUPs in a train to be small, the MUPT will usually be sparse.

Following is a description of each feature used in developing the FPVC.

(1) CV (coefficient of variation): $CV = \sigma/\mu$.

(2) CV_L (lower CV): $CV_L = \sigma_L/\mu$ where σ_L is the standard deviation of the IDI distribution of the MUPT calculated using only those IDIs with values below μ.

(3) CV_L/CV_U (the ratio of lower and upper CV): $CV_U = \sigma_U/\mu$ where σ_U is the standard deviation of the IDI distribution of the MUPT calculated using only those IDIs with values between μ and $\mu + 2\sigma$.

(4) PI (percentage of inconsistent IDIs): The PI for the IDIs of a MUPT is calculated by dividing the number of inconsistent IDIs by the total number of IDIs. An IDI is defined to be inconsistent with the firing behavior of a single MU if it is less than 25 ms, in a train for which μ cannot be estimated, or if it is less than $max(15ms, \mu - 2\sigma_*)$; where σ_* is the standard deviation of the IDI distribution of the MUPT calculated using only those IDIs with values between μ and $\mu + 2.4\sigma$.

(5) $LIDI_R$ (lower IDI ratio): The $LIDI_R$ is the number of IDIs having values less than 0.5μ, relative to the number of IDIs less than μ.

(6) r_1 (first coefficient of serial correlation): The coefficients of serial correlation for an IDI train are defined as [161]:

$$r_k = \frac{\sum\limits_{i=1}^{N-k}(IDI_i - \mu)(IDI_{i+k} - \mu)}{\sum\limits_{i=1}^{N}(IDI_i - \mu)^2} = \frac{\sum\limits_{i=1}^{N-k}(IDI_i - \mu)(IDI_{i+k} - \mu)}{(N-1)\sigma^2} \qquad (4.1)$$

The first coefficient of serial correlation, r_1, indicates cases where residuals ($IDI_i - \mu$) from adjacent elements in a train are not independent. To decrease the effect of very long IDIs, caused by MCEs, on the calculated value of r_1, only IDIs less than 1.9μ are used for estimating r_1.

(7) Skewness: is a measure of the symmetry of a distribution. By definition, a distribution is skewed if one of its tails is longer than the other. Skewness of an IDI distribution is defined as:

$$Skewness = \frac{\sum\limits_{i=1}^{N}(IDI_i - \mu)^3}{N\sigma^3} \qquad (4.2)$$

As when calculating r_1, only IDIs less than 1.9μ are used for estimating skewness.

(8) ID rate: identification rate (i.e. the probability of detection) is inversely related to the MCE rate of a train and is defined as:

$$ID\ rate = \frac{Number\ of\ MUPs\ in\ a\ MUPT}{Expected\ Number\ of\ MUPs\ in\ the\ MUPT} = \frac{(N-1) \times \mu}{Firing\ Interval} \qquad (4.3)$$

(9) IDI−MCD: mean consecutive difference of IDIs measures the average variability of consecutive IDIs. The sum of the absolute differences of consecutive IDIs is calculated and then divided by the number of IDIs used as follows[162]

$$IDI - MCD = \frac{\sum\limits_{i=1}^{N-2}|IDI_{i+1} - IDI_i|}{N-2} \qquad (4.4)$$

Again, to decrease the effect of very long IDIs caused by MCEs, only IDIs less than $\mu + 3\sigma$ are used for this calculation.

(10) FR−MCD: firing rate mean consecutive difference measures the variability in firing rate over time. An instantaneous firing rate (IFR) for each MUP occurrence in a MUPT was calculated by smoothing the firing rate with an 11‑ point Hamming window. Denoting IFR$_i$ as the estimated instantaneous firing rate at t_i (the occurrence time of the ith MUP), the FR−MCD value for a given MUPT with N MUPs is estimated as

$$FR - MCD = \frac{\sum_{i=1}^{N-2} \left| IFR_{i+1} - IFR_i \right|}{N - 2}$$ (4.5)

For the same reason mentioned above, IDIs greater than $\mu + 3\sigma$ are excluded from this calculation.

4.3 Classification Methods

Three classification methods were examined: Fisher discriminate analysis [105], [163], Pattern Discovery [164], [165], and Support Vector Machines [166], [167]. These classification methods are discussed briefly below.

Fisher discriminate analysis (FDA) [105], [163] is a very simple and powerful method for either linear supervised dimensionality reduction or linear classification. It is also very easy and computationally cheap to implement, especially after training.

Pattern Discovery (PD) [164], [165] is an associative rule-based classification method. Patterns discovered in training data and present in a feature vector to be classified are combined using information theory metrics for classification. A detailed description of how this methodology can be used for classification is provided by Hamilton-Wright et al. [168]. In this work, continuous data were quantized into 10 discrete bins per feature, and a confidence interval of 90% was used.

Support Vector Machines (SVMs): The foundations of SVMs were developed by Vapnik [166], [167]. A SVM is basically a linear classifier that formulates a hyperplane to optimally separate the two classes under study. The optimal decision surface is constructed by maximizing the distance to the nearest members of the classes (i.e., maximizing the margin). A SVM minimizes an upper bound on the generalization error while conventional learning algorithms (e.g., neural networks) minimize the error on the training data [166], [167]. In fact, this feature of a SVM makes it superior to conventional learning algorithms. For cases where the classes are not linearly separable, a kernel is applied to map the original feature space into a much higher feature space presumably making the separation linear in the new space. In this work, a Gaussian radial basis function of the following form was used as the kernel function.

$$K(x, x') = e^{-\xi \|x - x'\|^2}$$ (4.6)

where x is an input data point to the SVM, x' is the center of the kernel and ξ is the width of the kernel and specified a priori by the user.

In training a SVM, in addition to ξ there is another parameter which has to be selected by the user, the cost parameter, C. This parameter, which is also known as the regularization parameter, controls the tradeoff between allowing training errors and the complexity of the machine. For the objectives of this work, ξ and C were determined experimentally using cross validation [169].

In addition to these three classification methods a *Switching classifier,* which based on some measure of the input pattern switches between using the FDA and SVM classification methods, was developed. The motivation of developing a switching classifier is to take the advantage of both the speed of FDA and the accuracy of SVMs and therefore increase classification speed while maintaining classification accuracy. The idea is the same as used in multi-classifier techniques, but the difference is that here only one classifier (either an SVM or an FDA classifier) is used to find the label of the given example. In Sections 4.5 and 4.6 it is shown using simulated data that an SVM classifier is more accurate but slower than an FDA classifier. Therefore, the density function of the transformed features in the Fisher space was assessed to determine the region for each class for which the FDA classifier has 100% accuracy. In classifying a given MUPT using the Switching classifier, if the transformed features fall in one of these two regions the label given by the FDA classifier is used, otherwise the sample is classified using the SVM.

4.4 Evaluation Methodology

Classifiers, based on the methods discussed in Section 4.3, were trained using simulated data and tested using both simulated and real MU firing patterns.

For *simulated data,* trains of 75 IDIs, which on average correspond to EMG signals of 7.5s duration, were initially and independently generated using Gaussian distributions with mean IDI of 80, 90, 100, 110, or 120 ms and CV ranging from 10% to 30%, respectively. There were 20 replicates for each (mean and CV) set of values generated. Up to 5% FCE and from 0% to 70% MCE (in steps of 10%) was added to the single trains. Each possible pair of the generated trains (different mean, CV, false and missed classification rate) was then merged. On the whole, 90,000 valid trains and 90,000 invalid (merged) trains were generated.

For *real data,* EMG signals provided by M. Nikolic of Rigshospitalet, Copenhagen, Denmark [170] were used. These signals, which were detected from normal, myopathic and neurogenic individuals using a standard concentric needle electrode during constant low level voluntary contractions, were decomposed using DQEMG algorithms [7]. The resulting MUPTs were assessed manually to classify MUPTs as

single (with consistent MUP shapes and MU firing pattern) or merged. The single MUPTs were contaminated by adding up to 5% FCE and up to 70% MCE in steps of 10%. To generate merged (invalid) MUPTs, each pair of single MUPTs was merged. In total 5,055 single trains and 73,742 invalid trains were generated. This real MUPT data set was then divided into ten subsets each of which contained 506 valid and 7,375 invalid trains, respectively.

Considering the reference MUPTs as the gold standard data, the performance of the developed MUPT validation system was evaluated in terms of correctly classifying valid and invalid trains. Three accuracy indices were defined for this purpose: accuracy for valid trains (A_V), accuracy for invalid trains (A_{IV}), total accuracy (A_T). These three indices are given by:

$$A_V\% = \frac{Number\ of\ valid\ MUPTs\ correctly\ classified}{Total\ number\ of\ valid\ MUPTs\ tested} \times 100 \tag{4.6}$$

$$A_{IV}\% = \frac{Number\ of\ invalid\ MUPTs\ correctly\ classified}{Total\ number\ of\ invalid\ MUPTs\ tested} \times 100 \tag{4.7}$$

$$A_T\% = \frac{Number\ of\ \ MUPTs\ correctly\ classified}{Total\ number\ of\ \ MUPTs\ tested} \times 100 \tag{4.8}$$

4.5 Results

The classification performances of the developed MUPT classifier for both simulated and real data are summarized in Tables 4.1 and 4.2, respectively. Each table presents the estimated means and standard deviations of the three performance indices A_V, A_{IV}, and A_T. The numbers presented in Table 4.1 were obtained by running a 10–fold cross validation on the simulated data set used. The values presented in Table 4.2 for the real data were obtained by evaluating the classifiers trained using the entire simulated data on the 10 different subsets of the real MUPT data discussed in Section 4.4. The statistical comparison of the methods was conducted using the analysis of variance (ANOVA), at a 5% significance level and the Tukey-Kramer honestly significant difference test for pair-wise comparison of the mean values.

Each table summarizes the accuracy of the studied classifiers for the three ranges of MCE rates studied. The 0% to 70% range represents the expected levels of MCE rate in trains during the final iterations of EMG signal decomposition or once it is completed, while the 50% to 70% or 60% to 70% ranges model

the early stages of decomposition when the extracted MUPTs are sparse. The aim of using these ranges was to study the effectiveness of these classifiers at difference stages of EMG signal decomposition.

4.6 Discussion

According to the results shown in Table 4.1, the overall average accuracy of the classifiers studied as a FPVC is greater than 95% on average. For the data with 0% to 70% MCE rate, which is the general case in EMG signal decomposition, the SVM has an average accuracy of 99.5%, Switching 99.5%, FDA 99.0%, and PD 99.2%, respectively. Of these four classifiers, the SVM and Switching classifiers are the best performers. The accuracy of the FDA classifier is compatible with the SVM and Switching classifier, but the classification error for this classifier for single trains is higher which causes MUPT duplication during EMG signal decomposition. Based on these results and considering the runtime of the FDA classifier, this classifier may be preferred to the other classifiers studied for FPVC; nevertheless, the SVM and Switching classifiers have the highest accuracy (i.e., lowest error rates) and the Switching classifier is fast enough to be used both during EMG signal decomposition and once the decomposition is completed. The Switching classifier, with an average computation time of 7.7 ms per train, was 8 times faster than the SVM but 5 times slower than the FDA classifier. The processing was carried out in Matlab (The Mathworks, Natick, MA) on a computer with an Intel Core 2 Duo E8400 CPU (6M Cache, 3.00 GHz clock, 1333 MHz FSB) and 3GB of RAM.

The classifier performance using the real data, shown in Table 4.2, was consistent with that obtained using the simulated data because the IDIs of the real MUs studied (diseased and normal) were for the most part Gaussian distributed as were the simulated IDI training values. Specifically, the results for real data support the claim that the Switching classifier is the best choice as a FPVC. However, compared to the results presented in Table 4.1, the accuracy of the classifiers for real merged trains is lower than for simulated merged trains. One reason for this is that the selected trains may have had some MCEs that occurred during decomposition. Therefore, although up to 70% MCE was added to the trains, the exact MCE rate may have been greater. Our experience shows that the performance of a classifier drops if the MCE level in a train is greater than 70%. Nevertheless, the first two columns of Table 4.2 suggest that overall the FDA, SVM, and Switching classifiers all have admirable performance when applied to real data. Therefore, by using the developed classifiers, the probability of detecting a merged train during evaluation of a train's firing pattern or during the final step of EMG signal decomposition is greater than 0.98.

Table 4.1: The performance of the studied classifiers applied to simulated valid (single) or invalid (merged) MUPTs. In each column, individual or groups of methods indicated by an '*' and bolded performed significantly better than the others according to the analysis of variance (level of significance =5%) and the Tukey-Kramer honestly significant difference test in pair-wise comparison of the mean values. When two or more methods had statistically similar performance, they are all indicated by '*'.

	Missed-Classification Error Rate								
	0% to 70%			50% to 70%			60% to 70%		
	A_V (%)	A_{IV} (%)	A_T (%)	A_V (%)	A_{IV} (%)	A_T (%)	A_V (%)	A_{IV} (%)	A_T (%)
FDA	98.8±0.1	99.2±0.1	99.0±0.1	98.1±0.1	96.5±0.1	97.3±0.1	98.0±0.2	93.9±0.4	95.9±0.2
PD	99.3±0.1	99.1±0.1	99.2±0.1	99.1±0.1	96.1±0.2	97.7±0.1	99.2±0.1	92.7±0.3	96.0±0.1
SVM	*99.5±0.1	*99.5±0.1	*99.5±0.1	*99.3±0.1	*97.7±0.2	*98.5±0.1	*99.4±0.1	*95.7±0.2	*97.6±0.1
Switching	*99.6±0.1	*99.5±0.1	*99.5±0.1	*99.4±0.1	*97.7±0.2	*98.5±0.1	*99.4±0.1	*95.8±0.2	*97.6±0.1

Table 4.2: The accuracy of the four studied classifiers applied to real single/merge MUPTs. As in Table 4.1, the better classifiers are identified.

	Missed-Classification Error Rate								
	0% to 70%			50% to 70%			60% to 70%		
	A_V (%)	A_{IV} (%)	A_T (%)	A_V (%)	A_{IV} (%)	A_T (%)	A_V (%)	A_{IV} (%)	A_T (%)
FDA	*99.9±0.1	*95.7±0.3	*96.0±0.2	*99.8±0.1	*93.6±0.3	*94.3±0.3	99.6±0.2	*91.6±0.5	*93.0±0.3
PD	*99.9±0.1	94.1±0.3	94.5±0.4	*99.9±0.1	90.3±0.3	91.5±0.2	*99.7±0.2	89.9±0.3	91.4±0.3
SVM	*99.9±0.1	*95.6±0.2	*96.0±0.1	*99.9±0.1	*93.5±0.3	*94.2±0.3	*99.8±0.1	*91.7±0.3	*93.3±0.2
Switching	*99.9±0.1	*95.6±0.2	*95.8±0.1	*99.9±0.1	*93.5±0.2	*94.2±0.2	*99.8±0.1	*91.5±0.4	*92.9±0.3
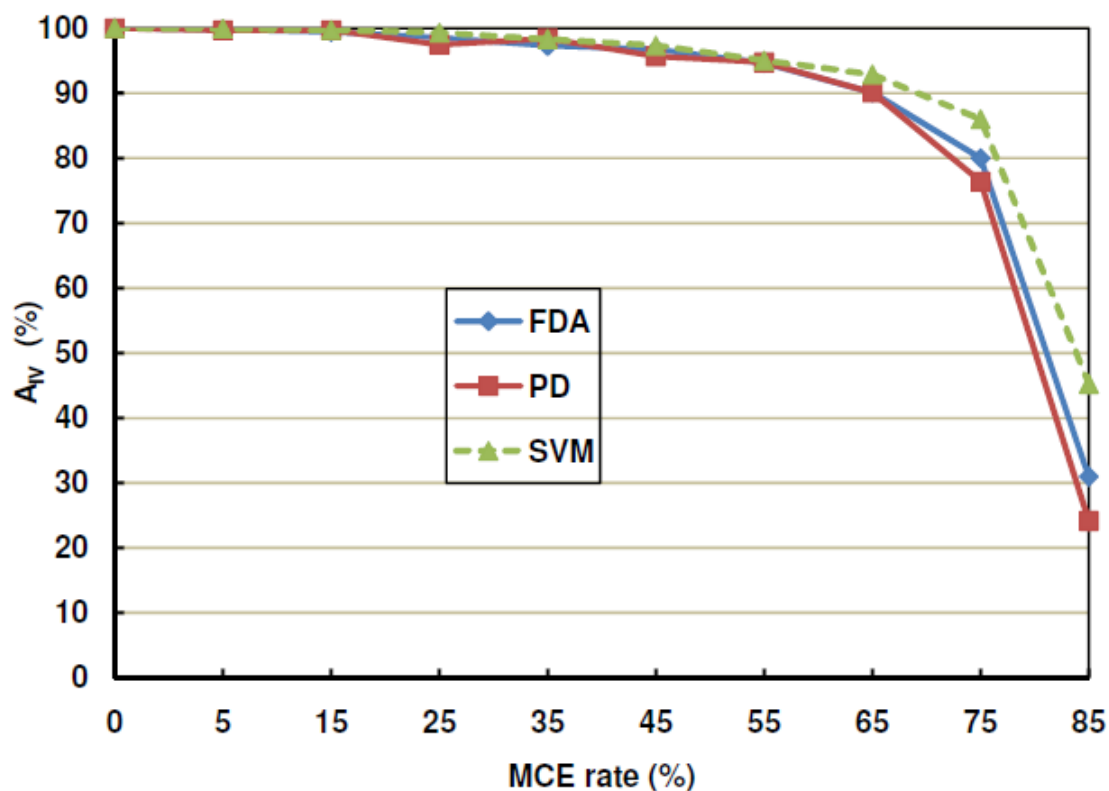
Figure 4.1: Accuracy of the classifiers studied for the FPVC in detecting invalid trains versus the MCE rate in the trains. The MCE rate represents the sparsity of the MUPT. Note: the plot for the Switching classifier is not given because it overlaps with that of the SVM.

A disadvantages of the developed FPVC is that its accuracy in detecting invalid (merged) MUPTs (A_{IV}) decreases as the MCE rate in the trains increases. Comparing the A_{IV} values presented in Tables 4.1 and 4.2 for three ranges of MCE rates supports this claim, such a trend also plotted in Figure 4.1 for the three classifiers evaluated for the FPVC. As shown, the A_{IV} value for the best, the SVM, classifier dropped to $< 60\%$ when the MCE rate was $>80\%$). One reason for this drop in classification accuracy is that the accuracy with which the MU firing pattern statistics (μ and σ) can be estimated and ultimately the estimation accuracy of the MU firing pattern features used decreases as a train becomes sparse. The EFE algorithm [140] that was used to estimate these two statistics works well, but for trains with high MCE or high CV it underestimates σ and overestimates μ. Therefore, for merged trains with high MCE rate the estimated value for CV is low and close to that of a single train while it is expected to be higher than that

58
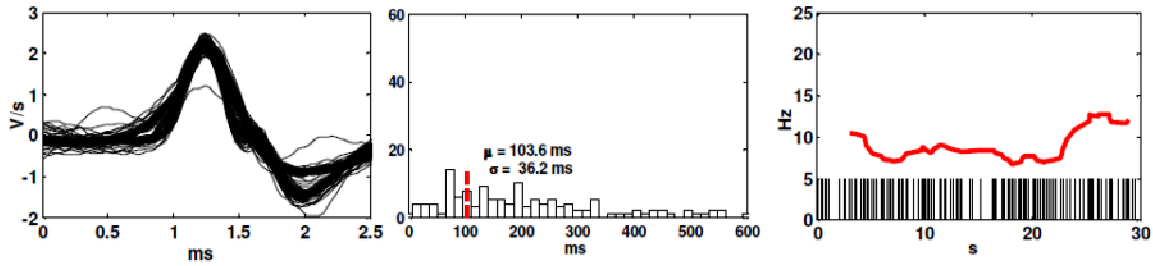
Figure 4.2: An example of an invalid MUPT that was misclassified by the classifiers studied for the FPVC. The first column shows the shimmer plot of the assigned MUPs, the second shows the IDI histogram and corresponding statistics. Finally, the last columns show the discharge patterns and instantaneous MU firing rates.

of a single train. The other reason for the drop in A_{IV} is that the percentage of inconsistent IDIs and FR−MCD values for incomplete invalid trains is not as high as for full invalid trains. An example of such merged MUPT that was misclassified by the three classifiers studied for the FPVC is shown in Figure 4.2. The inconsistency of the MUP-shapes in this MUPT confirms that the train is invalid, even though it misclassified by the FPVC due to their high MCE rate. Therefore, both MU firing pattern information and MUP shape information must be used in assessing the validity of a MUPT (see Chapter 6).

To investigate the possibility of reducing the dimension of the feature space, three different feature selection methods were used to rank features and to select a subset of features that maximizes the accuracy of the FDA classifier. Specifically, the Fisher discriminate analysis technique, in which features are ranked based on their separation ability between two classes, the sequential forward selection technique, and the sequential floating forward selection technique [171] were used. The FDA classifier was chosen for the feature selection consideration because it is one of the best performing classifiers and can be quickly trained and tested. The feature selection study, unfortunately, demonstrated that there is no unique subset of features that works well over the entire range of MCE rates. Furthermore, the effectiveness of the various features varies based on the level of MCE rate in a train. Nonetheless, in general, $LIDI_R$ and CV_L were the most effective features for most cases (across various rates of MCE), while r_1 was the least discriminate feature. If detecting invalid trains during the final iterations of EMG signal decomposition (when MCE rates in the extracted MUPTs are usually below 70%) is the objective, only the six features; CV_L, FR−MCD, IDI−MCD, CV_L/CV_U, Skewness, and PI are sufficient for the FPVC. The aim of this work was to develop classifiers that are effective in classifying MUPTs during and

59

after EMG signal decomposition. The classifiers should therefore be able to properly classify trains even when they have high MCE rates. As such, all of the features discussed in Section 4.2 were employed.

4.7 Conclusions

Supervised classification for automatic validation of a MUPT has been shown to correctly identify cases of single and merged trains. The classifier presented in this chapter, the FPVC, uses characteristics of MU firing patterns extracted from a given MUPT to determine whether a MUPT represents the firings of a single MU or the merged activity of more than one MU. Training based only on simulated firing times shows robust classification performance when tested on both simulated and real test data. Classifier construction has been shown to be best achieved through a hybrid "switching" classifier that first identifies the type of data and then classifies it using either the SVM algorithm or FDA, depending on data identification. This Switching classifier was notably better than the FDA classifier and faster than the SVM while as accurate as the SVM. The best-performing algorithm was significantly better than other algorithms studied. Considering classification speed and accuracy, the Switching classifier is the best as a FPVC.

The accuracy of the developed FPVC in categorizing merged trains was very high (> 90%) for most cases, but it decreases as the MCE rate in trains increases which suggests the need, in some cases, for the combined use of MU firing pattern and MUP shape information. Nevertheless, the results suggest that using these classifiers will be useful as a means to improve EMG signal decomposition results, and to facilitate automatic validation of a MUPT.

Chapter 5

Validating MUPTs using MUP Shape Information

5.1 Introduction

This chapter focuses on the possibility of using only MUP shape information to estimate the validity of a MUPT. Assuming the MUPs generated by a single MU are homogeneous in shape, the MUPT under study can be assumed to have MUP-shape validity when its MUPs have consistent shapes. As an example, the two MUPTs shown in the first two rows of Figure 3.1 have MUP–shape validity while the MUPT shown in the third of this figure does have MUP–shape validity. The objective of this chapter is to develop a robust, fast, and automated method that assesses the shape of the MUPs of a given MUPT to determine whether or not it accurately represent the activity of a MU or not.

Overall, the process of EMG signal decomposition can be considered a clustering problem because neither the number of MUPTs (i.e., clusters) nor the labels of the MUPs are known in advance. During EMG signal decomposition, detected MUPs are clustered into groups called MUPTs. Therefore, the MUP shape validity of a MUPT extracted by a decomposition algorithm can be considered a cluster validity problem and the decision to be made is whether the extracted MUPT represents one cluster in terms of the shapes of the assigned MUPs or not.

In this chapter, eight methods to assess the validity of an extracted MUPT using the shapes of its assigned MUPs were studied. The methods are based on existing cluster analysis algorithms, four are newly developed adaptive methods and four are existing cluster validation methods. These methods evaluate the shapes of the MUPs of a given MUPT to determine whether this train is valid (i.e., it represents the activity of a single MU) or not. The composition of these methods, their objectives and

61

how they were evaluated using both simulated and real data are presented in detail. The remainder of this chapter includes a summary of a group of methods proposed for determining the number of clusters in a data set, a discussion of MUPT validation using MUP shape information and a description of the methods developed for this purpose followed by Evaluation, Results and Discussion, and Conclusions sections.

5.2 Estimating the Number of Clusters in a Data set

Many methods have been developed to estimate the number of clusters ($\widehat{K}$) in a data set. Milligan and Cooper [172] and Gordon [173] provide a comprehensive survey of these methods. In general, a given data set first is clustered into K groups and the quality of clustering is measured using a criterion for a range of values of K. The best value for $\widehat{K}$ is then estimated by identifying the value of K for which the criterion used is optimal. The criteria, in general, are defined based on the within-cluster dispersion (W_K) and between-cluster variability (B_K) that are defined as [173]:

$$W_K = \sum_{i=1}^{K} \sum_{X \in c_i} (X - m_i)(X - m_i)^T \tag{5.1}$$

$$B_K = \sum_{i=1}^{K} N_i (m_i - m)(m_i - m)^T \tag{5.2}$$

where X is a vector of features representing each object of the given data set, m_i is the sample mean of the N_i objects assigned to cluster C_i, and m is the sample mean of the full data set.

Most of these methods cannot be used for testing one cluster versus multiple clusters in a data set and hence cannot be used for assessing the validity of an extracted MUPT. Of the developed methods, only the gap statistic [174], prediction strength [175], jump [176], Duda and Hart [105], and Beal [173] methods can be applied to single-cluster problems. Therefore, these methods can be used for deciding whether an extracted MUPT has MUP- shape validity or not. These methods and their advantages and disadvantages are summarized below.

The *gap statistic* [174] method estimates the number of clusters by comparing the difference (or gap) between W_K and its expected value ($W_K^{\#}$) estimated using an appropriate null reference distribution of the given data set. The optimal estimated number of groups is the minimum value of K which maximizes the gap between W_K and $W_K^{\#}$. Tibshirani et al. [174] proposed two methods to generate a reference data set for the gap statistic method. In the first method, the reference data set is sampled uniformly from the range of the observed values for each feature. In the second method, the reference data set is also sampled uniformly, but here over a box aligned with the principal components of the data. The gap statistic

method based on the first method is known as the gap/uni method and that based on the second method is known as the gap/pc method. The former is simpler than the latter but may not be as accurate because the latter considers the shape of the cluster in generating the reference data set and hence has a better estimation of $W_K^{\#}$.

The *prediction strength* [175] method considers clustering as a supervised classification problem. Generally in a classification task to choose the best classifier for a given data set, different techniques are studied and then the one that has the minimum classification error for the given data set is chosen. Here, the clustering algorithm is run for different values of K and prediction strength (accuracy) is estimated for each K. The optimal estimated number of clusters is the largest K on which the prediction strength is maximum. To estimate the prediction strength, the data set is divided into a training and testing set and each set is clustered by a clustering algorithm. The testing set is also classified by the cluster centers given from the training set. The prediction strength is a measure of how well the cluster cores in the training set predict the memberships in the testing set.

The *jump* method [176] applies an appropriate transformation to the curve of W_K and then determines the largest jump in the transformed curve. The value of K associated with this jump is considered as the best estimate for the number of groups in the given data set. Sugar and James [176] proposed the following transformation for W_K in the jump method

$$W_K^* = W_K^{-Y} \tag{5.3}$$

where Y is the transformation power. A typical value for Y is $d/2$ where d is the dimension of the feature space. Having this transformation, the jump index is given by

$$J_K = W_K^* - W_{K-1}^* = W_K^{-Y} - W_{K-1}^{-Y}, \ \ K=1,2,3,\ldots, K^*. \tag{5.4}$$

where $W_0^* = 0$ and K* is the maximum possible number of clusters in the given data set. The optimum number of clusters is the value of K for which J_K is maximized.

The typical value proposed for Y in Equation (3) does not work in general. In fact, the theoretical results provided by Sugar and James [176] show that $d/2$ is the best value for Y only when the feature values have a multivariate independent Gaussian distribution. For feature values where this assumption is not valid, they suggest trying several values of Y; however, it has been found that even a small variation in Y can lead to very different results [176].

The *Duda and Hart* (DH) method [105] tests the existence of clusters in a given data set by comparing its within cluster dispersion, W_1, to the resulting within cluster dispersion when the data set is partitioned into two clusters using a clustering algorithm, W_2, (These two parameters are obtained using Equation 5.1). Assuming the feature values have a multivariate Gaussian distribution, the null hypothesis of a single cluster is rejected in favor of multiple clusters at an α level of significance, if

$$J = \frac{-\frac{W_2}{W_1} + 1 - \frac{2}{\pi d}}{\left[\frac{2\left(1 - \frac{8}{(\pi^2 d)}\right)}{(Nd)}\right]^{0.5}} > z. \tag{5.5}$$

where N is the number of members in the full data set, and d is the dimension of the feature space, and z is defined by

$$\alpha = 100 \int_z^\infty \frac{1}{\sqrt{2\pi}} exp\left(-\frac{u^2}{2}\right) du = 50 \left(1 - erf\left(\frac{z}{\sqrt{2}}\right)\right). \tag{5.6}$$

The *Beal* method [173] also assumes a multivariate Gaussian distribution for the feature values and rejects the null hypothesis of one cluster if

$$BI = \frac{\left(\frac{W_2 - W_1}{W_2}\right)}{\left(\left(\frac{N-1}{N-2}\right)2^{2/d} - 1\right)} > F_{\text{critical}}. \tag{5.7}$$

where the value for F_{critical} is obtained from an $F_{d,(N-2)d}$ distribution at an α level of significance. The parameters N and d are as defined in Equation 5.5, and the parameter W_K is obtained using Equation 5.1.

5.3 Validating a MUPT Using MUP Shape Information

Here the goal is to assess if the MUPs of a MUPT extracted by a decomposition algorithm are homogeneous in terms of their shapes or not. If they are homogeneous, it is concluded that the extracted MUPT represents the MUPs of a single MU and the train is classified as valid; otherwise, the MUPT is classified as an invalid train. As discussed in the Section 5.1 above, this is a cluster validation problem and we need to determine whether a given MUPT represents one cluster in terms of the shapes of its assigned MUPs or not. MUPTs representing one cluster are considered to have MUP shape validity. The five methods discussed in the previous section were preliminarily evaluated for this purpose.

For each given MUPT, each of its MUP is represented using the 80 LPD filtered data samples centered about its peak value (i.e., d=80) and then the MUP shape validity of the given train was determined using one of the methods discussed in Section 5.2. To split the given train into two clusters, the K-means algorithm was used.

The LPD filtered samples were used instead of unfiltered samples because they discriminate between the MUPs generated by different motor units better than the raw samples (see Figure 2.5). The 1st-order LPD filter [49], [50] used is, in fact, a two-point central difference algorithm [177] that acts as a differentiator for the lower frequencies and as a low-pass filter for higher frequencies. Given that $x[n]$, n=1,2, ..,80 is the discrete time samples of a MUP, the LPD filtered of these time samples, $y[n]$, are calculated as

$$y[n] = \frac{x[n + L] - x[n - L]}{2 \times L \times T_s} \tag{5.8}$$

where L is the skip factor and T_S is the sampling interval. It is worth pointing out that a 2nd-order LPD filter was also evaluated for filtering the MUPs, but due to the low SNR of many of the filtered MUPs the accuracy obtained for classifying valid MUPTs was drastically decreased compared to the accuracy obtained when the MUPs are filtered using a 1st-order LPD filter. Therefore, a 1st-order LPD filter is preferred to a 2nd-order one.

Preliminary tests showed that when representing MUPs using first-order discrete derivative data points, the Beal [173] and the DH methods [105] (each with α =0.05) do not work well in classifying valid trains correctly. Their accuracy for classifying a valid train correctly was only 5% while that for an invalid train was 99%. In contrast, when using first-order discrete derivative data points as features, the gap statistic [174] and jump methods [176] work much better. However, these two methods are too computationally complex (i.e., slow) to be used during decomposition especially for algorithms to be employed in a clinical environment.

The Beal and DH methods are not accurate in classifying valid MUPTs correctly when using first-order discrete derivative data points as features mainly because these features are highly correlated and hence do not have a multivariate independent Gaussian distribution. In addition, it was discovered that both methods make classification errors depending on the variability of the shapes of the MUPs within a MUPT. For valid MUPTs with highly variable MUPs, both methods tend to conclude that the train under question is invalid (i.e., a false negative error). Therefore, to improve the accuracy of the Beal [173] and

DH methods [105] in classifying valid MUPTs, the two issues that these methods are sensitive to (i.e., feature correlation and within train inherent MUP shape variability) must be resolved.

In this work, in order to overcome these two issues and create fast and accurate methods for validating an extracted MUPT, new adaptive methods based on the Beal and DH methods were developed. One set of methods uses PCA, and the second uses gaps that exist in the shimmer plots of the MUPs assigned to the considered MUPT to select independent MUP features. Both sets of methods use an adaptive level of significance determined by the similarity of the MUPs within an extracted MUPT. Details of these methods are given below.

5.3.1 Adaptive PCA-Based MUPT Validation

These methods include three steps: 1) selecting the most effective features and estimating the effective dimension of the given data, 2) setting the parameter α adaptively, and 3) validating the MUPT. In the feature selection step, the MUPs are transformed to a new coordinate system using PCA. The first coordinate of this system is the principal component that accounts for the largest portion of the variance of the given data; the second coordinate is the principal component that accounts for the second largest portion of the variance of the given data and so on. By applying this transformation, the projected data is uncorrelated.

The most effective features in the given data are the first q $(q < 80)$ principal components that account for a specific portion, say $\gamma\%$, of the variance in the data. The value of d is the dimension of the feature space used to represent the MUPs of a given MUPT. The best value for the parameter γ was found empirically using simulated MUPTs (see Section 5.4 for more details).

The value of α (i.e., the level of statistical significance) is set adaptively by first splitting a considered MUPT into two sub-trains using the K-means algorithm. The pseudo-correlation (PsC) between the MUP templates of the two sub-trains is then calculated as a measure of their similarity. Assuming s_1 and s_2 are 80–dimensional vectors representing the templates of the resulting two sub-trains, the PsC value between these two templates is defined as [70]:

$$PsC(s_1, s_2) = max\left\{\frac{\sum_{i=1}^{80}\left(s_{1,i} \times s_{2,t+i} - |s_{1,i} - s_{2,t+i}| \, max\{|s_{1,i}|, |s_{2,t+i}|\}\right)}{\sum_{i=1}^{80} max\{|s_{2,i}|, |s_{2,t+i}|\}^2}\right\} \tag{5.9}$$

To mitigate the effects of sampling interval noise, when calculating PsC, t ranges from -5 to +5 (corresponding to 0.32 ms) and the maximum value is selected. PsC has a value of "1" for two perfectly

matched templates and values trending towards "0" and negative values as the templates become more dissimilar.

Having a PsC value, the parameter α is defined using the following empirically determined equation:

$$\alpha = \begin{cases} 0.03 & PsC \geq 0.75 \\ 0.05 & 0.4 \leq PsC < 0.75 \\ 0.1 & 0.3 \leq PsC < 0.4 \\ 0.2 & PsC < 0.3 \end{cases} \tag{5.10}$$

The adaptive setting of α makes the algorithm less likely to reject the null hypothesis that the given MUPT is valid when its MUPs are very similar to each other, and more likely to reject this null hypothesis when the MUPs of an extracted MUPT are less similar to each other.

Once the most effective features of the MUPs of the given train are determined, the MUPs are transformed into this new space and grouped into two sub-trains (clusters). Using these sub-trains, the parameter α is set and the given train is then validated (classified) using either the DH, or Beal criterion. The adaptive PCA-based MUPT validation method developed using the DH criterion is called the APDH method and that developed using the Beal criterion is called the APB method.

In short, the computational steps for these two adaptive PCA-based MUPT validation methods are as follows:

Step 1. Use PCA to transform the MUPs of a given MUPT into an uncorrelated space, estimate the effective dimension of MUPs and find the most effective MUP features.

Split the train into two sub-trains using a K-means algorithm; calculate W_1 and W_2 using Equation 5.1.

Step 2. Estimate the template of each sub-train in the original time sample feature space using the MUP labels obtained in Step 1.

Step 3. Calculate the PsC between these two templates using Equation 5.9 and then determine α using Equation 5.10.

Step 4. Assess the validity of the given MUPT using either the Duda and Hart or Beal criterion.

4.1 Using the Duda and Hart criterion [105]: if inequality 5.5 is satisfied, classify the train as invalid otherwise label it as valid.

4.2 Using the Beal criterion [173]: if inequality 5.7 is satisfied, classify the given train as valid otherwise label it as invalid.

5.3.2 Adaptive Gap-Based MUPT Validation

Similar to the PCA-based methods discussed in the previous sub-section, these methods include three steps: feature selection, parameter setting, and MUPT validation. The last two steps are as in the PCA-based methods, the parameter α is set adaptively based on the similarity of the templates of the resulting sub-trains and either the DH [105] or the Beal criterion [173] is used for MUPT validation. However, here a gap-based feature selection method is used to select effective features out of the d (80) first-order discrete derivative data points used to represent the MUPs of a MUPT. The goal is to select samples of the MUPs of a MUPT that are uncorrelated and also effective for discriminating between the MUPs created by two different MUs. This method is based on the way a human would assess the validity of a MUPT using its MUP shimmer plot. A human usually visually checks the homogeneity of the MUPs assigned to a MUPT by inspecting the existence of any gap or obvious differences between specific MUP time sample values.

The developed gap-based feature selection algorithm consists of two parts. In the first part, the algorithm estimates the gap values, gv_i, $i=1, 2, .., 80$, between the N MUPs assigned to a MUPT. In the second part, the samples with significant gap values are selected to represent these MUPs.

To estimate the gv_i values, the considered train is split into two sub-trains using a K-means algorithm and then their templates are calculated. Having these two templates, the raw gap value, rgv_i, is calculated as

$$rgv_i = |s_{1,i} - s_{2,i}|$$

(5.11)

where the 80-dimensional vectors s_1 and s_2 are defined as in Equation 5.9 above.

The estimated raw gap values are weighted such that more attention is focused on the features for which the MUPs of the entire MUPT are different and less attention on those samples for which the MUPs do not differ from each other. For each i, the value of the weight Wg_i is defined based on the variance of the sample values (σ_i^2) and the base line noise (ε^2) as follows.

$$Wg_i = \begin{cases} \max[\max{(rgv)}, \max(ds_{i,j})], & \sigma_i^2 >* \varepsilon^2 \\ \max(ds_{i,j}), & otherwise \end{cases}$$

(5.12)

where $ds_{i,j}$, $j=1, 2,.., N$-1 are the consecutive absolute differences between the sorted N sample values of the ith feature and $\sigma_i^2 >* \varepsilon^2$ represents a χ^2 statistics-based hypothesis test with N-1 degrees of freedom

68

at a 5% significant level. The two parameters σ_i^2 and $ds_{i,j}$ are computed using all of the MUPs of the considered MUPT.

The idea behind this weighting is that if all the MUPs assigned to the MUPT under question are created by a single MU, then the variance of the ith samples of these MUPs should be close to the baseline noise while for those created by different MUs this variance will be greater than the baseline noise.

Having the Wg_i's, gv_i is calculated as:

$$gv_i = \sqrt{Wg_i \times rgv_i} \ , i = 1,2, \ldots ,80. \tag{5.13}$$

Figure 5.1(b) shows an example of the estimated gap values for an invalid MUPT that the shimmer plot of its MUPs is plotted in Figure 5.1(a). Each MUP is represented using its 80 first-order discrete derivative data points. The plot of the gv_i values versus i is called a gap curve. As shown on Figure 5.1(b), the gaps occur at the samples for which the MUPs differ from each other the most.

Given a gap curve, the sample with maximum gap value in each active part is chosen as an effective feature. An active part is a segment of the gap curve with consecutive samples having gap values greater than the baseline noise. For example, the gap curve shown in Figure 5.1(b) includes four active parts. The first active part consists of samples 7 to 27, the second consists of samples 29 to 41, the third consists of samples 43 to 69, and the fourth consists of samples 71 to 74. In fact, each active part represents a range of time sample indices in which the time sample values of the MUPs of the MUPT differ. In order to decrease the effect of noise, short active parts with length of less than 5 samples (i.e., 0.16 ms) are ignored. In this example time samples 21, 36, and 54 are chosen as the best features. The fourth active part was ignored.

Finally, if the number of selected features (time samples) is less than six and the Beal criterion is to be used, additional samples from the gap curve are selected. Additional features, if required, are selected based on their gap value and also their intervals from the previous selected features. Each feature should have the maximum gap value among the remaining samples and also be at least eight samples (i.e. 0.26 ms) before or after any selected features. In the example given in Figure 1, time samples 13, 46, and 62 are additional features. All six selected time samples for this example are shown by bold stars in Figure 1(b). If the DH criterion is to be used, only the two features with the largest gap values are sufficient. If the required number of features cannot be found, the selected features are used and the algorithm continues with these features. These numbers of required features were found empirically to perform the

69

(a)

i^{th} **Sample**

(b)
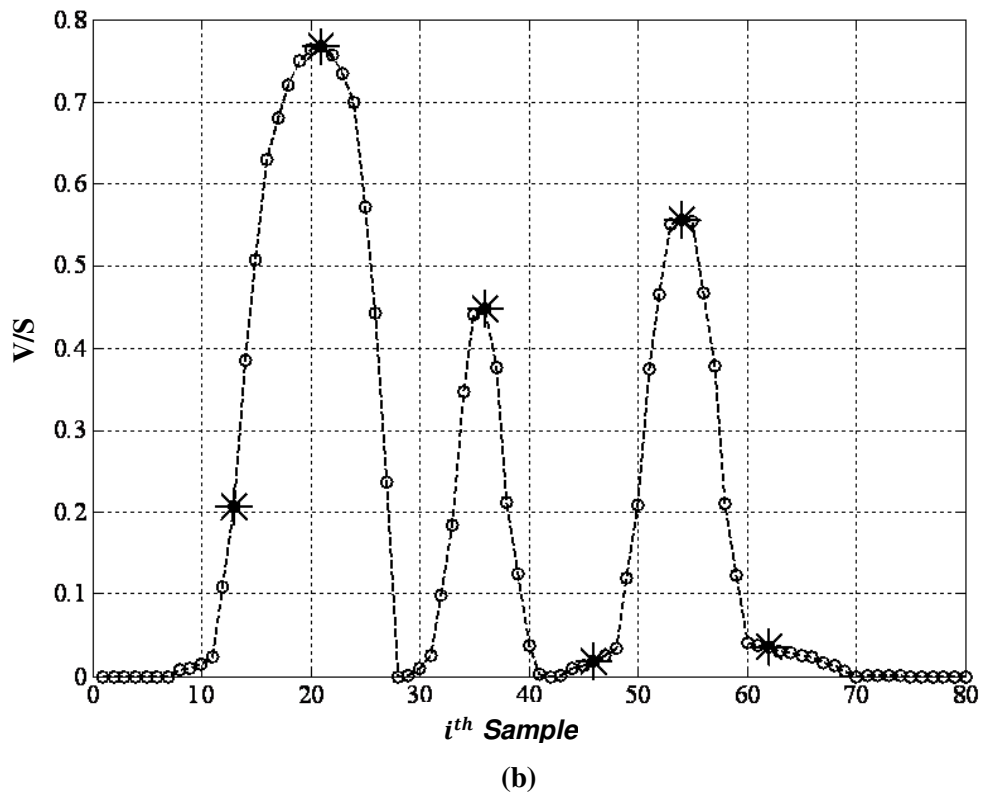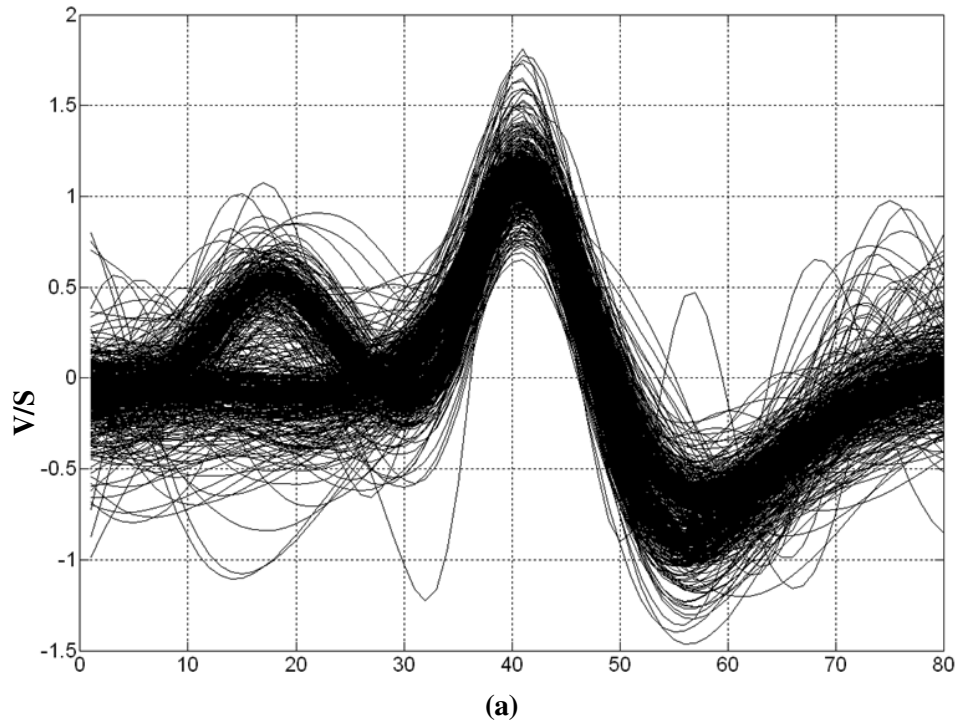
Figure 5.1: A shimmer plot of a motor unit potential train (a) and its resulting gap curve (b). The stars show the samples selected as effective features. Time samples 21, 36, and 54 are chosen based on the active parts of the gap curve. Time samples 13, 46, and 62 are additional selected samples.

70

best using exemplary simulated data (see Section 5.4 for a description of the data used). If no features can be selected, the given train is labeled valid.

Having selected the most effective features of the given train, the remaining steps for validating a given train are analogous to those presented for the PCA-based method discussed in the previous sub-section. Hence, the computation steps for the adaptive gap-based MUPT validation methods are similar to those presented for the PCA-based methods. The adaptive gap-based MUPT validation method using the Duda and Hart criterion [105] is called the AGDH method; and that using the Beal criterion [173] is called the AGB method.

5.4 Evaluation

The accuracies with which the four newly developed adaptive methods could categorize a given MUPT were estimated using both simulated and real data and compared to those of four existing methods (two gap statistic and two jump methods). The gap statistic methods were used for comparison because the gap statistic method was shown to work well in estimating the number of clusters for high dimensional data for both single cluster and multi-cluster data [174]. The jump methods [176] were used because the jump method is faster than both the gap statistic and prediction strength methods and its accuracy in finding the number of clusters in a data set is comparable with that of the gap statistic method. These gap statistic and jump methods were applied using 80 time samples as features and using a reduced number of uncorrelated features selected via PCA as for the adaptive PCA-based methods. The gap statistic (GS) and jump (J) methods using features selected using PCA are called the PCA-based gap statistic method (PGS) and PCA-based jump method (PJ), respectively. In total eight methods were evaluated.

For simulated data, EMG signals were generated using EMG signal simulation algorithms that were developed based on a physiologically and morphologically accurate muscle model [153]. These algorithms create simulated needle-detected EMG signals with different complexities, such as different numbers of MUs, different degrees of MUP shape and/or IDI variability (represented by the amount of jitter and CV of IDI, respectively), and different signal intensities (represented by the average number of MUP patterns per second). Using these algorithms, EMG signals can be simulated similar to those detected from normal, myopathic and neurogenic muscles with different degrees of involvement.

Two hundred and sixty one 30s EMG signals with different levels of intensity, ranging from 24 to 193 pps, with MUP jitter values ranging from 50 to 150μs, with IDI variability (i.e., CV) ranging from 0.10 to 0.45, and with various myopathic or neurogenic degrees of involvement ranging from 0 to 50% were

71

created. These data allowed us to study the performance of the developed methods related to signal intensity, number of trains and MUP shape variability.

The generated signals were decomposed using the DQEMG algorithms [7]. The resulting MUPTs were assessed visually and classified as valid or invalid. Additional valid trains were generated by selecting valid MUPTs with greater than 100 MUPs and randomly splitting them into sub-trains of at least 50 MUPs. For example, eight valid trains were created from a valid train having 210 MUPs. These eight trains include the original train, four trains with 50 MUPs, two trains with 100 MUPs, and one train with 150 MUPs. Additional invalid trains that are representative of invalid trains likely to be produced by a decomposition algorithm were generated by merging valid trains having similar MUP templates. MUP template similarity was measured by estimating the PsC between the MUP templates of the two selected MUPTs. Two trains were merged if the PsC between their MUP templates was ≥ 0.5. In total 20,386 MUPTs (18,000 valid and 2386 invalid trains) were generated. This data set was then divided into ten subsets each of which contained 1800 valid and 239 invalid trains.

For real data, three sets of EMG signals were used: single-channel EMG signals provided by M. Nikolic of Rigshospitalet, Copenhagen, Denmark [170]; single-channel EMG signals provided by K.C. McGill, VA RR&D Ctr, Palo Alto, US [178]; and multi-channel EMG signals provided by J.R. Florestal, P.A. Mathieu, and K.C. McGill [97]. The first set of signals were detected from normal, myopathic and neurogenic muscles using a standard concentric needle electrode during constant low level voluntary contractions. The signals in the second set were recorded by monopolar needle electrode during low level isometric contractions of the brachial biceps muscles of normal subjects. The signals in the third set (multi-channel signals) were recorded simultaneously from the brachioradialis muscles of three normal subjects using six or seven pairs of fine wire electrodes during low-level isometric contractions. In using this data set, the signals detected by each electrode were considered as single-channel EMG signals. These three data sets allowed us to study the performance of the developed methods across signals detected using different electrodes and instruments.

The same analysis as with the simulated data was completed using these signals. However, in analyzing the EMG signals provided by K.C. McGill et al. [97], [178], the results of manual decomposition completed by an expert investigator were used. As with the simulated data, the valid trains in these three data sets were split into sub-trains of at least 50 MUPs and those valid trains having similar MUP templates were merged to generate invalid trains. Consequently, 14,632 MUPTs (13,024 valid and 1608

invalid trains) were generated in total. This real MUPT data set was then divided into ten subsets each of which contained 1303 valid and 161 invalid trains.

Performance of the presented methods was evaluated and compared using the three performance indices: accuracy for valid trains (A_V), accuracy for invalid trains (A_{IV}), and total accuracy (A_T). These three indices are defined as in Chapter 4, Section 4.5.

5.5 Results

The results for the eight methods studied using the simulated and real data are presented and compared in Tables 5.1. The results presented were produced using the parameters listed in the second column of this table for each method studied. These user defined parameters were determined empirically using one of the ten subsets of the simulated data described above. Results for gap/pc method are reported because the gap/pc method performed better than the gap/uni method.

The third column of Table 5.1 shows normalized computation time, which is the processing time for each method normalized by that of the fastest method, the AGDH method, with an average computation time of 70 ms per train. The algorithms are currently encoded in Matlab (The Mathworks, Natick, MA) and processing was carried out on a computer with an Intel Core 2 Duo E8400 CPU (6M Cache, 3.00 GHz clock, 1333 MHz FSB) and 3GB of RAM.

The last six columns of both Table 5.1 show the estimated mean and standard deviation of the three indices A_V, A_{IV}, and A_T for the simulated and real MUPT data sets, respectively. The values reported for these three performance indices were obtained by testing each method using the ten different data subsets described in Section 5.4 above for each of the simulated and real data sets, respectively. In each column of these tables, the methods indicated by an '*' and also bolded had significantly better performance than the others as determined using the analysis of variance (ANOVA), at a 5% significance level and the Tukey-Kramer honestly significant difference test for pair-wise comparison of the mean values. Within groups of methods identified, performance was statistically similar.

The results for simulated data presented in Table 5.1 suggest that the newly developed adaptive methods are better able to detect valid trains than the gap statistic and jump-based methods (see results for A_V). Among the four adaptive algorithms, the two Duda and Hart criterion based methods (APDH and AGDH) with average $A_{IV} \geq 93.5\%$ perform statistically better than the two based on the Beal criterion (APB and AGB). The top three methods for classifying invalid trains (i.e., in terms of A_{IV}) were

Table 5.1: The parameters, normalized computation time, and accuracy of the eight methods studied for validating a MUPT using its MUP shape information applied to both simulated and real data. The normalized time presents the processing time for each method relative to that of the AGDH method with an average computation time of 70 ms per train (measures using simulated data). For each accuracy index, individual or groups of methods indicated by an '*' and bolded had significantly better accuracy than the others based on the analysis of variance (level of significance =5%) and the Tukey-Kramer honestly significant difference test in pair-wise comparison of the mean values. When two or more methods had statistically similar performance, they are all identified.

Method	Parameters	Normalized Time	Simulated data			Real data		
			A_V (%)	A_{IV}(%)	A_T (%)	A_V (%)	A_{IV}(%)	A_T (%)
GS	-	191.3	83.0±0.4	**85.7±0.8***	83.4±0.4	91.4±0.8	**87.4±2.3***	91.0±0.7
PGS	$\gamma = 90$	69.0	92.0±0.6	63.8±0.7	88.8±0.5	93.8±0.4	84.3±2.0*	92.7±0.5
Jump	$Y = 3$	94.5	81.5±0.8	55.3±1.3	78.5±0.6	91.4±2.1	66.3±2.9	88.6±2.1
PJ	$\gamma = 50, Y = 2$	41.0	86.2±0.6	50.4±1.0	82.0±0.5	93.5±2.1	71.7±4.5	90.7±1.7
APB	$\gamma = 93$	2.9	92.8±0.4	64.9±1.1	89.6±0.3	**95.6±0.6***	79.3±2.1	**93.8±0.6***
APDH	$\gamma = 50$	1.9	**93.5±0.5***	72.9±0.9	**91.1±0.4***	**95.8±0.5***	80.7±2.1	**94.1±0.6***
AGB	-	1.2	92.2±0.3	66.5±0.8	89.2±0.3	**95.0±0.6***	74.5±1.7	92.8±0.5
AGDH	-	1.0	**93.8±0.3***	73.9±1.0	**91.5±0.3***	**96.7±0.3***	80.4±1.2	**94.9±0.5***

the gap statistic, APDH, and AGDH methods. The improved ability of the gap statistic method to detect invalid trains was offset by its relatively poor ability ($A_V = 83\%$) for correctly detecting single trains. This in turn, would cause misclassification and consequently duplication of approximately 17% of the MUPTs created during EMG signal decomposition. Consequently, A_T for the gap statistic method were not as high as those for the best performing APDH and AGDH methods. The multivariate statistical analysis showed that all of the measured accuracies (A_V, A_{IV}, and A_T) of the APDH and AGDH methods are statistically similar and these two algorithms were in the group of the top four performing methods in all cases for the simulated data set used in this work.

In general, the results obtained using the real data (see the last three columns of Table 5.1) are similar to those presented for the simulated data. However, all of the eight methods studied performed better on the real data set than on the simulated data set. Both A_V and A_{IV} values estimated for the real data are slightly greater than the values estimated using the simulated data set. As a result, A_T values were improved for the real data. Specifically, for real data the four newly developed adaptive methods had the best accuracies for detecting valid trains, while both gap statistic-based methods were most accurate in detecting invalid trains, followed by the AGDH, APDH, and APB methods. With respect to A_T, three of the four newly adaptive methods (APB, APDH and AGDH) had the best performance. For all three performance indices A_V, A_{IV}, and A_T used, the performance of the three methods APB, APHD, and AGHD were statistically similar. As with the simulated data, for the real data used, the APDH and AGDH methods had statistically comparable performances and were in the group of the top performers with respect to A_V and A_{IV}.

For all of the methods studied and for both simulated and real data, the majority of the valid trains classified as invalid had highly variable MUP shapes caused by very high jitter (around 150 µs) or high numbers of superpositions (from signals with high intensity). Therefore, the accuracy of these methods for determining valid MUPTs should be higher for trains provided by EMG decomposition algorithms, such as MTLEMG [70], [97], EMGLAB [45], or EMGTools [69] that resolve superimposed MUPs. The A_V values estimated for real data are greater than the values estimated using the simulated data because the variably of the MUPs in the real data are lower than those of the simulated EMG signals. In fact, one possible reason for the improved A_V values obtained for the real data may be that a subset of the real MUPT data used was obtained using MTLEMG [70], [97] and EMGLAB [45] and had superimposed MUPs resolved.

In addition, for all of the methods studied and for both simulated and real data, the likelihood of an invalid (merged) train being labeled incorrectly was dependent on the similarity of the MUP templates of the MUPTs used to create the invalid train. Figure 5.2 demonstrates this trend; this figure presents A_{IV} values for the methods evaluated using the larger, simulated data versus the PsC between the templates of the two MUPTs selected for generating a merged train. The PsC value was used as a measure of the average similarity of the MUPs of the two trains selected to create an invalid train. As shown in Figure 5.2, the accuracy of the studied methods in detecting merged trains decreases as the MUP templates of the two trains merged become more similar (PsC increases) such that A_{IV} values decreased to less than 20% when the MUP templates of the MUPTs used to create an invalid MUPT have highly similar shapes (PsC > 0.8). An example of such merged MUPTs is shown in Figure 5.3. This is, in fact, an issue with all methods developed for estimating the number of clusters in a data set. Their accuracy decreases as the constituent clusters become less separable. This issue can be resolved by increasing γ in the PCA based methods, Y in the jump based method, or the number of selected features in the gap-based methods (AGB and AGDH). However, increasing these parameter values decreases the accuracy of the methods studied when classifying valid trains. In general, such MUPTs are hard to assess using only shape information. Motor unit firing pattern information can be useful in assessing such trains and labeling them correctly [19], [159], [179]. Probably, a reason why the A_{IV} values estimated using the real data used were slightly greater than the A_{IV} values estimated using the simulated data used is because the MUP templates of the extracted MUPTs selected to generate the invalid trains were, on average, less similar for the real signals than for the simulated signals.

Based on the results given in Tables 5.1 and Figure 5.2, the AGDH method is the best algorithm among the algorithms studied because this method is the fastest and one of the top four accurate methods in terms of all three performance indices used in this work. With respect to A_V and A_T, the AGDH method is one of the most accurate methods for both the real and simulated data used. The AGDH method was not as accurate as the best method, the gap statistic method, in classifying invalid MUPTs, but the gap statistic method has the lowest A_{IV} and is the slowest method. The performance of the APDH method is statistically similar to that of the AGDH. However, the APDH method is slower than the AGDH method.

5.6 Conclusions

Assuming MUPs generated by a single MU are homogeneous in shape (but with possibly different degrees of variability across different MUs), invalid MUPTs that represent the activity of more than one
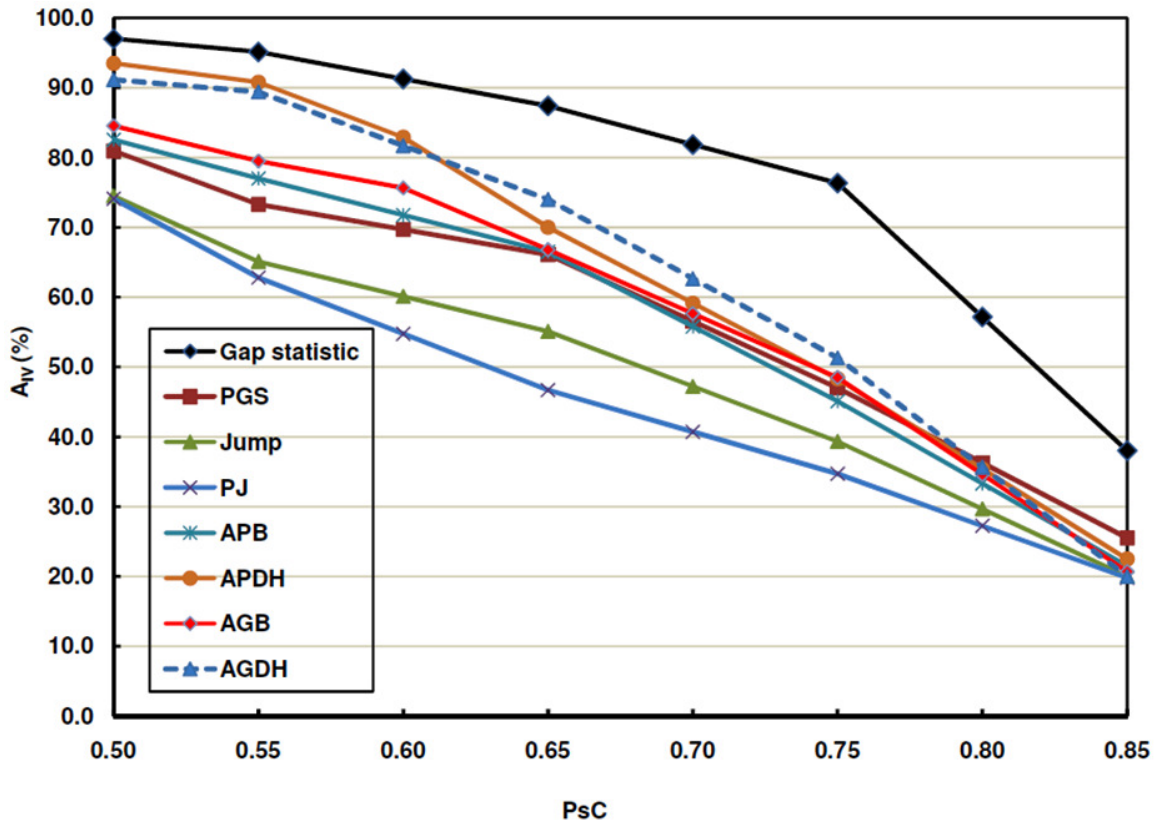
Figure 5.2: Accuracy in detecting invalid trains (A_{IV}) versus the pseudo-correlation (PsC) between the templates of two MUPTs merged to generate an invalid train. The parameter PsC was used to measure the average similarity of the MUPs of two MUPTs constituting an invalid MUPT. High values of PsC show the low separability between the MUPs of two trains. As the two trains constituting an invalid MUPT become less separable, the accuracy of the methods in detecting the invalid trains decreases.
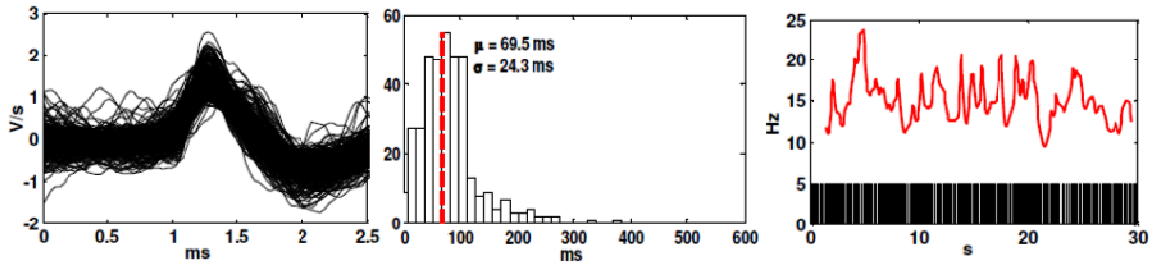
Figure 5.3: An example of invalid MUPT that was misclassified by the presented MUP-shape validation methods. The first column shows the shimmer plot of the assigned MUPs, the second shows the IDI histogram and corresponding statistics for each extracted MUPT. Finally, the last columns show the discharge patterns and instantaneous firing rates for each MUPT. The variability and the short spikes in the firing plots reveal that the train is invalid, although the train was classified as a valid MUPT.

MU can be detected as merged by assessing the homogeneity of its MUPs. Assessing MUP shape homogeneity can be considered as a cluster validation problem and the decision to be made is whether the MUPs of a MUPT represent one or more clusters. Four new adaptive algorithms for automatic MUP shape-based validation of MUPTs extracted by an EMG signal decomposition algorithm have been presented and evaluated in this chapter. These algorithms evaluate the MUP shapes of a given MUPT to see whether they are consistent or not. If the shapes of the MUPs assigned into a train are homogeneous, the train is classified as valid otherwise it is classified as invalid.

Evaluation results using both simulated and real data show that the ability of the algorithms studied to correctly classify a MUPT is encouraging. For all four performance indices used in this work the two new algorithms developed based on the Duda and Hart criterion (APDH and AGDH) were in the group of the top four methods for both simulated and real data. Considering classification speed and accuracy, the AGDH method outperforms the other seven methods studied. For invalid trains composed from MUPTs with similar MUP templates, the accuracy of the developed methods in classifying invalid trains was 73.9% for simulated data and 80.4% for real data. This accuracy, for simulated data, decreased to 20% when an invalid MUPT was composed of MUPTs with highly similar MUP templates, which suggests the need for the use of MU firing pattern as well as MUP shape information in evaluating such extracted MUPTs.

Chapter 6

Validating Motor Unit Potential Train using both MU Firing Pattern and MUP Shape Information

6.1 Introduction

In the previous two chapters several methods to estimate the validity of a MUPT using either its MU firing pattern information or MUP shape information were presented. As discussed, the accuracy of the FPVC, which estimates MU firing pattern validity, in detecting invalid trains decreases as the MCE rate in the MUPTs increases such that this accuracy was reduced to < 60% when the MCE rate was >80% (see Figure 4.1). Likewise, the accuracy of the MUP-shape based validation methods presented in Chapter 5 decreases as the separability between the trains used to create an invalid train decreases such that the methods failed to detect the majority (>80%) of invalid trains composed of MUPTs with highly similar MUP templates (see Figure 5.2). Using both the MU firing pattern and MUP shape information of a MUPT to estimate its validity was explored with the hope of overcoming these two issues; the achievements these efforts are presented in this chapter.

6.2 A System for Estimating MUPT Validity using Cluster Validation and Supervised Classification Techniques

One possible scheme for using both the MU firing pattern and MUP shape information of a MUPT in estimating its validity is combining the validity indices provided by the FPVC and one of the adaptive methods discussed in Chapter 5 using an "AND" logic; the overall procedure is shown in Figure 6.1. With such a MUPT validation system, a given MUPT is classified as valid if it satisfies both temporal and
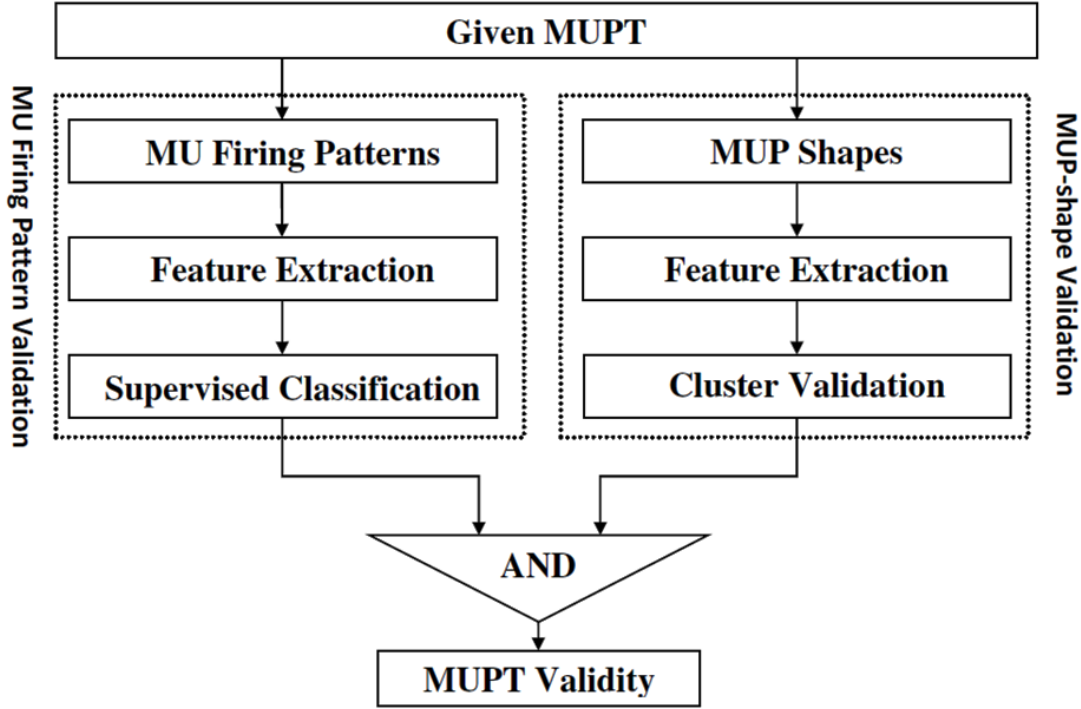
Figure 6.1: The procedure of the developed MUPT validation system that estimates the validity of a MUPT by combining its MU firing pattern validity and MUP shape validity estimated using a supervised classifier and a cluster validation technique.

shape criteria; otherwise, the train is labeled invalid. Using the switching classifier presented in Chapter 4 and the two adaptive gap-based methods presented in Chapter 5, two MUPT validation classifiers were developed and studied. The MUPT validation system that is based on the Beal criterion [173] is called the MVB method and the one developed using the Duda and Hart criterion [105] is called MVDH method.

The experimental results of evaluating the MVDH and MVB using the simulated and real reference data described in Section 5.4 of Chapter 5 showed that these two methods are more accurate than the FPVC, and the AGB and AGDH methods in correctly classifying invalid MUPTs (see Section 6.4). Specifically, using the MVDH and the MVB assists with improving the accuracy in classifying invalid MUPTs even ones having high MCE rates or composed of two valid trains with highly similar MUP templates (PsC > 0.7). However, both the MVB and MVDH misclassified valid MUPTs that had inherent MUP shape variability caused by jitter or jiggle [1], [24], [114], [180]. Ultimately, the A_V values for both the MVB and the MVDH were lower than that obtained for the FPVC.

80

The drop in the A_V values of the MVB and the MVDH compared to the A_V values of the FPVC reveals that the amount of MU firing pattern and MUP shape validity should be taken into account and weighted when classifying a given MUPT. The reminder of this chapter presents a system that first estimates the MU firing pattern and MUP shape validity of a given MUPT and then weights these amounts to estimate the overall validity for the MUPT.

6.3 A SVM-based System for Estimating MUPT Validity

Let C_1 represent the class of valid MUPTs and C_2 represent the class of invalid MUPTs, the objective of the developed SVM-based MUPT validation system is to estimate a posterior probability $P(C_i|\text{MUPT})$, i=1,2 for a given MUPT. For final classification (i.e., to determine the class label of a MUPT), a given train is classified as valid if $P(C_1|\text{MUPT}) > P(C_2|\text{MUPT})$. To determine the $P(C_i|\text{MUPT})$ values, both the MU firing pattern and MUP shapes of the MUPT are represented by several feature values which are then input to a supervised classification algorithm. The developed MUPT validation systems consist of three steps: preprocessing, feature extraction, and supervised classification.

6.3.1 Preprocessing

MUP preprocessing consisted of taking the first derivative of the 80 discrete time samples of a MUP using a two-point central difference algorithm [177]. The mathematical equation for this algorithm, which is also known as a 1st-order LPD filter, is given in Equation 5.8. MUP preprocessing was completed to increase the SNR of the MUPs, sharpen MUPs, and ultimately enhance the discrimination between the MUPs created by two or more different MUs but mistakenly assigned to one MUPT. An example of the effectiveness of using LPD filters in improving the discrimination of the MUPs created by three MUs is given in Figure 2.5. Details and examples of the effectiveness of using LPD filters during EMG signal decomposition are given in [49], [50]. For the same reason mentioned in Section 5.3, a 1st-order LPD filter was preferred to the a 2nd-order LPD filter, even though the latter filter enhances the difference between the MUPs of different MUs better than the first filter.

6.3.2 Feature Extraction

Eighteen features are used to represent a given MUPT for classification. Eleven features are extracted from MU firing patterns and the remaining seven features are extracted from the MUPs assigned to the MUPT.

The MU firing pattern features employed are the ten features discussed in Chapter 4 along with the MCE rate in the given train. The MCE rate was obtained using the following first order linear model; details related to the development of this model are given in [179].

$$MCE\ rate = -108.6 \times ID\ rate + 102.4 \qquad (6.1)$$

The seven features that are extracted from the MUPs assigned to the MUPT (MUP shape features) are defined and extracted based on the idea that the increase in the similarity of the MUP shapes of the sub-trains created when splitting a MUPT is greater for an invalid MUPT than for a valid MUPT. In addition, the similarity between the MUP templates of the two sub-trains created by splitting an invalid train is less than that for valid MUPTs. When calculating the MUP shape features, the N filtered MUPs of the MUPT are grouped into two sub-trains using a K-means clustering algorithm and MUP templates are estimated using the median trimmed mean averaging algorithm described in [143]. This averaging technique was used because it provides a good estimation of the MUP template of a MUPT by reducing the effect of interference from the MUPs of other motor units and noise [143]. A detailed description of the MUP shape features and how they are calculated is given below.

1. $N_{ratio} = \frac{\min{(N_1, N_2)}}{N}$, where N_1 and N_2 are the number of MUPs in the resulting two sub-trains to which the MUPs of the given MUPT are clustered, and $N = N_1 + N_2$.

2. PsC: The pseudo-correlation between the MUP templates of the two sub-trains.

3. PsC$_{norm}$: PsC between the MUP templates when each of these two templates is normalized using a min-max normalization technique [181] which transforms each sample of a template into the 0 to 1 range.

4. *Nac*: the number of active parts as determined in Chapter 5, Section 5.3.2.

5. W_{ratio}: is the ratio of W_1, the sum of squared distances between each MUP of the given train and its MUP template, to W_2, the corresponding sum of squared distances for the resulting two sub-trains. The distances are calculated using MUP and MUP template samples corresponding to the maximum gap value (i.e., gv_i) of each of the *Nac* active segments.

$$W_{ratio} = \frac{W_2}{W_1} \qquad (6.2)$$

6. *J-index*: an index proposed by Duda and Hart [105] to test the null hypothesis of one cluster versus multiple clusters in a data set. The *J-index* is calculated using Equation 5.5, the values obtained for

W_1 and W_2 in feature 5, and by replacing d with *Nac*.

7. *Beal index (Bi)*: an index proposed by Beal [173] to decide if a cluster should be subdivided into two sub-clusters. *Bi* is calculated using Equation 5.6 with the same setting as for calculating the *J-index.*

6.3.3 Classification

Two different classification schemes were evaluated to determine the validity of a given MUPT using both its MU firing pattern and MUP shape information: a single classifier approach, and a multiple classifier approach. For the single classifier scheme, a classifier uses all 18 features discussed in the previous section to estimate the validity of a given train. For the multi classifier procedure, the MU firing pattern validity and MUP shape validity of a given MUPT are determined separately using two distinct classifiers and then the estimated validity indices are combined by a fusion system to estimate the overall validity of the train under study; the overall procedure is shown in Figure 6.2. The classifier developed to estimate MU firing pattern validity is called the firing pattern validity classifier (FPVC). The classifier developed to estimate MUP shape validity is called the shape validity classifier (SVC).

For both the single and multiple classifier approaches, SVM-based classification [166], [167] with a Gaussian radial basis function as the kernel function is employed. The training parameters of the SVM were determined experimentally via cross-validation. The equation for the kernel function and the description of the training parameters are as given for the FPVC in 4.3 of Chapter 4.

The SVM-based classification was used for developing both FPVC and SVC because the SVM performed better than the FDA and PD classification scheme studied for estimating MU firing pattern validity (see Chapter 4). Likewise, the SVM outperformed the FDA, and logistic regression classifiers in estimating MUP-shape validity when evaluated using the simulated data experimental described in Section 5.4 of Chapter 5, details are given in [182].

The only disadvantage of using the SVM for MUPT validation is that this classifier is a binary classifier and does not provide posterior class probabilities for a given pattern. The objective of this work is to not only determine the validity of a train but also to estimate the posterior probabilities of the valid and invalid classes. Therefore, an extended SVM that provides such probabilities for each class is used [183]. The extended SVM first trains a standard SVM and then trains an additional sigmoid function to estimate the posterior probabilities for each class (see [183] for more details). Given x, is the input feature
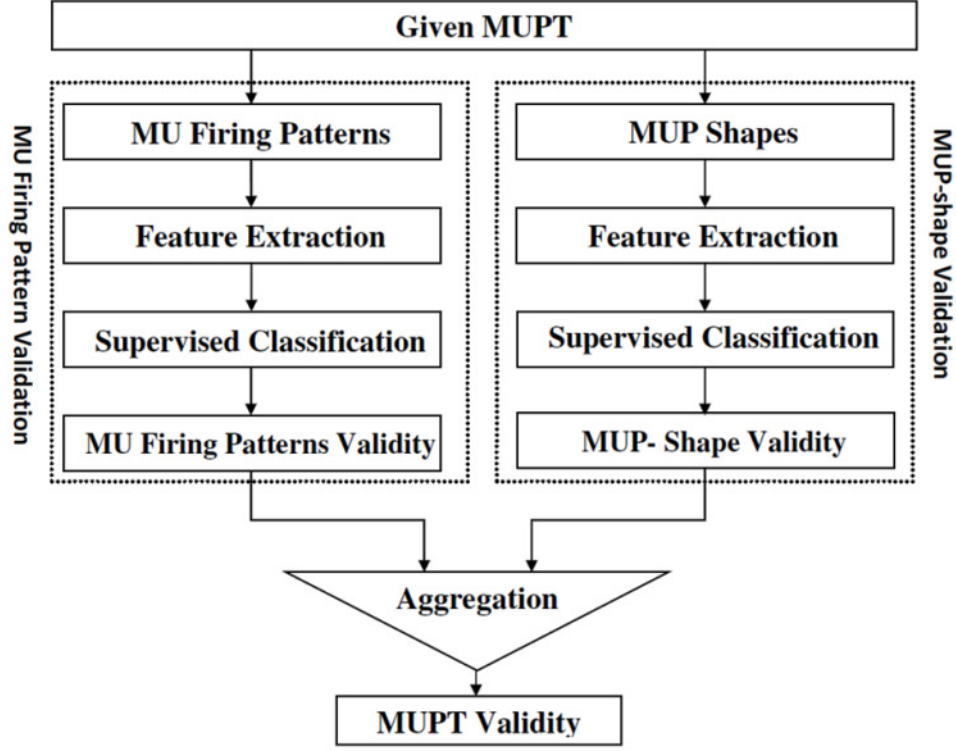
Figure 6.2: Classifier fusion technique for MUPT validation

vector representing a given MUPT in the feature space, *f(x)* is the un-thresholded output of a standard SVM. The probabilities $P(C_1|\text{MUPT})$ and $P(C_2|\text{MUPT})$ are given by:

$$P(C_1|\text{MUPT}) = \frac{1}{1 + \exp(\beta_1 f(x) + \beta_2)};$$

$$P(C_2|\text{MUPT}) = 1 - P(C_1|\text{MUPT})$$

(6.3)

Where, β_i are the parameters of the sigmoid function. In training the sigmoid function, the vector β is derived using a maximum likelihood estimation method such that $P(C_1|\text{MUPT})$ is maximized for each MUPT in the training data [184].

For the single classifier scheme, the values $P(C_i|\text{MUPT})$ provided by the SVM are used as a validity index for the given train and ultimately to classify the train; $P(C_1|\text{MUPT})= 1$ means that the train is most likely valid while $P(C_1|\text{MUPT}) = 0$ means that the train is most likely invalid. In the remainder of this paper, the single classifier developed to estimate the validity of a MUPT is simply called the SVM

validity classifier (SVMVC). For the multi-classifier scheme, however, the validity provided by the FPVC must be combined with the validity provided by the SVC to estimate the overall validity of the MUPT. For both the single classifier and multi-classifier schemes, the train is considered to be valid if the estimated probability $P(C_1|\text{MUPT}) > P(C_2|\text{MUPT})$.

Let $\Omega_{i,j}$ be an estimate of the a posterior probabilities, $P(C_i|\text{MUPT})$, offered by either the FPVC or SVC for a given MUPT. The overall support for class C_i, Ω_i, is estimated by combining $\Omega_{i,1}$ and $\Omega_{i,2}$ using a classifier fusion method $\mathcal{F}$ (i.e., $\Omega_i = \mathcal{F}(\Omega_{i,1}, \Omega_{i,2})$). The fusion method combines the degrees of support for a given class (i.e., valid or invalid), estimated by the base classifiers FPVC and the SVC to find the overall support for each class and ultimately assign the input to the class with the largest support. Both trainable and non-trainable fusion methods [185] were considered.

Average, product, and AND were studied as non-trainable fusion methods. The average and product fusion methods consider respectively the average and product of $\Omega_{i,1}$ and $\Omega_{i,2}$ as an estimation for Ω_i. The given train is labeled valid, if $\Omega_1 > \Omega_2$; otherwise it is labeled invalid. The AND logic, however, classifies a given train as valid if $\Omega_{1,1} > \Omega_{2,1}$ *and* $\Omega_{1,2} > \Omega_{2,2}$, otherwise the train is classified as invalid. In other words, the AND fusing method labels the train as valid when it has both MU firing pattern and MUP shape validity. The multi-classifier developed using the AND fusion method to estimate the validity of a MUPT is called the AND multi-classifier (ANDMC), those classifiers developed using the average and product fusion methods are called the average and product multi-classifiers (AVGMC and PRMC), respectively.

SVM and logistic regression classifiers were studied as trainable fusion methods to aggregate the output values provided by the FPVC and the SVC and ultimately estimate the validity of a given MUPT. The $\Omega_{i,j}$ values along with PsC and MCE rate are used as input features to a classifier that outputs the $P(C_i|\text{MUPT})$ for the given train. The MUPT classifier which uses a SVM classifier for fusion is called the SVM multi-classifier (SVMMC) and the one that employs a logistic regression classifier for fusion is called the logistic regression multi-classifier (LRMC).

Logistic regression is a probabilistic classification model that operates directly over the feature space and estimates a posterior probability for each class. If Z is a feature vector representing a given MUPT, the probabilities $P(C_1|\text{MUPT})$ and $P(C_2|\text{MUPT})$ for this train are estimated using Equation 6.3 by replacing *f(x)* with Z. The dimension of the vector β is equal to that of Z and the elements of β are derived using training data via a maximum likelihood estimation method [184].

6.4 Results

As with any supervised classification problem, training and testing a developed supervised MUPT validation system requires reference data (i.e., MUPTs whose validity or invalidity are known a priori). For this work, the simulated and real reference data described in Section 5.4 of Chapter 5 were used. Considering the reference MUPTs as the gold standard, the performance of the developed MUPT validation systems was evaluated, as the methods presented in Chapters 4 and 5, in terms of correctly classifying valid and invalid trains. Three accuracy indices as defined in, Section 4.5 of Chapter 4 were employed for this purpose: accuracy for valid trains (A_V), accuracy for invalid train (A_V), and total accuracy (A_T).

Classifiers, based on the methods discussed in 6.3.3, were trained using simulated data and tested using both simulated and real MUPTs. The performance of the developed classifiers were compared with that of the MVDH and MVB. The classification performances of the developed MUPT validation techniques for both simulated and real data are summarized in Table 6.1 which presents the estimated means and standard deviations of the three performance indices A_V, A_{IV}, and A_T. For classifiers studied, the numbers presented for simulated data were obtained by running a 10-fold cross-validation on this dataset while the values presented for the real data were obtained by evaluating the classifiers trained using the entire simulated data on the 10 different subsets of the real MUPT data discussed in Section 4.5. For comparison, the accuracies for the AGB and AGDH algorithms that are presented in Table 5.1 are repeated here. For the MVB and MVDH methods, the presented accuracy values were obtained by evaluating these methods using the same approach as with the methods presented in Chapter 5 (see Section 5.4 and 5.5), but the parameter of the AGDH and AGB algorithms (minimum number of required features) were readjusted to achieve the best performance for both MVB and MVDH. These parameters, as with the methods discussed in Chapter 5, were found empirically using one set of the simulated data sets discussed. Statistical analysis of the results was conducted using a multivariate analysis of variance, at a 5% significance level and the Tukey-Kramer honestly significant difference test for pair-wise comparison of the mean values.

6.5 Discussion

The results for the simulated data, which are presented in Table 6.1, demonstrate how well the developed methods/classifiers can correctly predict the class label of valid MUPTs, invalid MUPTs, and ultimately MUPTs obtained from decomposing an EMG signal. Of the methods studied, the estimated A_V values of

Table 6.1: Mean and standard deviations for the accuracy of the different MUPT validation methods applied to both simulated and real data. In each column of the table, individual or groups of methods bolded and indicated by an '*' had significantly better performance than the others as determined using a multivariate analysis of variance, at a 5% significance level and the Tukey-Kramer honestly significant difference test for pair-wise comparison of the mean values. For each performance index, when two or more methods had statistically similar performance, they are all indentified.

Method	Simulated data			Real data		
	A_V (%)	A_{IV} (%)	A_T (%)	A_V (%)	A_{IV} (%)	A_T (%)
AGB	92.2±0.3	66.5±0.8	89.2±0.3	95.0±0.6	74.5±1.7	92.8±0.5
AGDH	93.8±0.3	73.9±1.0	91.5±0.3	96.7±0.3	80.4±1.2	94.9±0.5
SVC	98.6±0.2	74.0±2.7	95.7±0.4	97.1±0.5	60.0±5.9	93.1±0.9
FPVC	**99.8±0.1**[*]	95.9±0.7	99.4±0.1	98.2±0.6	96.2±1.4	98.0±0.5
MVDH	93.7±0.7	**99.1±0.2**[*]	96.4±0.5	95.2±0.7	**99.7±0.2**[*]	94.4±0.3
MVB	98.2±0.2	98.6±0.3	98.4±0.2	98.0±0.6	99.1±0.3	**98.3±0.3**[*]
SVMVC	**99.3±0.2***	**99.3±0.5**[*]	99.3±0.2	97.8±0.4	91.5±2.5	97.1±0.5
ANDMC	98.1±0.2	**99.8±0.2**[*]	98.3±0.2	95.4±0.6	**99.7±0.3**[*]	95.9±0.5
AVGMC	**99.8±0.1**[*]	95.6±1.2	99.3±0.2	**98.9±0.3**[*]	95.8±1.4	**98.6±0.3**[*]
PRMC	**99.8±0.1***	95.7±0.8	99.3±0.2	**98.9±0.2**[*]	95.8±1.4	**98.6±0.1**[*]
LRMC	**99.4±0.2**[*]	**99.5±0.4**[*]	**99.4±0.2**[*]	98.2±0.4	**99.6±0.4**[*]	**98.4±0.3**[*]
SVMMC	**99.7±0.1**[*]	**99.3±0.6**[*]	**99.6±0.1**[*]	97.7±0.2	**99.4±0.6**[*]	97.9±0.2

the FPVC, AVGMC, PRMC, and the SVMMC were statistically similar to each other and were higher than the A_V values of the remaining methods/classifiers. In terms of A_{IV}, all the systems that use MU firing pattern and MUP shape information, except the AVGMC and the PRMC, outperformed the algorithms that use only MU firing pattern or MUP shape information. The MVDH, SVMVC, ANDMC, LRMC, and the SVMMC were the top-five methods/classifiers for correctly classifying invalid MUPTs. With respect to A_T, the LRMC and the SVMMC, which fuse the validities provided by the FPVC and the SVC using trainable fusion methods, were in the group of the top-three systems.

In general, the results obtained using the real data are consistent with those presented for the simulated data. The average and product classifier fusion techniques resulted in no further improvement of

A_{IV} compared to the FPVC results, but the estimated A_V values of these two classifiers were statistically better than the other methods studied. The AGB, AGDH methods and the SVC that use only MUP shape information had the lowest A_{IV}. The MVDH, ANDMC, LRMC, and the SVMMC had the highest A_{IV}. However, the estimated A_{IV} value of the SVMVC, which is based on a single SVM, decreased significantly compared to its performance using simulated data and was significantly lower than the A_{IV} values of the MFPC and the other five multi-classifiers which use both MU firing pattern and MUP shape information.

For both simulated and real data, the accuracies of the AVGMC and the PRMC were almost identical because both methods assess the same criterion in classifying a given MUPT, even though they use two different methods for fusing the probabilities provided by the SVC and the FPVC. In fact, for both the AVGMC and the PRMC a given MUPT is classified as valid if $\Omega_{1,1} + \Omega_{1,2} > 1$.

The estimated A_V of the ANDMC, MVDH, and the MVB, which combine the MU firing pattern validity and MUP shape validity using an AND operation, is slightly lower than the A_V value of the methods that only use MU firing pattern and MUP shape information to estimate the validity of a given train. This result is caused by the number of valid MUPTs that are misclassified by base methods used to estimate MU firing pattern validity (e.g., the FPVC) and MUP shape validity (e.g., the AGDH and the AGB methods or the SVC). This is a weakness of the AND fusion operation, which does not take into account the amount of MU firing pattern and MUP shape validity, when classifying a given MUPT. In fact, the ANDMC, MVDH, and the MVB are rigorous in labeling a MUPT as valid; the MUPT must have both MU firing pattern validity and MUP shape validity to be considered valid. Such conservative classification however, resulted in an improvement in A_{IV}. As shown in Table 6.1, the estimated A_{IV} for the ANDMC (as an example) was around 25% and 3% higher than that of the SVC and the FPVC, respectively. The statistical analysis conducted on the results of Table 6.1 shows that the ANDMC and the MVDH were in the group of top- four systems in terms of A_{IV} for both the simulated and real data.

Figures 6.3 to 6.4 illustrate the advantage of using both MU firing pattern and MUP shape information for MUPT validation (except the AVGMC and the PRMC) compared to using either one set of this information.

Figure 6.3 presents A_{IV} values versus the PsC between the templates of the two MUPTs selected for generating an invalid train for the classifiers studied. The PsC value represents a measure of the average similarity of the MUPs of the two trains selected to create an invalid train. The results for the AVGMC

and the PRMC were not plotted because these two classifiers not only did not provide better A_{IV} values over the base FPVC but also performed worse than the FPVC for PsC > 0.8. As shown, MUPT validation systems that fuse both MU firing pattern and MUP shape information in assessing invalid MUPTs trains composed of two MUPTs with PsC > 0.8 improved the ability to correctly predict their class labels. The A_{IV} values of the methods that use both MU firing pattern and MUP shape information were > 98% for most cases. For the worst case scenario (high PsC), the estimated A_{IV} values of the ANDMC and the LRMC (the two classifiers with the highest A_{IV} values) were around 98%, which is at least 52% higher than that of the SVC and the AGB and AGDH methods. On average, the estimated A_{IV} of the ANDMC and the LRMC was 1.3 times of that of the SVC and the AGDH method and 1.5 times of the A_{IV} of the AGB method.

An example of an invalid MUPT (from simulated data) composed of valid trains with high PsC is given in Figure 6.4. It is clear that assessing the validity of this train using only MUP shape information is difficult such that it was misclassified by the SVC and AGB and AGDH methods, but the MVB, MVDH, ANDMC and the LRMC, which use both MU firing pattern and MUP shape information classified the train correctly.

Figure 6.5, which plots A_{IV} values of the algorithms studied versus the MCE rate in invalid MUPTs, demonstrates another advantage of using both MU firing pattern and MUP shape information in assessing the validity of a MUPT over using just firing pattern or shape information. As shown, A_{IV} for the FPVC decreases as the MCE rate in the trains increases such that the algorithm misclassified around 60% of the invalid trains having a MCE rate > 80%. One reason for this drop in classification accuracy is that the accuracy with which the MU firing pattern statistics can be estimated and hence the accuracy of the MU firing pattern features used decreases as a train becomes sparse (see Chapter 4 or [159] for more details). As demonstrated in Figure 6.5, the MUPT validation systems that use both MU firing pattern and MUP shape information (specifically the MVDH, ANDMC, and the LRMC) performed better than the FPVC in correctly classifying invalid trains having high MCE rate. For the worst-case scenario (MCE rate > 80%), A_{IV} for the MVDH, ANDMC, and the LRMC was 31%, 30%, and 15% higher than the A_{IV} of the FPVC, respectively, which is a significant improvement in detecting invalid trains especially during the early stages of an EMG signal decomposition.
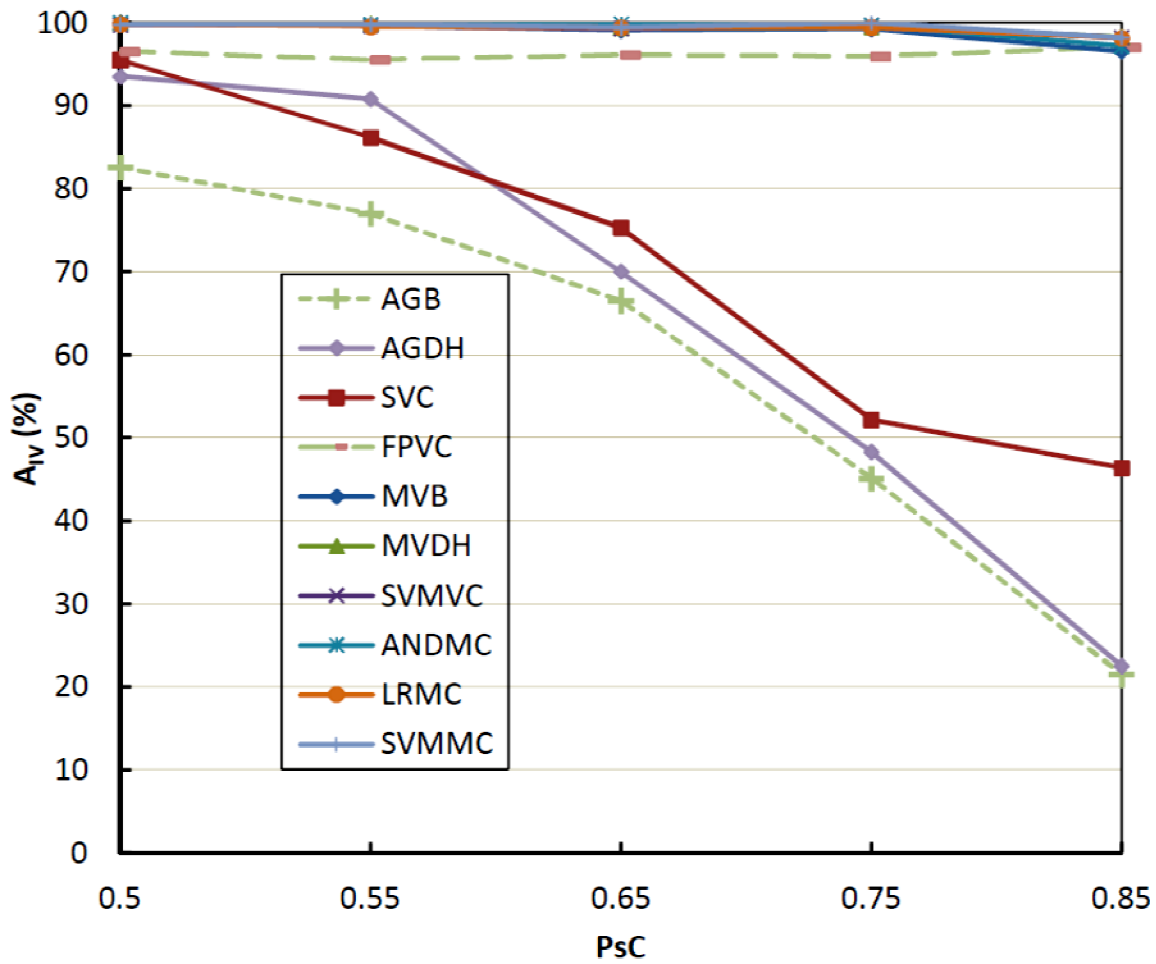
Figure 6.3: Accuracy in detecting invalid trains (A_{IV}) versus the pseudo-correlation (PsC) between the templates of two valid MUPTs merged to generate an invalid train. High values of PsC show the high similarity of the templates and ultimately low separability of the two valid MUPTs comprising an invalid MUPT. As shown, the systems that use both MU firing pattern and MUP shape information (e.g., MVB, MVDH, SVMVC, ANDMC) are more accurate in detecting invalid trains than the systems that employ only one source of this information in estimating the validity a given MUPT (AGB, AGDH, SVC, FPVC). Note: the A_{IV} plots for several methods overlapped.
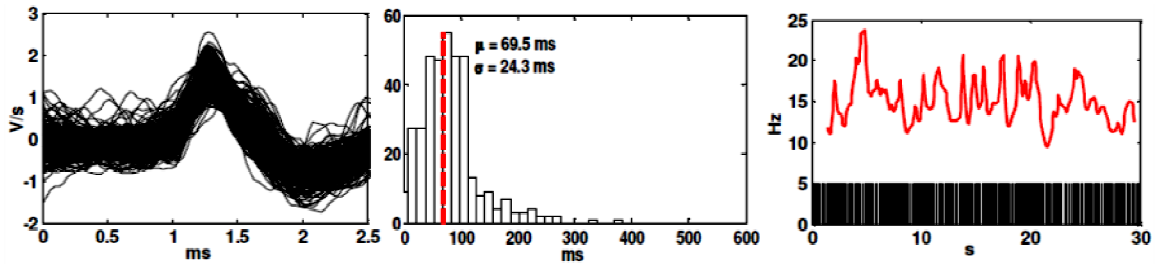
Figure 6.4: An example of an invalid MUPT that is misclassified by the AGDH and AGB methods and also by the SVC, but correctly classified by both the majority of the systems that employ both MU firing pattern and MUP shape information (e.g., MVB, MVDH, ANDMC, LRMC, and SVMMC). The first column shows the shimmer plot of the assigned MUPs, the second shows the IDI histogram and corresponding statistics for the extracted MUPT. Finally, the last columns show the discharge patterns and instantaneous firing rates for the MUPT.

An example of an invalid MUPT that was misclassified by the FPVC due to its high MCE rate is given in Figure 6.6. The inconsistency of the MUP-shapes in each MUPT confirms that the train is invalid. This shape inconsistency was recognized by the SVC and the AGB and AGDH methods. Consequently, the train was correctly classified by the majority of the systems (e.g., the MVDH, ANDMC, and the LRMC) that use both MU firing pattern and MU shape information in assessing the train.

The ANDMC and the LRMC have several advantages over the single SVMVC. In addition to their higher A_{IV} values for real data (see Table 6.1), they performed better in correctly classifying invalid trains with MCE rates > 75% than the SVMVC (Figure 6.5). Providing the reason for invalidity is another advantage of using the multi-classifier techniques over using of the single SVMVC for MUPT validation. Knowing that a MUPT is invalid because of its MU firing pattern or MUP shape validity can assist with efficient correction of invalid trains created during decomposition.

Based on the results given in Table 6.1 and Figure 6.5, the LRMC is the best method among the methods studied because this classifier is one of the four most accurate methods in terms of all three performance indices used. The SVMMC is as accurate as the LRMC, but the LRMC is simpler and faster than the SVMMC. The only drawback with the LRMC is that its A_{IV} was not as high as that of the MVDH and ANDMC for highly sparse invalid MUPTs (see Figure 6.5). In addition, for the FPVC used in the ANDMC a switching classifier presented in Chapter 4 can be used instead of the SVM. Using the switching classifier will improve the computation time of the ANDMC. The ANDMC is 2.4 times faster

91
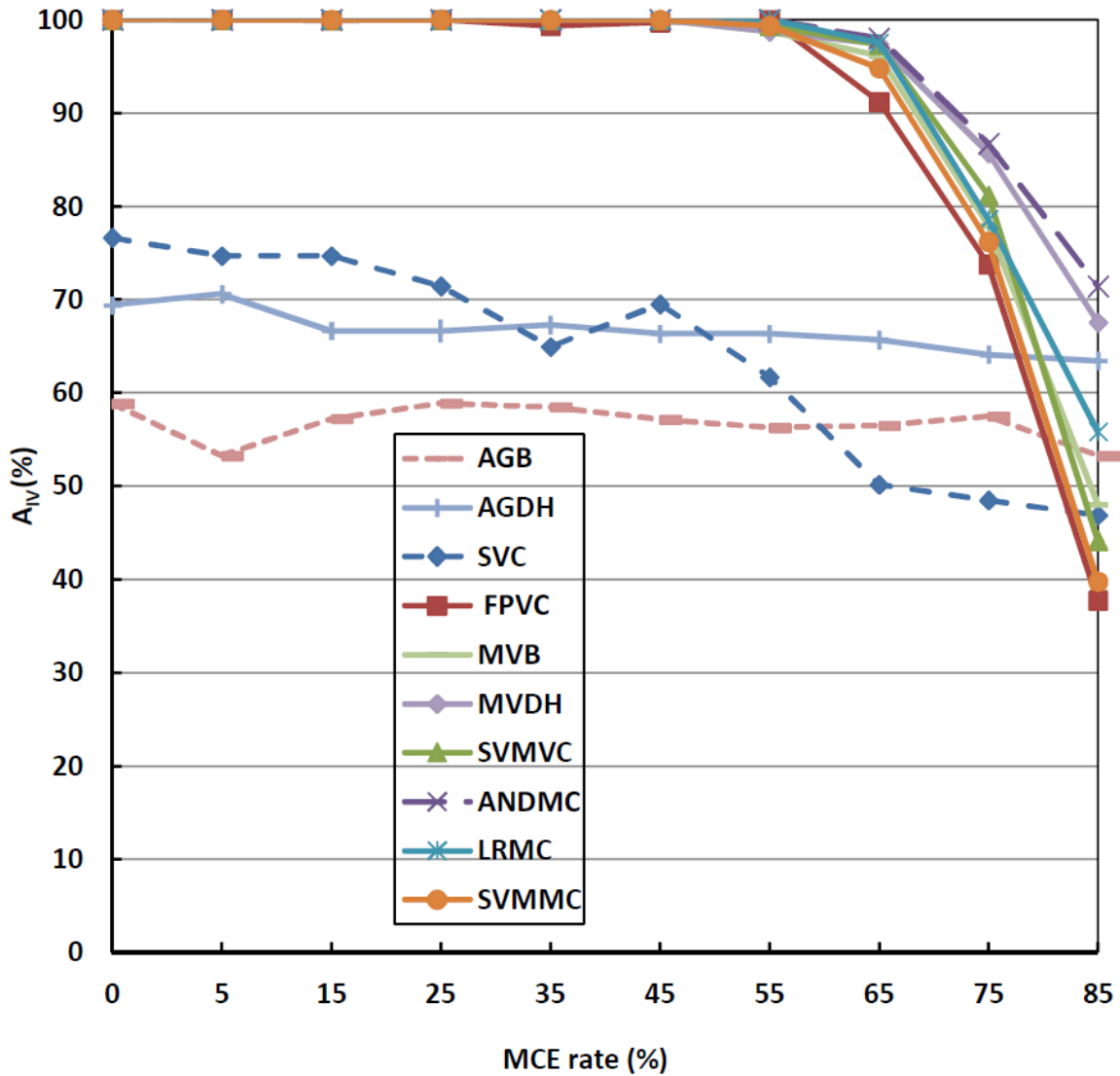
Figure 6.5: Accuracy in detecting invalid trains (A_{IV}) versus the MCE rate in the invalid trains. The MCE rate represents the sparsity of the MUPT. The MUPT validation systems that use both MU firing pattern and MUP shape information (e.g., the MVB, MVDH, SVMVC, and the ANDMC) are more accurate in detecting invalid trains having high MCE rate (> 65%) than the methods that employ only one type of this information (AGB, AGDH, SVC, FPVC) in estimating the validity a MUPT.
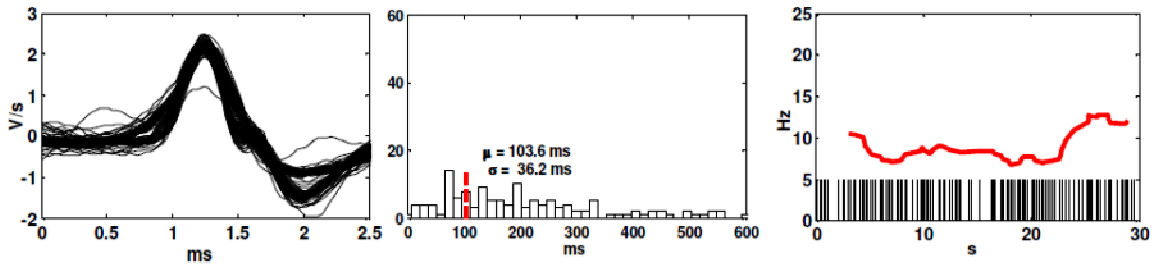
Figure 6.6: An invalid MUPT that is misclassified by the FPVC due to its high MCE rate, but correctly classified by the MVB, MVDH, ANDMC, and LRMC that estimate MUPT validity using both MU firing pattern and MUP shape information. The first column shows the shimmer plot of the assigned MUPs, the second shows the IDI histogram and corresponding statistics. Finally, the last column shows the discharge patterns and instantaneous firing rates for each MUPT.

than the LRMC with average processing time of 71ms for a train. The MVDH is not preferred to the ANDMC because its A_V value is significantly (around 5%) lower than the ANDMC. Therefore, using the ANDMC during the early stages of an EMG signal decomposition, when the MCE rates in the extracted MUPTs are high, may be more practical than using the LRMC. The LRMC can be used during the latter stages of EMG signal decomposition, when MCE rates in the trains are < 65%, or it can be used passively for post processing of extracted MUPTs after decomposition. Figure 6.7 demonstrates two examples showing the advantage of using the LRMC for post processing of extracted MUPTs over using of the ANDMC for this propose. Both MUPTs are valid even though they have high MUP shape variability due to high jitter values. These two valid MUPTs were misclassified by the SVC and hence the ANDMC but both were correctly classified by the LRMC.

It is important to point out that the presented methods do not provide the absolute validity for a MUPT. They only estimate the class label of a MUPT (i.e., valid/invalid) and provide a degree of support for the decision made. The proposed methods are to: 1) assist with improving the accuracy and completeness of decomposition results; and 2) facilitate the use of EMG signal decomposition results for clinical applications of quantitative electromyography by excluding or highlighting invalid MUPTs.

The developed MUPT validation classifiers can be used both during decomposition, for detecting invalid extracted MUPTs (i.e., actively), or after decomposition, for post-processing of the extracted MUPTs before using them for further analysis (i.e., passively). For passive use of the LRMC, the validity of each MUPT extracted by a decomposition algorithm is determined and invalid trains are excluded from further analysis. For active use of either the LRMC or the ANDMC, the validity of each MUPT is
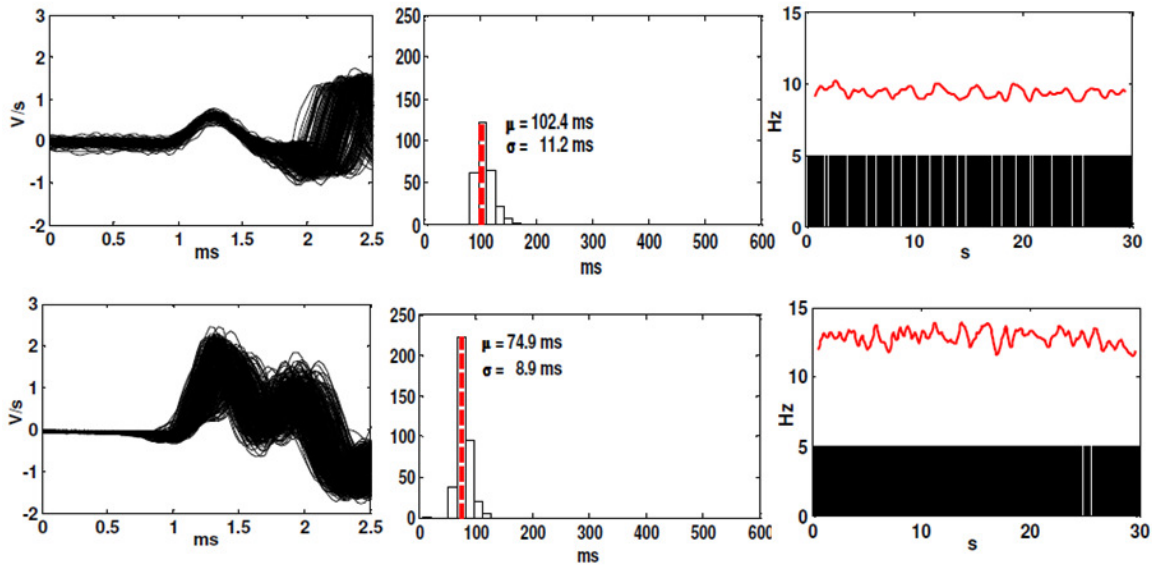
Figure 6.7: Two examples of valid MUPTs that are misclassified by the SVC and the ANDMC but correctly classified by the LRMC. The first column shows the shimmer plot of the MUPs assigned to each MUPT; the second and third columns present the MU firing pattern information. The second column illustrates the IDI histogram and the last one demonstrates the discharge patterns and instantaneous firing rates for each MUPT.

estimated after each pass during decomposition. Invalid trains can then be split into several valid trains before decomposition continues. Splitting can be completed using the information provided by the FPVC and the SVC such that the clustering algorithm (e.g., K-means) employed for splitting is seeded based on the MUPs that caused either the IDI inconsistency or the MUP shape inconsistency. Having invalid trains corrected, more MUPs will be assigned correctly into the extracted trains. Chapter 8 reveals the effectiveness of using the developed MUPT validation classifiers during EMG signal decomposition.

6.6 Conclusions

Combining MU firing pattern and MUP shape information for automatic validation of a MUPT has been shown to correctly identify cases of both valid and invalid trains. In this chapter, several methods that fuse both the MU firing pattern and MUP shape information of a MUPT to estimate its validity are developed and evaluated using both simulated and real data. Overall, the methods that use only shape or only firing pattern information did not perform as well as the ones that use both types of information,

especially for invalid trains. Of the methods studied, the LRMC that separately estimates MU firing validity and MUP-shape validity of a MUPT and then estimate the validity of the train by fusing these two indices using a logistic regression classifier outperformed the others in terms of computation time and classification accuracy (i.e., in terms of A_T). However, the ANDMC performed better than the LRMC in correctly categorizing highly sparse invalid trains and could be used in early stages of decomposition.

Chapter 7

Detecting and Editing Contaminated MUPTs during EMG Signal Decomposition

7.1 Introduction

As discussed in Chapter 3, several characteristics of the contaminated MUPTs (trains with a high number of FCEs) differ from that of valid trains. The IDI distributions of contaminated MUPTs are skewed to the left (Figure 3.4) and their MU firing pattern statistics are often underestimated due to the increased number of shortened IDIs while the IDI distribution of a valid train follows a Gaussian distribution. The percentage of short IDIs in contaminated MUPTs are, in general, higher than that in valid trains. The MU firing pattern variability of contaminated MUPTs may be higher than that of the valid trains. For an example of a contaminated MUPT created by DQEMG applied to a real EMG signal see MUPT# 3 in Figure 2.6. As shown, the FR−MCD, which presents the variability of the firing rate over time, for this invalid train are higher than that for the two first MUPTs that are valid. These facts motivate the development of a supervised classifier that use the features of the IDIs of a MUPT to verify the class label (contaminated or non-contaminated) for a MUPT.

This chapter describes a method developed for: 1) determining whether a given MUPT is contaminated with a high number of FCEs and needs to be edited; 2) removing the FCEs from a contaminated train. Using motor unit firing pattern information provided by each MUPT, the developed algorithm first determines if a given MUPT is contaminated with a high number of FCEs and needs to be edited or not. For contaminated MUPTs, the method uses both MU firing pattern and MUP shape information to detect MUPs that were erroneously assigned to the train (i.e., represent FCEs).

96

As discussed in Chapter 3 (Section 3.2), our experience reveals that from a clinical perspective, an FCE rate of up to 5% does not have a significant effect on the estimated characteristics of MUPTs and MUP templates (i.e., MU mean firing rate or firing rate variability; MUP peak to peak voltage, duration, area, number of phases and number of turns). Therefore, a train with an FCE rate less than 5% is considered as a single (non-contaminated) train.

7.2 A Supervised Classifier for Detecting Contaminated MUPTs

To verify whether a given MUPT can be considered a single train or if it is a contaminated train a supervised classifier called here a single/contaminated classifier (SCC) was developed. The SCC uses a supervised classification scheme and MU firing pattern information of the given MUPT to determine its class label. The MU firing pattern information is represented by ten features extracted from the IDIs and MU firing pattern of the given MUPT. The majority of these features target the left side of the IDI distribution of the given MUPT, where short IDIs (i.e., the errors of interest) are reflected. The features , classifiers, and the training methods employed to develop the SCC are the same as does used to develop the FPVC (Chapter 4). However, a different dataset was utilized to develop the SCC (see Section 7.4). Therefore, three classification methods were examined for developing the SCC: FDA [105], [163], SVM [166], [167], and PD (Pattern Discovery) [164], [165], [168].These classifiers are briefly discussed in Section 4.3.

7.3 Detecting FCEs in a Contaminated MUPT

The FCE detection algorithm employs both MU firing pattern and MUP shape information to classify the MUPs of a contaminated MUPT as being either a FCE or a correct MUP assignment. Initially, erroneously assigned MUPs (i.e., FCEs) are detected using shape information. The goal is to detect those MUPs whose shape is inconsistent with the shapes of the majority of the MUPs in the MUPT. With the information provided by the EMG decomposition algorithm used, each MUP in the given MUPT is represented by a window of 80 sample points (representing an interval of 2.56 ms at a sampling rate of 31.25 kHz) within the EMG signal band-pass filtered using a 1st –order LPD filter [49], [50]. Among these 80 samples, the L uncorrelated samples for which the N MUPs of the contaminated MUPT significantly differ from each other are selected and then used to detect FCEs using only MUP shape information. A gap-based feature selection algorithm was developed for finding these L features.

Let $A = [a_{i,j}]_{N \times 80}$ represent the N MUPs assigned to a contaminated MUPT, $a_{i,*}$ (i th row of matrix A) includes the 80 filtered time sample of the ith MUP. By calculating the largest change, the gaps, in the sorted $a_{*,j}$ values, the L values with the largest gap that are also at least 8 samples (0.26 ms) apart are used as effective features to represent the MUPs assigned to the MUPT under study.

Let L-dimensional vector b_i denotes the L effective time samples representing the ith MUP in the given contaminated MUPT; the L-dimensional vector s represents the L corresponding samples of the MUP template of the given MUPT; and ε denotes an estimate of the root mean square value of the noise contaminating the MUPs. For each MUP, the percentage of shape inconsistency (PSI) and its distance from the MUP template (d) are calculated as:

$$PSI_i = \frac{1}{L} \sum_{l=1}^{L} \{ U(b_{i,l} - s_l - 3\varepsilon) + U(-b_{i,l} + s_l - 3\varepsilon) \} \tag{7.1}$$

$$d_i = \frac{1}{\varepsilon^2} \sum_{l=1}^{L} (b_{i,l} - s_l)^2 \tag{7.2}$$

where $U(t)$ is the unit step function.

Using χ^2 statistics and the calculated values for PSI_i and d_i, MUPs of a contaminated MUPT are classified into three classes based on their shape: 1) *definitely* a FCE if $d_i > \chi^2(L, \theta)$ AND $PSI_i > 0.8$; 2) *potentially* a FCE if $d_i > \chi^2(L, \Delta)$; and 3) a correctly assigned MUP.

In the second step of detecting FCEs, erroneously assigned MUPs are detected using MU firing pattern information. MUPs that cause IDI inconsistencies are detected and classified into three categories based on their firing pattern: 1) *Semi-definitely* a FCE if $IDI_i < \mu\text{-}3\sigma$; 2) *potentially* a FCE if $IDI_i < \mu\text{-}2\sigma$; and 3) *do not know* if $IDI_i > 2\mu$. Where μ and σ are the mean and standard deviation of the IDIs of the given train estimated using the EFE algorithm that provides accurate estimates of these IDI statistics of a MUPT even when contaminated by a high MCE rate [140].

In the third step, a MUP is classified as a FCE if it was assigned into either: 1) the *definitely* a FCE based on shape class; or 2) the *potentially* a FCE based on shape class AND the *do not know* based on firing pattern class; or 3) the *potentially* a FCE based on shape class AND the *potentially* a FCE based on firing pattern class. In addition, a MUP is labeled as a FCE if it is assigned into the *Semi−definitely* based on firing pattern and its PSI > 0.4. Otherwise, it is classified as a correctly assigned MUP.

7.4 Evaluation

Each part of the developed method was tested separately. Specifically, the three classification methods studied for the SCC discussed in Section 7.2 were trained using simulated data and tested using both simulated and real MU firing patterns. The FCE detection algorithm was tested using several MUPTs extracted by decomposing 43 simulated EMG signal.

For training and evaluating the SCC, the same simulated and real MU firing patterns used for training the FPVC were employed (see Chapter 4, Section 4.4), but here instead of merging the obtained single MUPTs they were contaminated by adding up to 20% FCE and 70% MCE in steps of 1% and 10% respectively. Specifically, for simulated data from 0% to 70% MCE and from 0 to 15%, including both acceptable and unacceptable levels of contamination, were added to the trains. For real data, up to 70% MCEs and up to 15% FCEs were added to the train. The simulated data set created contains 35,000 non-contaminated trains (with an acceptable FCE rate) and 35,000 contaminated trains (with an unacceptable FCE rate). The real data set generated includes 21,899 non–contaminated trains and 58,162 contaminated trains.

For studying the effectiveness of the FCE detection algorithm 535 MUPTs extracted from 43 EMG signals each of 10s length with different levels of intensity, ranging from 24 to 193 pps, with jitter values ranging from 50 to 150μs, and with IDI variability (i.e., coefficient of variation) ranging from 0.10 to 0.45 generated using the EMG signal simulator developed by Hamilton-Wright and Stashuk [153] were used. These data allowed us to study the performance of the developed method in relation to various degrees of MUP shape and IDI variability. Generated signals were decomposed using the DQEMG algorithm [7]. MUPs were added to each train extracted from an EMG signal at random points in time until the FCE rate of the train was between 5% and 20% (with 5% intervals). The added MUPs were selected randomly from the remaining MUPTs extracted from the same EMG signal.

The performance of the classifiers studied for SCC was evaluated and compared in terms of correctly classifying contaminated and non–contaminated trains. Three accuracy indices were defined for this purpose: accuracy for non–contaminated trains (A_{NCT}), accuracy for contaminated trains (A_{CT}), total accuracy (A_T). These three indices are given by:

$$A_{NCT}\% = \frac{Number\ of\ non-conaminated\ MUPTs\ correctly\ classified}{Total\ number\ of\ non-conaminated\ MUPTs\ tested} \times 100 \qquad (7.3)$$

$$A_{CT}\% = \frac{Number\ of\ contaminated\ MUPTs\ correctly\ classified}{Total\ number\ of\ contaminated\ MUPTs\ tested} \times 100 \qquad (7.4)$$

$$A_T\% = \frac{Number\ of\ MUPTs\ correctly\ classified}{Total\ number\ of\ MUPTs\ Tested} \times 100 \qquad (7.5)$$

The performance of the developed FCE detection algorithm was evaluated using three indices: Sensitivity, specificity, and accuracy. These three indices are given by

$$Sensitivity = \frac{N_{FCECD}}{N_{FCE}} \times 100 \qquad (7.6)$$

$$Specificity = \left(1 - \frac{N_{FCED} - N_{FCECD}}{N_C}\right) \times 100 \qquad (7.7)$$

$$Accuracy = \frac{N_{FCE} \times Sensitivity + N_C \times Specificity}{N_T} \qquad (7.8)$$

where the parameters N_C, N_{FCE}, N_T, N_{FCED}, and N_{FCED} are defined as follows.

N_C : Number of MUPs that correctly assigned to the MUPT by the decomposition system used. These MUPs all generated by the corresponding MU and should be left in the MUPT.

N_{FCE}: Number of FCEs added to the MUPs.

N_T : Total number of MUPs in MUPT; $N_T = N_C + N_{FCE}$.

N_{FCECD}: Number of FCEs that correctly detected by the FCE detection algorithm.

N_{FCED}: Number of MUPs that detected as FCE by the FCE detection algorithm ($N_{FCED} \geq N_{FCECD}$).

7.5 Results

The performances of the three classification methods considered to implement the SCC for both simulated and real data are summarized in Tables 7.1 and 7.2, respectively. Each table presents the estimated means and standard deviations of the three performance indices A_{NCT}, A_{CT}, and A_T for the three ranges of MCE rates studied. The aim of using these ranges was to study the effectiveness of these classifiers at different stages of EMG signal decomposition. The values presented in Table 7.1 were obtained by running a 10–fold cross validation on the simulated data set used. While the values presented in Table 4.2 were obtained by evaluating the classifiers trained using the entire simulated data on the real

Table 7.1: Mean and standard deviations of the accuracy of the three studied classifiers applied to simulated MU firing patterns having acceptable and unacceptable FCE rate. In each column of the table, individual or groups of classifiers bolded and indicated by an '*' had significantly better performance than the others as determined using a multivariate analysis of variance, at a 5% significance level and the Tukey-Kramer honestly significant difference test for pair-wise comparison of the mean values. For each performance index, when two or more methods had statistically similar performance, they are all identified.

	Missed-Classification Error Rate								
	0% to 50%			0% to 70%			60% to 70%		
	A_{NCT} (%)	A_{CT} (%)	A_T (%)	A_{NCT} (%)	A_{CT} (%)	A_T (%)	A_{NCT} (%)	A_{CT} (%)	A_T (%)
FDA	80.7±0.6	***87.3±0.5**	***84.0±0.4**	78.1±1.0	***85.5±0.6**	***81.1±0.6**	71.9±2.1	***71.0±1.3**	***71.4±1.2**
PD	79.6±0.8	85.8±0.5	82.7±0.2	78.0±0.9	82.4±0.3	80.2±0.4	***76.0±3.0**	66.3±1.8	***71.1±2.2**
SVM	***82.7±0.6**	85.5±0.6	***84.1±0.6**	***80.1±0.9**	82.1±0.6	***81.1±0.6**	***76.2±1.8**	68.1±1.5	***72.1±1.1**

Table 7.2: The performance of the three classifiers applied to real MU firing patterns having acceptable and unacceptable FCE rate. As in Table 7.1 above, individual or groups of classifiers that had significantly better performance than the others are identified.

	Missed-Classification Error Rate								
	0% to 50%			0% to 70%			60% to 70%		
	A_{NCT} (%)	A_{CT} (%)	A_T (%)	A_{NCT} (%)	A_{CT} (%)	A_T (%)	A_{NCT} (%)	A_{CT} (%)	A_T (%)
FDA	***87.4±0.4**	***85.7±0.5**	***86.1±0.4**	***83.9±0.4**	***79.2±0.8**	**80.8±0.5**	76.7±1.1	***70.3±1.5**	***72.3±0.5**
PD	82.5±0.7	82.1±0.6	82.2±0.5	***83.7±0.6**	75.1±1.0	77.4± 0.8	***79.2±0.9**	61.7±2.0	66.2±1.7
SVM	84.2±0.6	83.0±0.5	83.2±0.4	***83.8±0.5**	76.6±0.9	78.6± 0.6	***79.8±1.2**	66.5±1.8	70.2±1.3

Table 7.3: The performance of the FCE detection algorithm obtained using 535 MUPTs obtained from the decomposition of 43 simulated EMG signals.

Sensitivity (%)	Specificity (%)	Accuracy (%)
84.4±0.7	93.4±0.1	92.1±1.0

dataset when this dataset is divided in 10 different- equalize subsets. The statistical comparison of the methods were conducted using the analysis of variance, at a 5% significance level and the Tukey-Kramer honestly significant difference test for pair-wise comparison of the mean values.

The calculated means and standard deviations across the MUPTs studied for the sensitivity, specificity and accuracy of the FCE detection algorithm with $L = 5, \theta = 0.01$, and $\Delta = 0.05$ are presented in Table 7.3. These settings were empirically found to perform better based on experimentation with several MUPTs.

7.6 Discussion

Based on the results presented in Table 7.1, the SVM performs better than the FDA and PD classifiers in correctly classifying non-contaminated trains. On the other hand, the FDA classifier is best at correctly classifying contaminated MUPTs. Overall, the FDA classifier is better than the SVM and PD classifiers for the SCC because of the following three reasons. 1) The FDA classifier is the best classifier in terms of A_T. For the data with 0% to 70% MCE rate, which is the general case, the FDA classifier has an average accuracy of 81.7%, while the SVM and PD classifiers had accuracy of 81.0%, and 80.2%, respectively. 2) The FDA classifier has the best performance in correctly classifying MUPTs with unacceptable FCE rate as contaminated. It is clear that misclassifying a contaminated MUPT as a single (i.e., valid) train is more costly than misclassifying a single train as contaminated. 3) The FDA classifier is the fastest classier among the three classifiers studied. Therefore, the FDA classifier is the best choice for detecting MUPTs contaminated with a high number of FCEs during decomposition.

The results shown for the real data used in Table 7.2 also support the statement that an FDA classifier is the best choice as a SCC. As, shown for both 0% MCE and the general case, 0% to 70% MCE range, the FDA classifier had the highest accuracy in detecting contaminated MUPTs. For the worst case, 50%
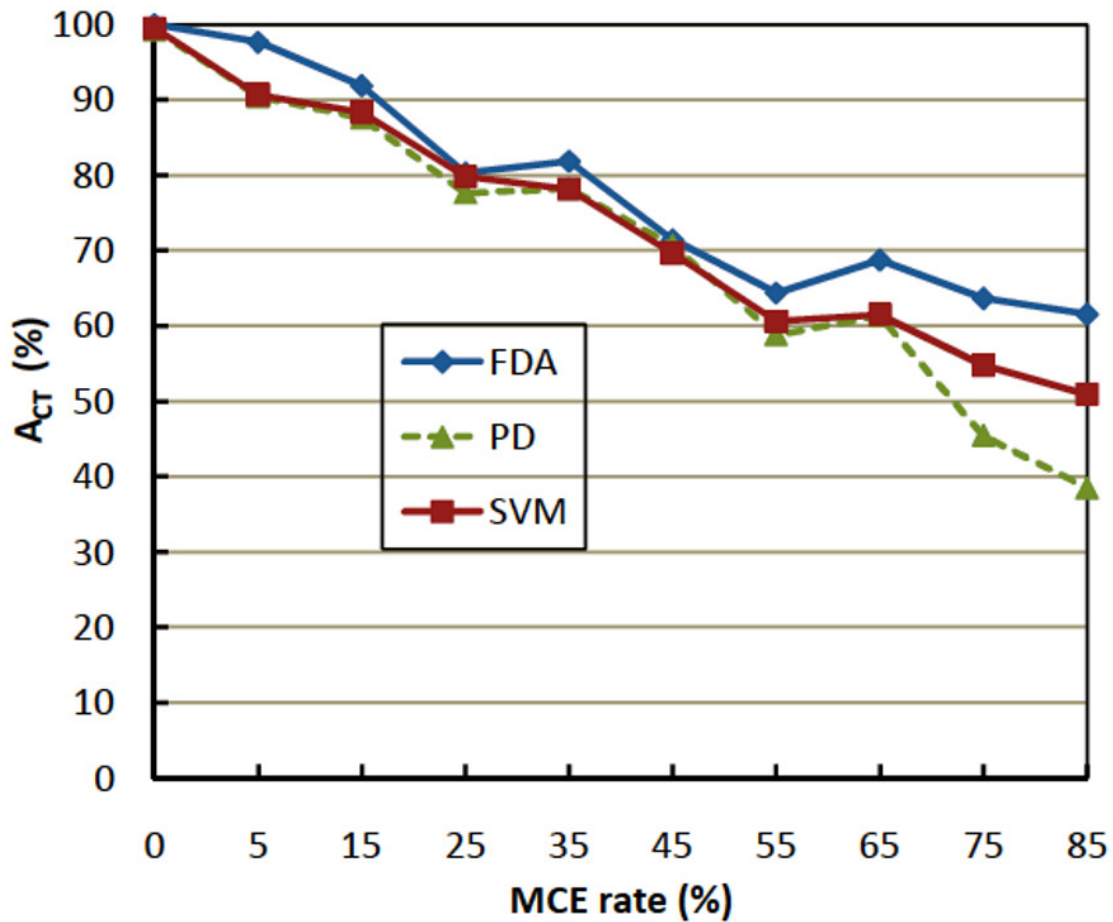
Figure 7.1: Accuracy of the classifiers studied for the SCC in correctly labeling a contaminated MUPT versus the MCE rate in the train.

to 70% MCE rate range, the FDA classifier performed significantly better than the SVM and PD classifiers in detecting contaminated trains.

The accuracy of the SCC in correctly classifying contaminated MUPTs decreases as the MCE rate in the train increases. Comparing the numbers presented for A_{CT} in Tables 7.1 and 7.2 for three ranges of MCE rate reveal this fact.

Figure 7.1 shows this trend for the three classifiers studied for the SCC. As shown, the FDA-based SCC (as the best classifier) correctly detected approximately only 65% of the contaminated MUPTs having MCE rates between 55% and 85%. A possible reason for the drop in performance of the SCC with increased MCE rate is that the accuracy of estimating the IDI statistics, especially the standard deviation,
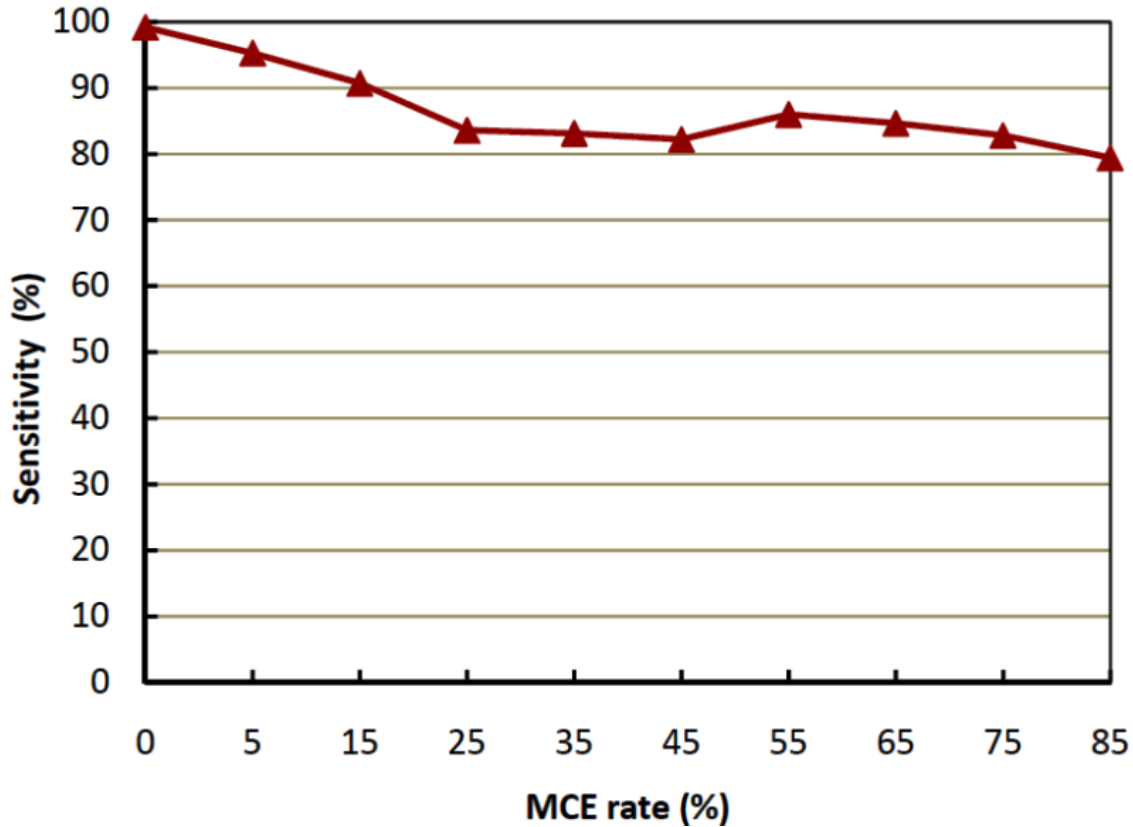
Figure 7.2: Sensitivity of the FCE detection algorithm in correctly detecting FCEs in a contaminated MUPT versus the MCE rate of the train.

decreases as the train becomes sparse [74]. The other reason is that the percentage of inconsistent IDIs for incomplete invalid trains is not as high as for full invalid trains. Figure 7.1 demonstrates another advantage of the FDA over the SVM and PD classifiers for developing a SCC. As shown, the FDA is more accurate than the other two classifiers evaluated in correctly classifying highly sparse contaminated MUPTs.

The results presented in Table 7.3 show that the FCE detection algorithm can detect the majority of the added FCE errors and was also able to correctly classify most of the correctly assigned MUPs. However, for the same reason mentioned for the SCC the sensitivity of the FCE detection algorithm decreases as the MCE rate in the contaminated MUPTs increases (see Figure 7.2). As shown, the sensitivity of the algorithm for contaminated MUPTs having MCE rate between 25% and 85% was approximately 80%.
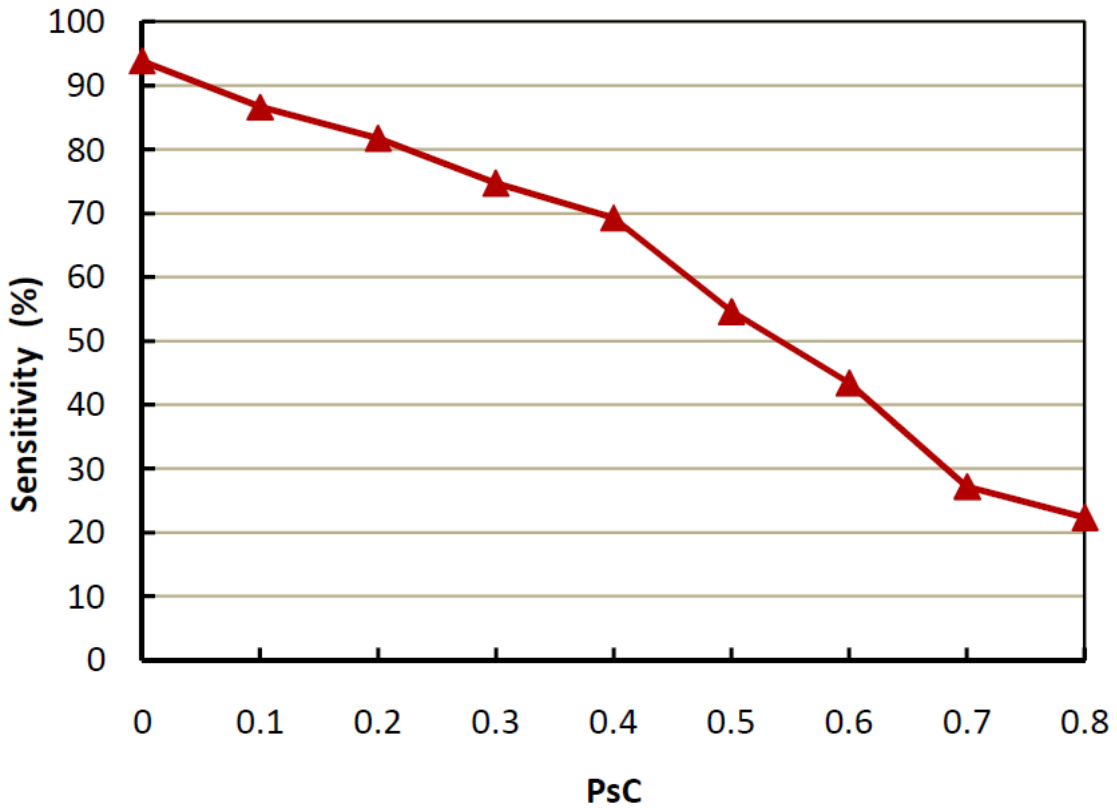
Figure 7.3: Sensitivity of the FCE detection algorithm in correctly detecting a MUP erroneously assigned to a contaminated MUPT versus the pseudo-correlation (PsC) between the MUP and the template of the MUPT.

Figure 7.3 illustrates the estimated values for the sensitivity of the FCE detection algorithm versus the similarity between the MUP template of the contaminated MUPT and an erroneously assigned MUP measured using the PsC [70]. As shown, the sensitivity of the algorithm decreases as the similarity between the incorrectly assigned MUP (i.e., the FCE) and the MUP template of the contaminated MUPT increases such that in the worse case (PsC = 0.8) the algorithm failed to detect approximately 78% of the FCEs created by MUPs that are very similar to the MUP template. Sensitivity for such cases can be improved by increasing θ or classifying at least one of the two MUPs creating an IDI $< \mu$-3σ as an FCE, but such an adjustment may cause specificity to decrease. Nevertheless, the performance of the algorithm on average is promising in terms of detecting and removing FCEs from contaminated MUPTs.

7.7 Conclusions

A robust method for detecting MUPTs contaminated by a high number of false classification errors and then detecting the erroneously assigned MUPs in a contaminated MUPT was presented. Evaluation based on both simulated and real data shows that the FDA-based SCC developed for discriminating between contaminated and non-contaminated MUPTs outperformed the SVM-based SCC and the PD-based SCC. The accuracy of the FDA-based SCC is 84% and 81% for simulated and real data, respectively. The FDA-based SCC, on average, correctly classified around 87.3% and 85.7% of the contaminated MUPTs created by a decomposition algorithm.

The obtained results using several simulated contaminated MUPTs also revealed that the FCE detection algorithm can on average detect 84.4% of the FCEs in a given MUPT. However, the accuracy of both the SCC and the FCE detection method decreases as the percentage of MCEs in a MUPT increases. In addition, the sensitivity of the FCE detection algorithm in detecting an MUP erroneously assigned decreases as the similarity between the MUP and the MUP template of the MUPT increases. Nevertheless, the overall accuracy of the method (92.1%) is encouraging and suggests using the method during EMG signal decomposition to improve the results or to facilitate editing extracted MUPTs.

Chapter 8

EMG Signal Decomposition using MUPT Validity

8.1 Introduction

EMG signal decomposition is the process of resolving an EMG signal into its component MUPTs. The purpose of EMG signal decomposition is to provide an estimate of the firing pattern and MUP template of each active MU that contributed significant MUPs to the composite EMG signal. Numerous automatic and semi-automatic EMG signal decomposition methods, as summarized in Table 1.2 and discussed in Chapter 2, have been proposed. These algorithms have been shown to be able to successfully decompose both the simulated and real EMG signals used for their evaluation. However, the obtained results still depend on several factors such as the parameters used by the algorithms, the decomposability of the signal, and the MUP shape and MU firing pattern variability over the entire signal. In addition, the accuracy of an EMG signal decomposition depends on the validity of the MUPTs obtained by the decomposition algorithm which in turn depends on the criteria and parameters used to merge or split MUPTs.

This chapter describes a newly developed EMG signal decomposition system that uses MUPT validity and how it was evaluated. The newly developed validity-based decomposition system is, in essence, an enhanced version of the decomposition algorithms of DQEMG [7]. In DQEMG, the detected MUPs are grouped into several MUPTs using STBC [74] and a supervised certainty-based classifier (CBC) [72]. The STBC algorithm is a customized K-means clustering method that uses both MUP shape and MU firing pattern information to cluster MUPs. In STBC, MUPTs are split or merged based on several heuristic criteria. Assuming the MUPTs provided by the STBC algorithm are valid, they are augmented

by the CBC algorithm in which a MUP is assigned to the MUPT that has the greatest certainty value, if this value is greater than a certainty assignment threshold. Otherwise, the MUP is left unassigned. In the CBC algorithm, two MUPTs are merged if the resulting MUPT satisfies several predefined criteria but the MUPTs are not split nor assessed for splitting. The new validity-based decomposition system employs the algorithms presented in Chapters 6 and 7 to merge, split, or edit MUPTs. The new system also adjusts the assignment threshold for each individual MUPT adaptively based on the validity information extracted from the train. At the end of each classification pass through the set of detected MUPs, during supervised classification, the validity of each obtained MUPT is evaluated. Invalid MUPTs either have their FCEs corrected or are split into valid trains. In addition, during supervised classification, the minimum certainty MUP assignment thresholds for invalid trains are increased while the thresholds for valid trains are decreased (i.e., adaptive adjustment of the assignment criteria). This adjustment controls the minimum confidence required to assign a MUP to a specific MUPT. Details of the newly developed decomposition algorithms along with its evaluation using several simulated and real EMG signals are given in the following sections.

8.2 MUPT Validity-based Decomposition System

The validity-based EMG signal decomposition system decomposes a detected EMG signal off-line. The system consists of four major steps: signal preprocessing, MUP detection, and clustering and supervised classification of the detected MUPs. A brief description of the objective of each step is given in Figure 8.1. Signal preprocessing, MUP detection, and clustering of detected MUPs are completed using methods similar to that in DQEMG [7]. The main contribution of this work is in the supervised classification step in which the user-defined parameters and heuristic criteria used in the DQEMG algorithms are replaced by the signal dependent parameters and several supervised classifiers, respectively. Following is a description of these steps.

8.2.1 Signal Preprocessing

The signal preprocessing step is involved with filtering the signal to improve the SNR of the signal, decrease MUP temporal overlap, to accentuate the differences between MUPs created by different MUs, and to increase the separation between MUPs and the background noise. For this purpose, a 1st-order LPD filter [49], [50] as defined in Equation 5.8 is employed. Figure 8.2 shows the effectiveness of LPD filtering of an EMG signal. As shown, filtering flattens the signal baseline and makes the MUPs into narrower and more recognizable spikes.

```
┌─────────────────┐              ┌─────────────────┐
│  Decomposition  │              │    Objective    │
│      Steps      │              │  of Each Step   │
└─────────────────┘              └─────────────────┘
       ▽                                ▽
┌─────────────────┐    ┌──────────────────────────────────┐
│     Signal      │    │ Improve the ability to detect the │
│  Preprocessing  │    │ signals by removing background    │
│                 │    │ noise and reducing MUPs overlap.  │
└─────────────────┘    └──────────────────────────────────┘
       │
       ▼
┌─────────────────┐    ┌──────────────────────────────────┐
│    Detecting    │    │ Identify the positions of MUPs in │
│ Individual MUPs │    │          the filtered signal.     │
└─────────────────┘    └──────────────────────────────────┘
       │
       ▼
┌─────────────────┐    ┌──────────────────────────────────┐
│  Clustering of  │    │ Form MUPTs by grouping the MUPs   │
│ Detected MUPs   │    │ of similar shapes (working with   │
│                 │    │        just part of data).        │
└─────────────────┘    └──────────────────────────────────┘
       │
       ▼
┌─────────────────┐    ┌──────────────────────────────────┐
│   Supervised    │    │ Assign the rest of the MUPs to the│
│ Classification  │    │ extracted MUPTs based their shapes│
│      of MUPs    │    │   and MU firing time consistency. │
└─────────────────┘    └──────────────────────────────────┘
```

Figure 8.1: The main steps of the validity−based decomposition system along with the objective of each step.

8.2.2 MUP Detection

MU detection identifies the position of the MUPs in a given EMG signal. The positions of suitable MUPs in the filtered signal are detected using a threshold crossing technique by which the prefilterd EMG signal is scanned and the peaks that satisfy several criteria [7] are detected and considered as the occurrence times of MUPs. In general, the amplitudes of detected MUPs are higher than the baseline noise. Figure 8.2 illustrates the segmentation procedure for an EMG signal.

For clustering and supervised classification, each detected MUP is represented using the 80 filtered data samples (i.e., 2.56 ms at 31250 Hz sampling rate), centered about its peak value (i.e., about the position of maximum slope of the unfiltered MUP data).
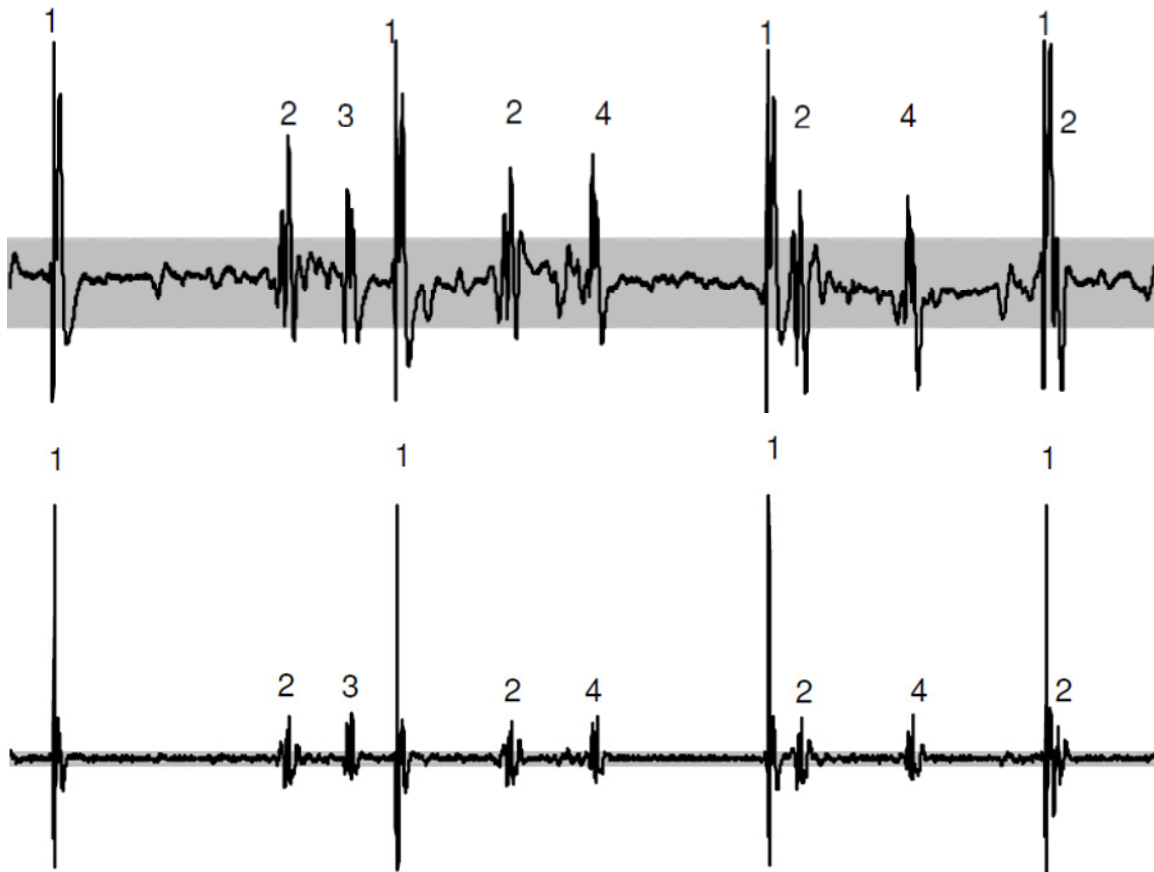
Figure 8.2: The effectiveness of LPD filtering and the segmentation procedure for an EMG signal. A portion of the signal containing ten MUPs (top row). The LPD filtering results for this portion. Gray region shows the estimated level of baseline noise.

8.2.3 Clustering of the Detected MUPs

Detected MUPs are clustered to obtain the initial information required for supervised classification such as estimates of the number of MUPTs, their prototypical MUP shapes (or templates), and their MU firing pattern statistics. To extract such information, the MUPs detected in a specified portion (a 5 second interval with the highest number of detected MUPs) of the EMG signal are input to the STBC algorithm [74] that groups the detected MUPs into several MUPTs using both firing time and shape information across multiple iterations. The initial estimate of the number of clusters (number of active MUs) is equal to the maximum number of MUPs and the initial cluster centers are the actual MUPs in the 30 ms interval

within the selected 5 second interval. Having estimates for the number of clusters and their centers, each detected MUP is assigned to the closest cluster, if its distance to the core of the closest cluster is smaller than 0.25 times that of the second smallest distance from the candidate MUP and the cluster centers. In STBC, a MUPT will be split into two trains if it includes a MU firing-pattern inconsistency. Similar MUPTs are merged if their MUP templates are close and the firing pattern of the merged MUPT satisfies several criteria [74]. The MUP assignment, cluster splitting, editing, and merging steps are repeated until the resulting MUPTs are stable. Detail of the STBC algorithm can be found in [74].

8.2.4 Supervised Classification of Detected MUPs

Having the initial information about possible MUPTs provided by the clustering step, the detected MUPs are assigned to MUPTs using a supervised classifier. The objective here is to assign each MUP to the MUPT for which the MUP's time of occurrence and shape are more consistent with respect to the MU firing times and MUP shapes of the selected MUPT, respectively, than to the other MUPTs. Each of the MUPTs should have low MCE and FCE rates and represent the activity of a single MU that contributed detected MUPs to the given EMG signal. In this work, a new adaptive certainty-based classifier was developed for this purpose.

The certainty-based classifier [72] is a supervised classifier that combines both MUP shape and MU firing pattern information to calculate the confidence of assigning a candidate MUP to a MUPT. The candidate MUP is assigned to the MUPT that has the greatest certainty value, if this value is greater than a certainty assignment threshold (C_{AT}). Otherwise, the MUP is left unassigned.

The certainties for assigning a candidate MUP are evaluated for the two trains that have the most and the next most similar MUP templates. These two trains are found by calculating the Euclidian distance between the candidate MUP and the MUP template of each MUPT. The certainties are calculated using MUP shape and MU firing pattern information. MUP shape certainty includes normalized absolute shape certainty (C_{ND}) and relative shape certainty (C_{RD}). The first represents the distance from the candidate MUP to the template of a train, normalized by the energy of the template. The second represents the distance from the MUP to the most similar MUP template relative to the distance of the MUP to the next most similar MUP template. Assuming a_j represents the feature vector of the MUP_j being classified and, s_1 and s_2 respectively represent the feature vectors of the closest and the next closest MUP template to MUP_j, C_{ND}^j and C_{RD}^j are evaluated as

111

$$C_{\text{ND } i}^{j} = max\left\{1 - \frac{r_i}{\|s_i\|^2}, 0\right\} \; ; \; i = 1,2 \tag{8.1}$$

$$C_{\text{RD } i}^{j} = 2 - i + (-1)^i \frac{r_1}{2r_2}; \; i = 1,2 \tag{8.2}$$

where r_i is the Euclidean squared distance between the MUP and s_i and is given by

$$r_i = (a_j - s_i)(a_j - s_i)^T. \tag{8.3}$$

Firing pattern certainty, C_{FC}, measures the consistency of the occurrence time of the candidate MUP relative to the established MU firing pattern of a MUPT. Denoting t_j as the occurrence time of the given MUP (i.e., MUP$_j$) and t_{pi} and t_{ni} as the occurrence times of the previous and next MUPs in MUPT$_i$, the firing pattern certainty of assigning MUP$_j$ to MUPT$_i$ ($C_{\text{FC}i}^{j}$) is given by:

$$C_{\text{FC}i}^{j} = C_{fi}^{j}\left(|t_j - t_{pi}|\right) \times C_{fi}^{j}\left(|t_j - t_{ni}|\right) \tag{8.4}$$

Where

$$C_{fi}^{j}\left(|t_j - t_{pi}|\right) = \sum_{n=1}^{40} \frac{1}{\sqrt{n}} \exp\left(-\frac{\left(|t_j - t_{pi}| - n\mu_i\right)^2}{2n\sigma_i{}^2}\right). \tag{8.5}$$

The two parameters μ_i and σ_i represent the mean and standard deviation of the IDIs of MUPT$_i$ estimated using the EFE algorithm [140]. If μ_i and σ_i are not available or $|t_j - t_{pi}| > \mu_i + 3\sigma_i$, $C_{fi}^{j}\left(|t_j - t_{pi}|\right)$ is set equal to 0.2. The value for $C_{fi}^{j}\left(|t_j - t_{ni}|\right)$ is estimated as $C_{fi}^{j}\left(|t_j - t_{pi}|\right)$ by replacing t_{pi} with t_{ni} in Equation 8.5.

The firing pattern certainty function given in Equation 5 for $C_{fi}^{j}\left(|t_j - t_{pi}|\right)$ is based on a multi-modal Gaussian model representing the IDI distribution of a MUPT with different levels of MCE rate. This model, which estimates the probability density function of the IDIs of a MUPT, is given in Equation 3.1.

Having the shape certainties and the firing pattern certainty, the overall certainties for assigning the MUP$_j$ to one of the two selected MUPTs are estimated by multiplying the shape and firing pattern certainties as

$$C_i^{j} = C_{\text{ND } i}^{j} \times C_{\text{RD } i}^{j} \times C_{\text{FC } i}^{j}; \; i =1,2 \tag{8.6}$$

If $C_i^{j} > C_{AT}$, the candidate MUP is assigned to the MUPT which has the greatest certainty value,

otherwise it is left unassigned.

In order to accommodate non-stationarity in MUP shapes, the algorithm updates the MUP templates with each MUP assignment. The MUP templates are calculated using a moving average for which the weights are the certainties with which MUPs are assigned to the MUPTs. If MUP$_j$ is assigned to MUPT$_i$ with certainty C_i^j higher than the updating threshold (0.6 in this work) the template of MUPT$_i$ (s_i) is updated as [72]:

$$s_i^{New} = \frac{s_i + C_i^j a_j}{1 + C_i^j} \tag{8.7}$$

where a$_j$ is the feature vector of MUP$_j$.

Once each pass is completed and before decomposition continues, the validity of each extracted MUPT is assessed using the methods discussed in Chapters 6 and 7. Invalid trains are detected, corrected and have their C_{AT} adjusted. Trains that are classified as merged by the ANDMC or LRMC are split into valid trains using a K-means clustering algorithm; the single MUPTs that were classified as contaminated by the SCC have their FCEs corrected using the automated MUPT editing algorithm presented in Chapter 7.

To decrease the number of MCEs and FCEs in the MUPTs, the C_{AT} value for each MUPT is adjusted based on its validity (i.e., an adaptive adjustment of the assignment threshold). For invalid MUPTs (either merged or contaminated), the C_{AT} is increased by a step of 0.005 while the C_{AT} for valid trains is adjusted based on the PsC between the MUP template of this train and that of the closet train as follow.

$$C_{AT}^{New} = 0.005 + [max(0.02, C_{AT}) - 0.005] \times exp(-N_{itr}/\eta) \tag{8.8}$$

Where N_{itr} is the number of iterations that the classification algorithm has passed through in assigning all of the MUPs and η is the decreasing rate of the C_{AT} for a valid MUPT and is given by

$$\eta = \begin{cases} 1/3 & PsC \leq 0.1 \\ 1 & 0.1 < PsC \leq 0.3 \\ 2 & 0.3 < PsC \leq 0.5 \\ 4 & PsC > 0.5 \end{cases} \tag{8.9}$$

The C_{AT} value of a MUPT is not decreased or increased below 0.005 or above 0.99, respectively.

In addition to splitting or editing invalid MUPTs, the chance of merging single MUPTs is evaluated. Pairs of MUPTs that have similar MUP templates are merged if the resulting train is valid. MUP template

113

similarity is measured by estimating the pseudo-correlation, the PsC value, between the MUP templates of the two selected MUPTs. Two trains are merged if the PsC between their MUP templates is ≥ 0.4.

The MU firing pattern statistics of each MUPT are updated. The MUP assignment and MUPT splitting, editing, and merging steps are repeated until either, the maximum number of iterations is exceeded or the MUPTs are stable. If trains are merged or split at least one more supervised classification pass will be completed.

A flowchart of the validity-based EMG signal decomposition system is presented in Figure 8.3. The adaptive nature of the validity-based decomposition system, which adjusts the C_{AT} value for each MUPT based on the estimated validity of the train assists with improving the decomposition results in terms of estimating the correct number of MUPTs represented in the set of detected MUPs and decreasing MCE and FCE rates in each MUPT.

8.3 Evaluation Methodology

The performance of the validity-based decomposition algorithm was evaluated using several simulated and real EMG signals. For each EMG signal, the MU discharge patterns provided either by the EMG signal simulator used or by a human expert operator were used as reference. Following are details of each data set.

For simulated data, 32 EMG signals were generated using a physiologically-based EMG signal simulation algorithm [153]. This EMG signal generation tool creates simulated intramuscular EMG signals with different complexities such as different numbers of active MUs, different degrees of MUP shape and/or IDI variability (represented by the amount of jitter and CV of IDI), and different signal intensities (represented by the average number of MUPs per second (pps)). Using these algorithms, EMG signals can be simulated similar to those detected from normal, myopathic and neurogenic muscles with different degrees of involvement.

For real data, several single-channel EMG signals provided by K.C. McGill, VA RR&D Ctr, Palo Alto, US [178]; and multi-channel EMG signals provided by J.R. Florestal, P.A. Mathieu, and K.C. McGill [97] were used. The single-channel signals were recorded using a monopolar needle electrode during low-level isometric contractions of the brachial biceps muscles of normal subjects. The multi-channel signals were recorded simultaneously from the brachioradialis muscles of three normal subjects using six or seven pairs of fine wire electrodes during low-level isometric contractions. Of the MUs contributed to
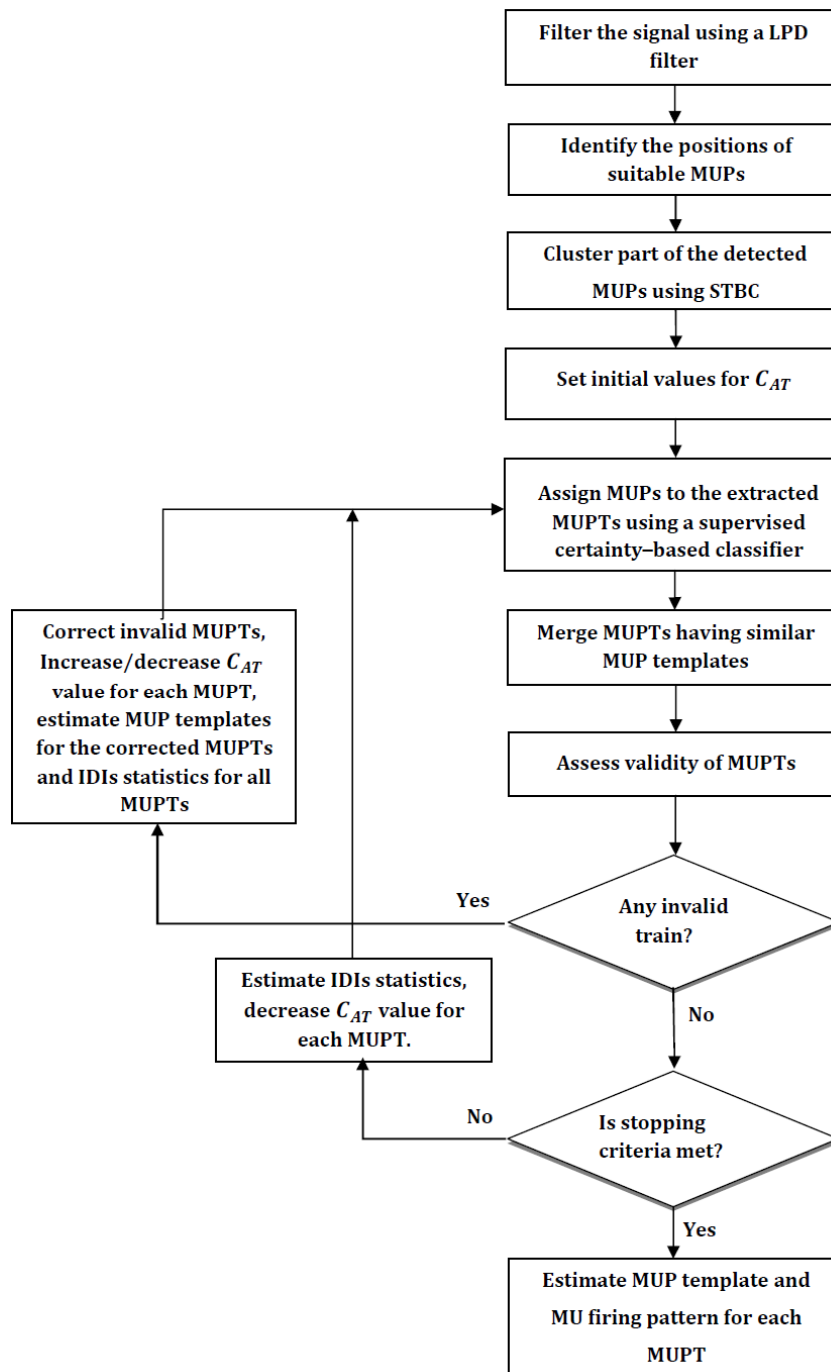
Figure 8.3: Flowchart of the validity–based EMG signal decomposition system.

each signal, only the discharge patterns of those MUs that were selected by the expert as accurately identified patterns and the amplitude of their MUP templates were >0.01V/S were considered as reference and used for evaluation. For this data set, the signals detected by each electrode were considered as single-channel EMG signals.

Four indices were used for evaluation: assignment rate (A_r), accuracy (A_c), correct classification rate (CC_r), and error in finding the correct number of MUPTs (E_{NMUPTS}). These four indices are given by:

$$A_r\% = \frac{Number\ of\ MUPs\ assigned}{Total\ number\ of\ MUPs\ detected} \times 100 \tag{8.10}$$

$$A_c\% = \frac{Number\ of\ MUPs\ correctly\ classified}{Total\ number\ of\ MUPs\ assigned} \times 100 \tag{8.11}$$

$$CC_r\% = \frac{Number\ of\ MUPs\ correctly\ classified}{Total\ number\ of\ MUPs\ detected} \times 100 \tag{8.12}$$

$$E_{NMUPTs} = Number\ of\ extracted\ MUPTs\ -\ Number\ of\ expected\ MUPTs \tag{8.13}$$

where the number of expected MUPTs equals to the number of MUPTs identified by the human expert or identified by the simulator as significant.

8.4 Results and Discussion

Performance results for the validity-based decomposition system and that of the original decomposition algorithms of DQEMG for both simulated and real data are summarized in Tables 8.1 and 8.2, respectively. For each data set, the performance for each signal used along with the mean and standard deviation (STD) for the performance indices over all signals is reported. Statistical comparison of the average values was conducted using paired t-tests ($\alpha = 0.05$), while comparison of the STD values was conducted using F-tests ($\alpha = 0.05$).

For the simulated data set (i.e., Table 8.1), the validity-based decomposition system has significantly improved decomposition results in terms of all four performance indices ($p < 0.00001$). In addition, the validity-based system has lower STD for all performance measures ($p < 0.02$), which shows that the system has better overall and less variable performance. The improvement in decomposition results (especially CC_r and E_{NMUPTs}) increases as the complexity of the signal increases, such that for the last four

Table 8.1: Characteristics of the simulated EMG signals used along with the performance of the decomposition algorithms of the DQEMG and the validity-based decomposition system for these signals. Note: for E_{NMUPTs} the mean absolute value is presented.

Signal	Intensity (pps)	No. of MUPTs	Jitter (ms)	IDI-CV	Original DQEMG				Validity-based system			
					A_r (%)	A_c (%)	CC_r (%)	E_{NMUPTs}	A_r (%)	A_c (%)	CC_r (%)	E_{NMUPTs}
1	30.5	3	100	0.15	92.1	97.2	89.5	0	98.1	98.3	96.4	0
2	35.3	4	50	0.15	93.5	99.4	92.9	0	98.6	100.0	98.6	0
3	41.8	5	100	0.15	87.8	97.5	85.6	0	97.4	97.4	94.8	0
4	45.6	4	50	0.15	88.8	93.1	82.7	0	97.8	96.4	94.3	0
5	54.0	6	50	0.15	92.6	98.0	90.7	0	97.4	99.6	97.0	0
6	59.4	7	100	0.15	90.7	95.9	87.0	0	95.8	99.6	95.4	0
7	61.4	6	75	0.15	78.0	96.4	75.2	1	93.5	98.1	91.7	0
8	62.6	6	150	0.10	70.7	74.4	52.6	4	87.7	92.0	80.6	0
9	62.6	6	150	0.30	72.3	80.4	58.1	3	90.2	88.6	79.9	1
10	68.2	7	50	0.15	90.2	96.4	86.9	0	94.6	98.4	93.1	0
11	70.7	7	100	0.15	73.3	96.9	71.0	3	95.3	98.5	93.9	0
12	79.3	8	25	0.15	91.0	82.3	74.9	0	93.6	99.1	92.8	0
13	82.5	8	100	0.15	83.5	89.8	75.0	2	90.2	95.3	86.0	0
14	85.2	9	50	0.15	89.3	87.3	78.0	-1	93.2	97.9	91.2	0
15	88.4	9	75	0.20	98.1	68.8	67.5	-1	90.5	96.3	87.1	0
16	91.7	7	50	0.15	80.5	85.8	69.0	1	87.8	95.8	84.1	0
17	94.6	9	50	0.20	87.2	89.6	78.2	1	91.3	91.5	83.5	1
18	94.6	9	150	0.15	78.8	85.4	67.3	3	91.1	90.9	82.9	0
19	95.6	9	50	0.30	87.0	80.9	70.4	3	94.3	90.6	85.5	0
20	95.6	9	75	0.30	77.3	85.9	66.4	4	88.7	86.0	76.2	1
21	95.9	9	50	0.10	87.9	81.7	71.8	3	92.7	96.2	89.1	0
22	96.0	9	150	0.30	75.7	72.0	54.5	5	90.8	85.8	77.9	1
23	97.5	10	100	0.15	87.6	84.8	74.3	1	91.8	95.8	87.9	0
24	105.2	9	50	0.15	80.6	87.1	70.2	4	91.3	97.6	89.1	0
25	109.5	9	75	0.15	88.1	83.4	73.5	1	90.6	96.7	87.6	0
26	116.5	8	75	0.15	71.9	90.3	65.0	5	88.7	96.7	85.8	0
27	119.4	10	75	0.15	78.5	70.2	55.2	2	86.3	87.5	75.5	1
28	120.6	11	50	0.15	72.9	87.3	63.6	4	87.6	90.0	78.8	1
29	127.5	11	50	0.15	81.6	83.7	68.3	4	87.6	94.7	83.0	0
30	135.2	10	75	0.30	68.2	80.2	54.7	5	88.0	88.6	78.0	1
31	134.5	10	50	0.30	76.8	89.5	68.8	5	90.7	89.5	81.1	1
32	135.8	10	150	0.30	62.4	82.3	51.3	7	79.0	84.6	66.9	2
		Mean			**82.3**	**86.7**	**71.6**	**2.3**	**91.6**	**94.2**	**86.4**	**0.3**
		STD			**8.6**	**8.3**	**11.5**	**2.0**	**4.2**	**4.6**	**7.5**	**0.5**

117

Table 8.2: The performance of the original decomposition algorithms of the DQEMG system and the validity-based decomposition system for real EMG signals. Note: for E_{NMUPTs} the mean absolute value is presented.

Signal	Intensity(pps)	No. of MUPTs	Original DQEMG A_r (%)	A_c (%)	CC_r (%)	E_{NMUPTs}	Validity-based system A_r (%)	A_c (%)	CC_r (%)	E_{NMUPTs}
1	26.7	3	100.0	100.0	100.0	0	99.8	99.8	99.6	0
2	33.8	4	100.0	100.0	100.0	0	100.0	100.0	100.0	0
3	48.9	5	93.0	99.9	92.9	0	97.9	100.0	97.9	0
4	63.9	6	99.3	99.8	99.1	0	99.8	100.0	99.8	0
5	65.4	6	99.7	100.0	99.7	0	99.6	99.8	99.4	0
6	65.6	7	98.1	99.8	97.9	0	99.8	100.0	99.8	0
7	65.7	7	99.8	100.0	99.8	0	100.0	100.0	100.0	0
8	66.9	7	94.4	100.0	94.4	0	99.6	99.6	99.2	0
9	71.7	7	84.7	99.8	84.4	1	98.6	98.7	97.3	0
10	74.1	7	96.4	99.4	95.7	0	98.1	99.9	98.0	0
11	79.4	8	91.7	99.4	91.2	0	97.8	99.2	97.0	0
12	80.2	8	95.1	97.8	93.1	0	96.3	98.5	94.9	0
13	115.8	9	94.6	98.9	93.5	0	96.6	99.7	96.3	1
14	70.5	10	98.7	87.9	86.8	-1	99.1	99.5	98.6	0
15	90.3	10	96.8	99.8	96.7	0	97.3	99.4	96.8	0
16	86.6	10	96.6	99.0	95.7	0	98.1	99.2	97.3	1
17	105.0	10	95.7	99.9	95.6	0	98.9	99.7	98.6	0
18	116.2	10	96.4	72.3	69.7	-3	97.8	99.4	97.2	0
19	105.8	11	95.6	98.2	93.9	0	97.7	99.1	96.8	0
20	112.3	11	88.4	87.9	77.7	3	94.8	98.2	93.1	0
21	112.4	11	82.7	97.0	80.2	4	91.0	95.4	86.7	0
22	114.3	11	86.6	98.8	85.6	0	94.8	98.2	93.1	0
23	89.7	12	99.1	61.7	61.2	-5	99.1	99.5	98.6	0
24	120.7	12	94.6	98.6	93.3	0	97.1	99.3	96.4	0
25	119.7	13	91.6	98.5	90.2	1	94.4	99.4	93.8	2
26	130.3	13	90.1	98.6	88.9	1	96.6	98.9	95.5	0
27	146.1	14	86.6	89.9	77.8	1	93.9	98.7	92.7	0
28	152.8	14	90.1	98.6	88.9	1	93.2	98.3	91.7	0
29	157.4	15	91.4	90.6	82.8	-1	96.1	98.8	94.9	0
30	155.0	15	86.1	98.7	84.9	1	93.0	98.5	91.5	1
Mean			**93.8**	**95.7**	**89.7**	**0.8**	**97.2**	**99.1**	**96.4**	**0.2**
STD			**5.0**	**8.7**	**9.3**	**1.3**	**2.4**	**0.9**	**3.1**	**0.5**

signals, each having intensity > 134 pps, the CC_r values are improved by at least 12.4 % and either A_r or A_c or both are significantly improved.

The results presented in Table 8.1 reveal that both the validity-based system and the original decomposition algorithms of the DQEMG can successfully decompose EMG signals with low to moderate complexity and with varying MUP shapes and MU firing pattern variability. These accuracies may be sufficiently high for clinical application of EMG decomposition results when several physiological parameters, such as the MUP template and the mean firing rate for each MU, are required. The performance of both the validity-based system and the decomposition algorithms of the DQEMG decreases as the complexity of the signal increases, but the validity-based system performed better than the DQEMG for complex signals. In fact, the advantage of the validity-based system for relatively simple signals may not be as evident as for highly complex signals. As shown, for the first six EMG signals, which have low complexity, both algorithms correctly estimated the number of expected MUPTs and decomposed the signal with A_r > 93.1% and A_c > 87.1 %. However, for the last nine signals, each having an intensity > 100 pps, the DQEMG extracted 37 extra MUPTs (4.1 extra MUPTs/signal) while the validity-based developed system extracted only 6 extra MUPTs (0.7 extra MUPTs/signal). In addition, the average CC_r for the DQEMG for these nine signals is 63.4 % while that of the validity-based system is 80.6 % (+17.2% improvement). The significant reduction in E_{NMUPTs} and CC_r achieved using the validity-based system for the last nine signals demonstrate the advantage of the validity-based system over the DQEMG.

In general, the results obtained using the real data presented in Table 8.2 are consistent with those presented for the simulated data; the validity-based decomposition system outperformed the DQEMG in terms of the average and STD values of all four performance measures, which shows that the validity-based system has higher overall and less variable (or more robust) performance. However, both systems performed better on the real data set than on the simulated data set. One possible reason is that the MU firing pattern and MUP shape variability in the real signals are lower than that in the simulated signals. The other possible reason is that the similarity between MUPs created by different MUs in the real data used are lower than that in the simulated data.

Figures 8.4 and 8.5 present decomposition results for simulated EMG signal 14 for both the DQEMG and the validity-based system, respectively. The EMG signal used is composed of 9 MUPTs and was simulated to have a jitter value of 50 µs and an IDI- CV of 0.15. For each MUPT, the accuracy and

identification rate (ID rate) are presented. Comparing MU firing patterns plots and the accuracy and identification rate values presented for each train in these two figures reveals the advantages of using the validity-based system. As shown, both the accuracy and completeness (ID rate) of the majority of the trains created by the validity-based system are improved relative to those created by the DQEMG. Similar improvement can also be seen in the IDI histogram and MU firing rate plot of each MUPT. More importantly, the decomposition algorithms of the DQEMG underestimated the expected number of MUPTs. Two MUPTs (Trains 4 and 9 according to Figure 8.5) were mistakenly merged and reported as Train 4. On the other hand, the validity-based system correctly estimated the number of expected MUPTs.

For the example shown in Figures 8.6 and 8.7 both systems correctly estimated the number of MUPTs composed the EMG signal used, but the MUPTs obtained using the validity-based decomposition system are more accurate and complete than the trains obtained using the decomposition algorithms of the DQEMG. With the validity-based decomposition system, the accuracy for train # 2 was improved by 11% and the assignment rate (ID rate) for trains 4, 5, and 6 was improved by 25%, 23%, and 39%, respectively. Comparing the MU firing plots (last column) for the trains obtained by these two systems reveals the consequence of this improvement.

Increases in MU firing pattern or MUP shape variability can decrease the performance of a decomposition system. Nonetheless, for the EMG signals with relatively high jitter and IDI–CV values studied, the improvement gained using the validity-based system was significant.

The DQEMG and the validity-based system are for decomposing intramuscular EMG signals mainly for clinical application where several physiological parameters, such as the MUP template and mean MU firing rate for each MUPT, are required. Since these parameters can be estimated from incomplete MUPTs, superimposed MUPs are not resolved by these two systems. In fact, the majority of MUPs left unassigned by these algorithms are superimposed MUPs. In addition, low amplitude MUPs, which are composed of low frequency components and created by MUs with no muscle fibers close to the electrode detection surface, are neither detected nor considered for clustering and supervised classification. If such MUPs were detected and then considered for clustering and supervised classification, the accuracies of both systems may not be as high as those presented in Tables 8.1 and 8.2. Finally, the accuracies of both DQEMG and the validity-based system for EMG signals contaminated by high levels of noise may be lower than the values reported for the simulated and real EMG signals used in this work.

Both the DQEMG and the validity-based system assume the mean and standard deviation of the IDIs of the MUs that contributed to the signal being decomposed did not change during signal detection. Such assumptions are valid for EMG signals detected during short-term isometric contraction; however, these assumptions may not be realistic for EMG signals detected during either force-varying or long contractions. Such limitations restrict the use of both DQEMG and the validity-based system for research applications where the decomposition of signals detected during non-isometric or long-term contractions are required. Nevertheless, DQEMG has been used successfully for the decomposition of intramuscular EMG signals detected for clinical applications [7], [8], [12], [13], [18], [20], [21], [32].

Validating MUPTs during EMG decomposition and correcting invalid MUPTs takes time. The average processing time of the DQEMG for the simulated data used was 15.9 s while that for the validity-based system was 23.6s; the DQEMG is approximately 1.5 times faster than the validity-based system. The algorithms are currently encoded in Matlab (The Mathworks, Natick, MA) and processing was carried out on a computer with an Intel Core 2 Duo E8400 CPU (6M Cache, 3.00 GHz clock, 1333 MHz FSB) and 3GB of RAM. For both systems, the processing time is proportional to the number of MUPTs and the number of MUPs assigned. The average rate of increase of computation time versus intensity (pps) for DQEMG and the validity-based system was estimated to be 0.3 s/pps and 0.5 s/pps, respectively. Nonetheless, both DQEMG and the validity-based system are fast enough to be useful for clinical applications.

8.5 Conclusions

An innovative program for EMG signal decomposition has been presented. The MUPs comprising a given EMG signal are first detected using a threshold-based algorithm and then grouped into several MUPTs using STBC and a certainty-based algorithm. The developed system uses MUPT validity techniques to efficiently estimate the numbers of MUPTs comprising a given EMG signal by splitting merged MUPTs and merging MUPTs having similar MUP templates. To reduce the number of FCEs and MCEs in the extracted MUPTs: a) contaminated MUPTs are indentified and corrected; b) the assignment threshold for each train is increased or decreased based on the estimated validity of the train. The rate of decrease is dependent on the similarity of MUP templates between trains (i.e., adaptive classification). Evaluation results using several simulated and real EMG signals demonstrate that the validity-based system is more robust and accurate but slower than the decomposition algorithms of DQEMG.
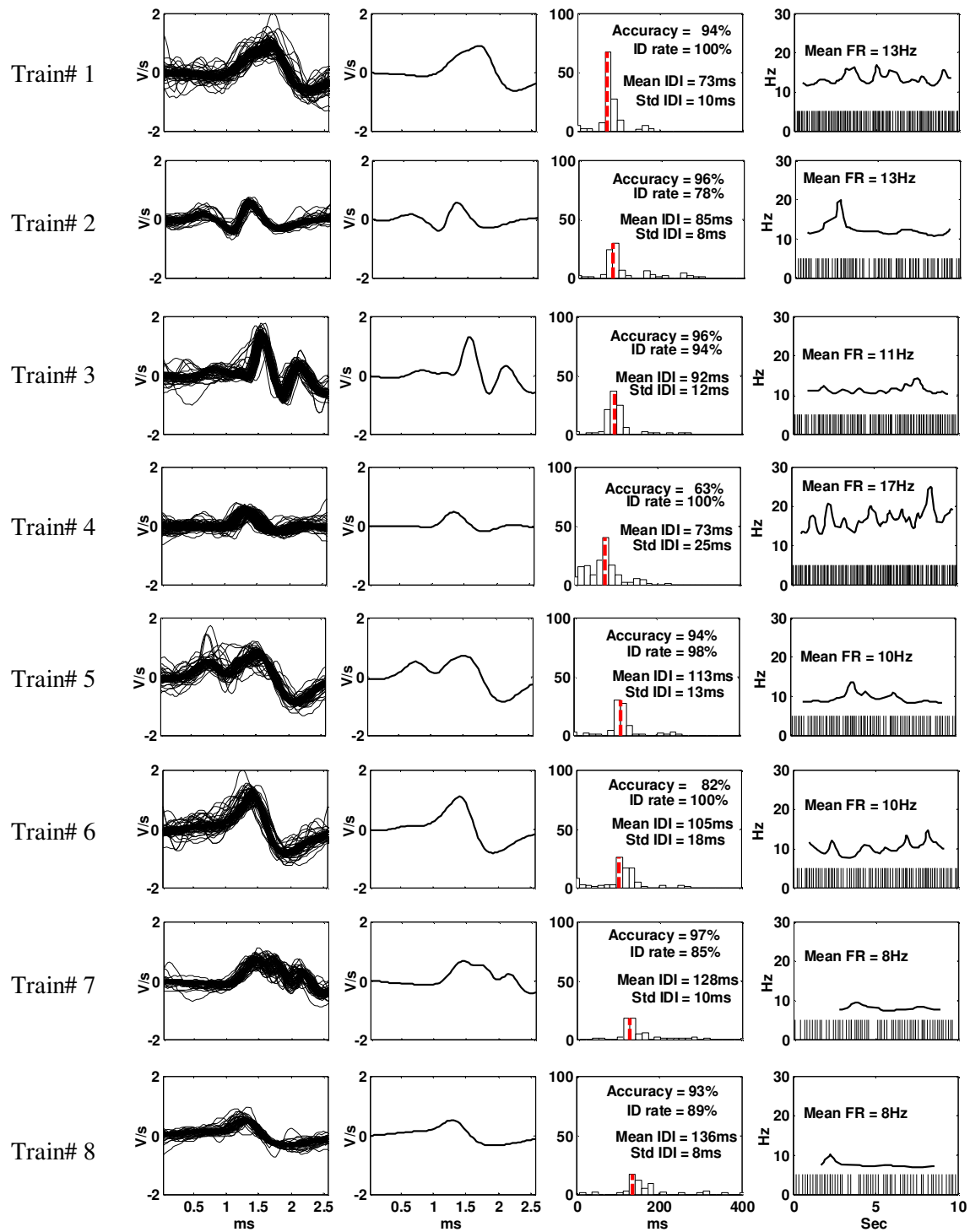
Figure 8.4: Decomposition results for simulated EMG signal 14 obtained using the decomposition algorithms of the DQEMG.

122
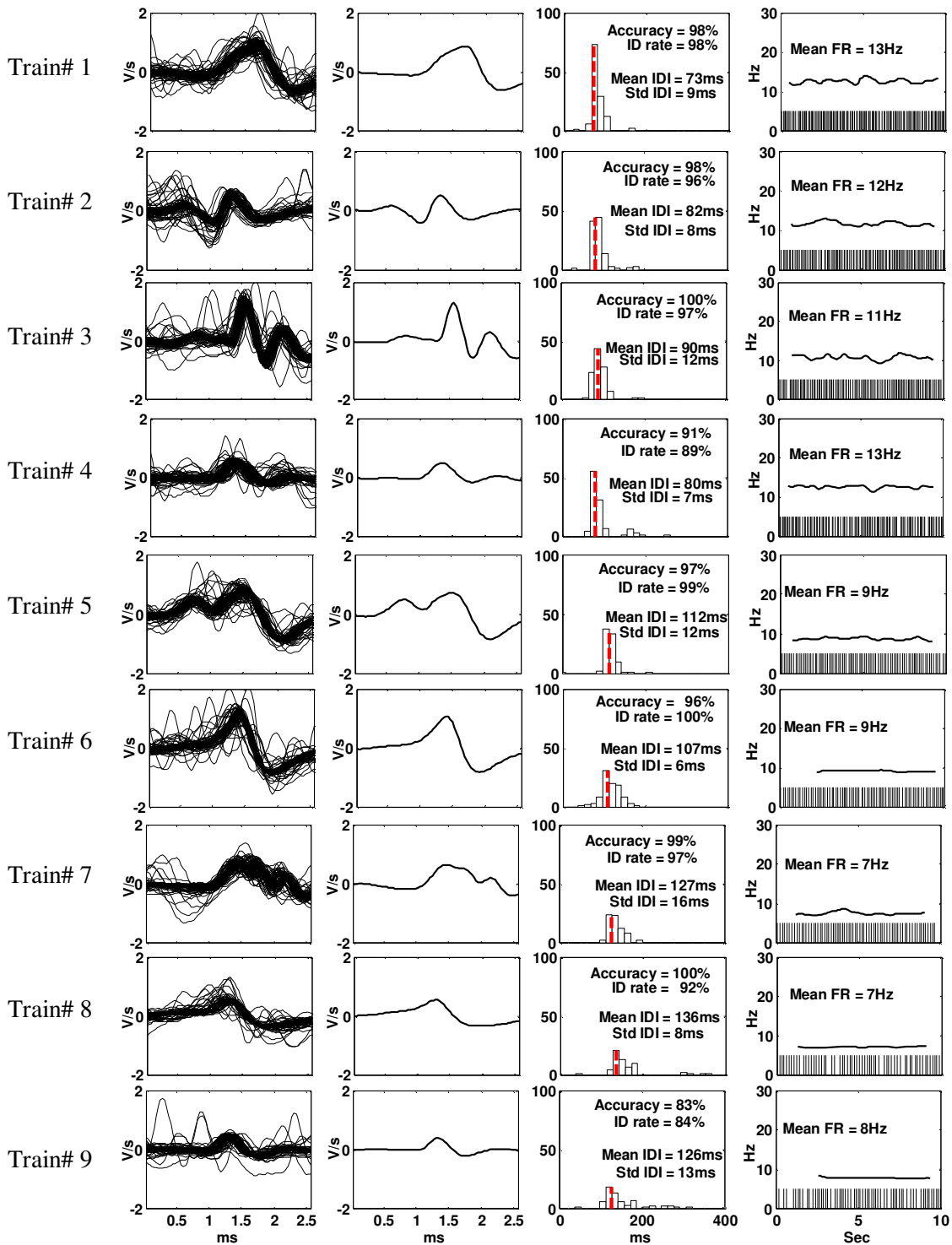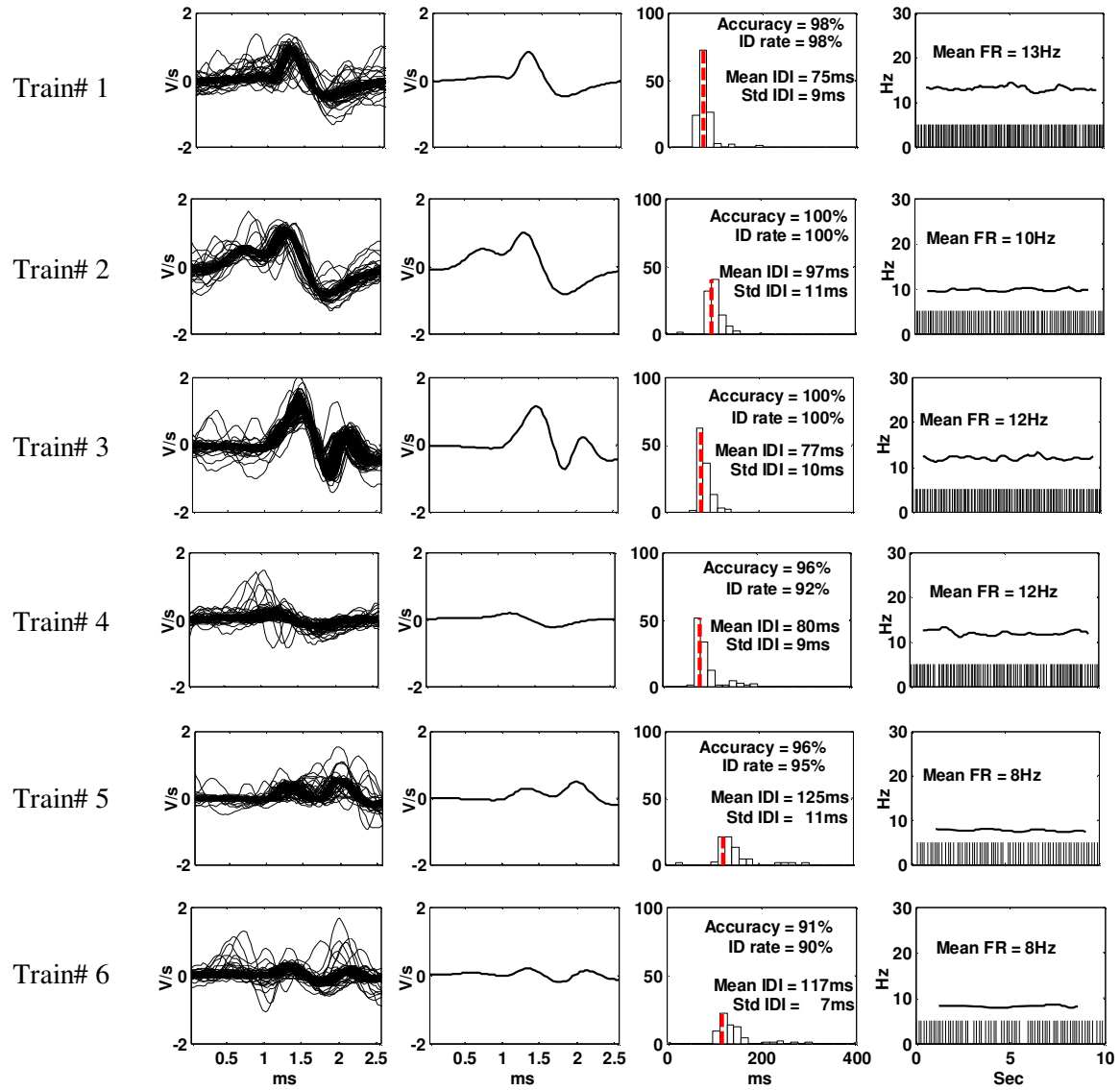
Figure 8.5: Decomposition results for simulated EMG signal 14 obtained using the validity-based decomposition system.
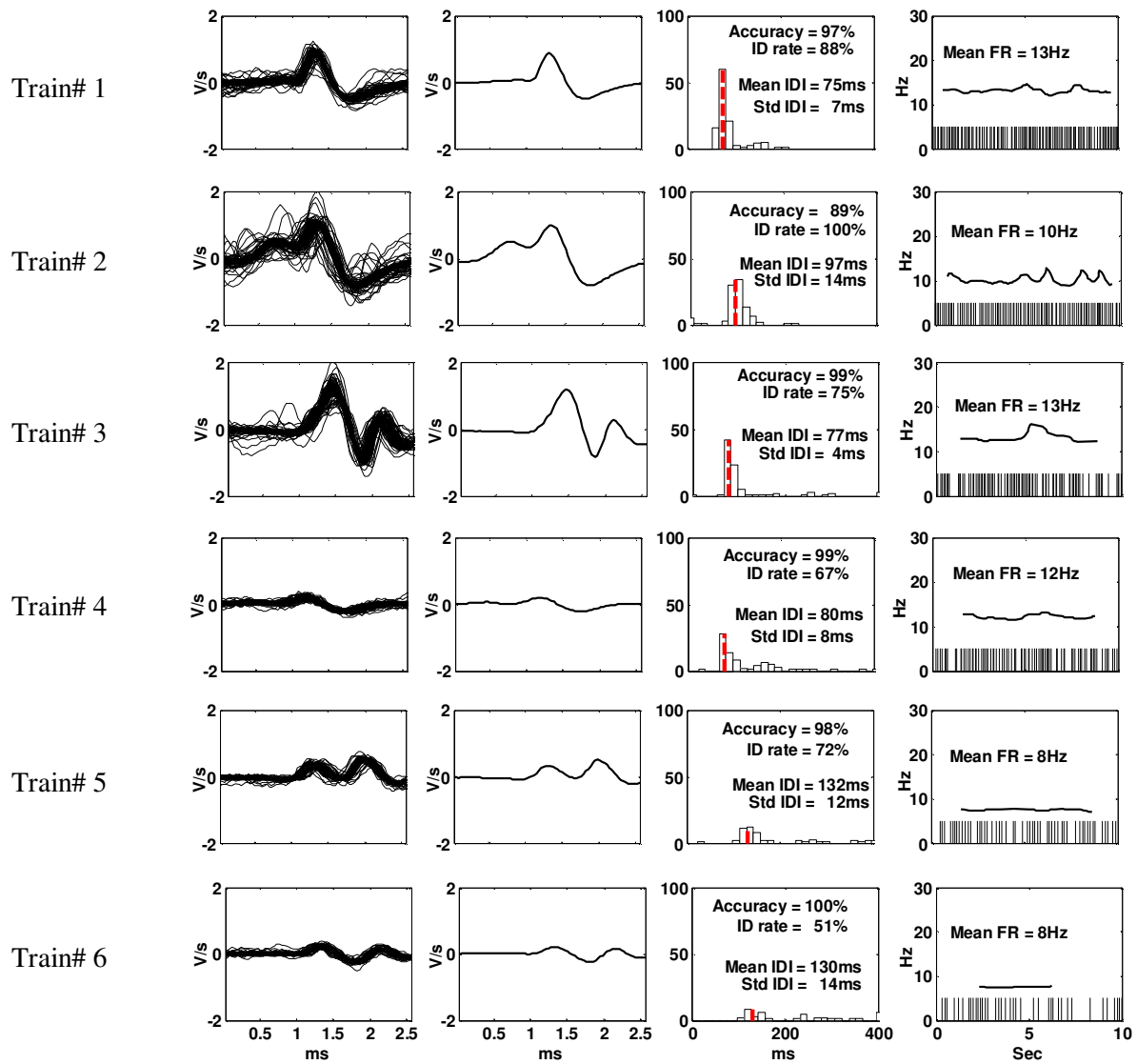
Figure 8.6: Decomposition results obtained using the decomposotion algorithms of the DQEMG for an EMG signal composed of 6 MUPTs.

Figure 8.7: Decomposition results obtained using the validity-based decomposition sysetm for the same signal of Figure 8.6.

Chapter 9

Conclusions and Future Work

9.1 Conclusions

Decomposition of an EMG signal may result in several invalid MUPTs that do not accurately represent the activity of a signal MU; such invalid MUPTs must be identified and then either corrected or excluded before extracted MUPTs are quantitatively analyzed. In addition, detecting and then correcting invalid MUPTs during decomposition can improve the results in terms of finding the correct numbers of MUPTs that constitute a given signal as well as decreasing the MCE and FCE rates in the extracted trains.

Characteristics of IDI histograms, MU firing rates over time and within-train MUP shape inconsistencies of MUPTs extracted during EMG decomposition can be used to estimate their validity. The existing qualitative MUPT validation methods, which typically need human operator supervision, are time consuming, related to operator experience and skill, and cannot assist with improving the performance of automatic EMG decomposition systems. To overcome these issues, in this thesis the possibility of developing automatic MUPT validation algorithms has been explored. Several algorithms, based on pattern recognition techniques, have been developed and evaluated using both simulated and real data. With the methods presented in this work, the validity of a MUPT is estimated using either its MU firing pattern information or its MUP shape information or both types of information. Based on the results obtained, the methods that use only shape or only firing pattern information did not perform as well as the ones that used both types of information, especially for invalid trains.

Among the supervised classifiers developed and evaluated to estimate MU firing pattern validity of a train, the Switching classifier that first identifies the type of data and then classifies it using either the SVM algorithm or FDA, depending on data identification, showed the best performance. The accuracy of classifiers in categorizing invalid trains was very high (> 95%) for most cases, but it decreases as the MCE rate in trains increases and suggests the need, in some cases, for the combined use of MU firing pattern and MUP shape information.

Classical cluster validation methods employed to estimate MUP-shape validity of a MUPT are either computationally complex (the gap statistic and jump methods) or inaccurate in classifying valid trains (the Beal and DH methods) when using 80 first-order discrete derivative data points as MUP features. However, the newly developed adaptive methods are sufficiently fast and accurate to be used during or after the decomposition of EMG signals. The fastest methods, the adaptive gap-based Duda and Hart method with an average computation time of 70 ms per train, had relatively high accuracy in correctly categorizing the MUPTs extracted during decomposition. The estimated average accuracy of this algorithm was 91.5% and 94.9% for simulated and real data, respectively, but the accuracy with which invalid MUPTs can be detected is dependent on the similarity of the MUP templates of the MUPTs comprising an invalid train, which suggests the need for the use of MU firing pattern as well as MUP shape information in evaluating such extracted MUPTs

For the systems that use both MU firing pattern and MUP shape information to estimate the validity of a MUPT, the methods that separately estimate MU firing validity and MUP-shape validity and then estimate the validity of the train by fusing these two indices using trainable fusing methods performed better than the single classifier scheme that estimates MUPT validity by a SVM, especially for the real data used. The MVDH that combines the outputs of the FPVC and that of the AGDH using an AND operation had the lowest accuracy in classifying valid MUPTs. Of the fusion methods evaluated, the trainable techniques on average outperformed the non-trainable ones such that the LRMC in which the MU firing pattern validity and MUP shape validity are aggregated using a logistic regression classifier showed robust classification performance in classifying MUPTs ($A_T > 98.4\%$). However, the ANDMC which combines these two validity indices using an AND operation performed better than the LRMC for rejecting invalid trains, especially for invalid trains with high MCE rate. In addition, the ANDMC could be faster than the LRMC. Consequently, using the ANDMC during the early stages of decomposition and

then the LRMC during the latter stages of decomposition and/or after decomposition for post processing the extracted MUPTs may be the most practical way of using these two MUPT validation classifiers

A method for detecting MUPTs contaminated with a high number of FCEs during EMG signal decomposition and then removing the FCEs from a contaminated train was also developed and evaluated. Of the supervised classifiers used to determine the class label of MUPTs (i.e., contaminated train or non-contaminated train) the FDA showed the best overall performance with $A_T > 84$ %. For a given contaminated MUPT, the FCE-detection algorithm on average correctly detected 83.4% of the FCEs and left 93.4% of the correctly assigned MUPs. The accuracy of the MUPs classified to a MUPT was estimated to be 92.1% on average. For the FDA classifier the accuracy in classifying contaminated MUPTs decreases as the percentage of MCEs in a MUPT increases. Likewise, the sensitivity of the FCE detection algorithm in detecting a FCE assigned decreases as either the similarity between the MUP and the MUP template of the MUPT or the MCE rate in the train increases. Nevertheless, the overall accuracy of both FDA and the FCE detection algorithm is promising and they can be used to improve the decomposition results or to facilitate editing extracted MUPTs.

Finally, the effectiveness of using the developed MUPT validation systems and the MUPT editing methods during EMG signal decomposition was investigated by integrating these algorithms into a certainty-based EMG signal decomposition algorithm. The new validity-based decomposition system employs: a) the ANDMC or LRMC to merge and split MUPTs, b) the FDA-based SCC and the FCE detection algorithm to detect and then edit contaminated MUPTs. The system also adjusts the assignment threshold for each individual MUPT adaptively based on its validity and the similarity between its MUP template and that of the closest train. When these changes were made to the certainty-based EMG signal decomposition algorithm used, the decomposition accuracy was improved by 7.5% (from 86.7% to 94.2%) on average; moreover a significant improvement was achieved in correctly estimating the number of MUPTs represented in a set of detected MUPs.

9.2 Future Work

For extending this research, several major directions as summarized below are proposed:

1. When developing the SVM-based MUPT validation system, the best MU firing pattern and MUP-shape classifiers were combined. Even though the developed system was both fast and accurate to be used during decomposition, there is a possibility that aggregating the other classifiers used in

this work or even existing classification techniques that were not studied here will provide a system as accurate as, but faster than, the current one.

2. As discussed above, the accuracy of the FDA-based SCC classifier decreases when the MCE rate in a MUPT increases. Using classifier fusion techniques may resolve this issue. Using several MUP-shape features along with the MU firing pattern features used may also improve the performance of the SCC. The MUP-shape features can be extracted based on the methods presented for finding the outliers in a cluster [186-188] or even the methods developed for detecting super-imposed MUPs in a MUPT [189].

3. The EFE algorithm underestimates σ and overestimates μ for trains with either high MCE rate or high CV. Developing a new algorithm or modifying the EFE algorithm to improve the estimation error, especially for trains with a high MCE rate, may improve the accuracy of the SVM-based MUPT validation system, the FDA-based SCC, the FCE detecting algorithm, and decomposition results.

4. The certainty-based classifier only measures the confidence in assigning a MUP to the two closet trains found using a distance measure. Re-designing this classifier such that it provides the certainty values for all extracted MUPTs instead of just the first and second closest MUPTs may improve the decomposition accuracy.

5. In the current validity-based decomposition system, the certainty assignment threshold for a valid MUPTs is decreased based the pseudo-correlation between the MUP template of this train and that of the closet train. Such a strategy can be used for an invalid train as well; the rate of increasing the assignment threshold can be adjusted based on the similarity between the MUP templates of the extracted trains. In addition, using other similarity measures to estimate the similarity between MUPTs may give better performance than the pseudo-correlation, which measures the similarity between the centers of the trains. When the similarity between the centers of two trains is low, there is no guarantee that these two trains are separate. The similarity measures proposed to measure the similarity between two clusters can be explored.

6. Further analysis of the developed decomposition system, especially using clinical EMG signals acquired: a) from with myopathic and neurogenic muscles; b) during force-varying contractions.

Bibliography

[1]   D. Stashuk, "EMG signal decomposition: how can it be accomplished and used?," *J Electromyogr Kinesiol.*, vol. 11, no. 3, pp. 151-173, Jun. 2001.

[2]   J. V. Basmajian and C. J. D. Luca, *Muscles Alive: Their Functions Revealed by Electromyography*, 5th ed. Williams & Wilkins, 1985.

[3]   C. J. De Luca, "Physiology and mathematics of myoelectric signals," *IEEE Trans Biomed Eng.*, vol. 26, no. 6, pp. 313-325, Jun. 1979.

[4]   [Online]. Available: http://www.operativemonitoring.com/emg.htm.

[5]   R. S. Lefever and C. J. De Luca, "A Procedure for Decomposing the Myoelectric Signal Into Its Constituent Action Potentials - Part I: Technique, Theory, and Implementation," *IEEE Trans Biomed Eng.*, vol. 29, no. 3, pp. 149-157, 1982.

[6]   R. S. Lefever, A. P. Xenakis, and C. J. De Luca, "A Procedure for Decomposing the Myoelectric Signal Into Its Constituent Action Potentials-Part II: Execution and Test for Accuracy," *IEEE Trans Biomed Eng.*, vol. 29, no. 3, pp. 158-164, 1982.

[7]   D. W. Stashuk, "Decomposition and quantitative analysis of clinical electromyographic signals," *Med Eng Phys.*, vol. 21, no. 6, pp. 389-404, Jul. 1999.

[8]   C. Farkas, A. Hamilton-Wright, H. Parsaei, and D. W. Stashuk, "A review of clinical quantitative electromyography," *Crit Rev Biomed Eng.*, vol. 38, no. 5, pp. 467-485, 2010.

[9]   E. V. Stalberg and B. Falck, "The role of electromyography in neurology," *Electroencephalogr Clin Neurophysiol.*, vol. 103, no. 6, pp. 579-598, Dec. 1997.

[10]   A. Fuglsang-Frederiksen, "The role of different EMG methods in evaluating myopathy," *Clin Neurophysiol.*, vol. 117, no. 6, pp. 1173-1189, Jun. 2006.

[11]   M. Tröger and R. Dengler, "The role of electromyography (EMG) in the diagnosis of ALS," *Amyotroph Lateral Scler*, vol. 1, no. 2, pp. 33-40, Jan. 2000.

[12]   L. J. Pino, D. W. Stashuk, and S. Podnar, "Bayesian characterization of external anal sphincter muscles using quantitative electromyography," *Clin Neurophysiol.*, vol. 119, no. 10, pp. 2266-2273, Oct. 2008.

[13]   L. J. Pino, D. W. Stashuk, S. G. Boe, and T. J. Doherty, "Motor unit potential characterization using 'pattern discovery'," *Med Eng Phys.*, vol. 30, no. 5, pp. 563-573, Jun. 2008.

[14]   C. J. de Luca, R. S. LeFever, M. P. McCue, and A. P. Xenakis, "Behaviour of human motor units in different muscles during linearly varying contractions," *J Physiol.*, vol. 329, no. 1, pp. 113-128, Jan. 1982.

[15]   C. J. De Luca, R. S. LeFever, M. P. McCue, and A. P. Xenakis, "Control scheme governing concurrently active human motor units during voluntary contractions," *J Physiol.*, vol. 329, pp. 129-142, 1982.

[16]   P. Contessa, A. Adam, and C. J. De Luca, "Motor unit control and force fluctuation during fatigue," *J Appl Physiol*, vol. 107, no. 1, pp. 235-243, Jul. 2009.

[17] Z. C. Lateva and K. C. McGill, "Estimating motor-unit architectural properties by analyzing motor-unit action potential morphology," *Clin Neurophysiol.*, vol. 112, no. 1, pp. 127-135, Jan. 2001.

[18] A. Hamilton-Wright and D. W. Stashuk, "Clinical Characterization of Electromyographic Data Using Computational Tools," in *IEEE Symposium on Computational Intelligence and Bioinformatics and Computational Biology(CIBCB 06). 2006*, 2006, pp. 1-7.

[19] H. Parsaei, D. W. Stashuk, S. Rasheed, C. Farkas, and A. Hamilton-Wright, "Intramuscular EMG Signal Decomposition," *Crit Rev Biomed Eng.*, vol. 38, no. 5, pp. 435-465, 2010.

[20] S. G. Boe, D. W. Stashuk, W. F. Brown, and T. J. Doherty, "Decomposition-based quantitative electromyography: Effect of force on motor unit potentials and motor unit number estimates," *Muscle Nerve*, vol. 31, no. 3, pp. 365-373, 2005.

[21] K. M. Calder, D. W. Stashuk, and L. McLean, "Physiological characteristics of motor units in the brachioradialis muscle across fatiguing low-level isometric contractions," *J Electromyogr Kinesiol.*, vol. 18, no. 1, pp. 2-15, Feb. 2008.

[22] W. Boron, *Medical physiology: a cellular and molecular approach*, 2nd ed. Philadelphia PA: Saunders/Elsevier, 2009.

[23] D. Farina, R. Merletti, and D. F. Stegeman, "Biophysics of the Generation of EMG Signals," in *Electromyography: Physiology, Engineering, and Noninvasive Applications*, P. P. Roberto Merletti, Ed. 2004, pp. 81-105.

[24] E. V. Stålberg and M. Sonoo, "Assessment of variability in the shape of the motor unit action potential, the 'jiggle,' at consecutive discharges," *Muscle Nerve*, vol. 17, no. 10, pp. 1135-1144, 1994.

[25] S. H. Nawab, R. P. Wotiz, and C. J. De Luca, "Decomposition of indwelling EMG signals," *J Appl Physiol*, vol. 105, no. 2, pp. 700-710, Aug. 2008.

[26] D. W. Stashuk, D. Farina, and K. Søgaard, "Decomposition of Intramuscular EMG Signals," in *Electromyography*, P. P. Roberto Merletti, Ed. 2004, pp. 47-80.

[27] S. Rasheed, D. W. Stashuk, and M. S. Kamel, "Integrating Heterogeneous Classifier Ensembles for EMG Signal Decomposition Based on Classifier Agreement," *IEEE Trans Inf Technol Biomed*, vol. 14, no. 3, pp. 866-882, 2010.

[28] D. Zazula, D. Korosec, and A. Sostaric, "Computer-assisted decomposition of the electromyograms," in *11th IEEE Symposium on Computer-Based Medical Systems, 1998.*, 1998, pp. 26-31.

[29] U. Windhorst and H. Johansson, *Modern techniques in neuroscience research*. Springer, 1999.

[30] R. Merletti and P. Parker, *Electromyography: Physiology, Engineering, and Non-Invasive Applications*. Wiley-IEEE Press, 2004.

[31] R. Merletti and D. Farina, "Analysis of intramuscular electromyogram signals," *Philosophical Transactions of the Royal Society A: Mathematical, Physical and Engineering Sciences*, vol. 367, no. 1887, pp. 357-368, Jan. 2009.

[32] T. J. Doherty and D. W. Stashuk, "Decomposition-based quantitative electromyography: Methods and initial normative data in five muscles," *Muscle Nerve*, vol. 28, no. 2, pp. 204-211, 2003.

[33] K. C. McGill, M. Z. Kermani, and Z. C. Lateva, "Estimation of recruitment and firing rate in EMG signals," in *19th IEEE Eng Med Biol Soc*, 1997, vol. 3, pp. 1247-1248 vol.3.

[34] L. J. Dorfman, J. E. Howard, and K. C. McGill, "Motor unit firing rates and firing rate variability in the detection of neuromuscular disorders," *Electroencephalogr Clin Neurophysiol.*, vol. 73, no. 3, pp. 215-224, Sep. 1989.

[35] P. K. Kasi et al., "Motor unit firing characteristics in patients with amyotrophic lateral sclerosis," in *35th IEEE Ann. Bioeng. Conf., 2009:1-2.*, 2009, pp. 1-2.

[36] P. E. Barkhaus, S. D. Nandedkar, and D. B. Sanders, "Quantitative EMG in inflammatory myopathy," *Muscle Nerve*, vol. 13, no. 3, pp. 247-253, 1990.

[37] T. Brannagan, A. Hays, D. Lange, and W. Trojaborg, "The role of quantitative electromyography in inclusion body myositis," *Journal of Neurology, Neurosurgery, and Psychiatry*, vol. 63, no. 6, pp. 776-779, Dec. 1997.

[38] C. J. De Luca, A. Adam, R. Wotiz, L. D. Gilmore, and S. H. Nawab, "Decomposition of Surface EMG Signals," *J Neurophysiol*, vol. 96, no. 3, pp. 1646-1657, Sep. 2006.

[39] R. Merletti, M. Aventaggiato, A. Botter, A. Holobar, H. Marateb, and T. M. M. Vieira, "Advances in surface EMG: recent progress in detection and processing techniques," *Crit Rev Biomed Eng.*, vol. 38, no. 4, pp. 305-345, 2010.

[40] M. Gazzoni, D. Farina, and R. Merletti, "A new method for the extraction and classification of single motor unit action potentials from surface EMG signals," *J Neurosci Methods.*, vol. 136, no. 2, pp. 165-177, Jul. 2004.

[41] G. A. Garcia, R. Okuno, and K. Azakawa, "A decomposition algorithm for surface electrode-array electromyogram," *IEEE Eng Med Biol Mag.*, vol. 24, no. 4, pp. 63-72, Jul. 2005.

[42] B. U. Kleine, J. P. van Dijk, B. G. Lapatki, M. J. Zwarts, and D. F. Stegeman, "Using two-dimensional spatial information in decomposition of surface EMG signals," *J Electromyogr Kinesiol.*, vol. 17, no. 5, pp. 535-548, Oct. 2007.

[43] C. J. De Luca and W. J. Forrest, "An Electrode for Recording Single Motor Unit Activity During Strong Muscle Contractions," *IEEE Trans Biomed Eng.*, vol. 19, no. 5, pp. 367-372, 1972.

[44] H. P. Clamann, "Activity of single motor units during isometric tension," *Neurology*, vol. 20, no. 3, p. 254-, 1970.

[45] K. C. McGill, Z. C. Lateva, and H. R. Marateb, "EMGLAB: An interactive EMG decomposition program," *J Neurosci Methods.*, vol. 149, no. 2, pp. 121-133, Dec. 2005.

[46] E. Stålberg, "Macro EMG, a new recording technique.," *J Neurol Neurosurg Psychiatry*, vol. 43, no. 6, pp. 475-482, Jun. 1980.

[47] C. E. Shannon, "Communication in the Presence of Noise," in *Proc. Institute of Radio Engineers*, 1949, vol. 37, pp. 10-21.

[48] C. E. Shannon, "Communication In The Presence Of Noise," *Proceedings of the IEEE*, vol. 86, no. 2, pp. 447-457, 1998.

[49]   K. C. McGill, "A method for quantitating the clinical electromyogram," PhD dissertation, Stanford University, 1984.

[50]   K. C. McGill, K. L. Cummins, and L. J. Dorfman, "Automatic Decomposition of the Clinical Electromyogram," *IEEE Trans Biomed Eng.*, vol. 32, no. 7, pp. 470-477, Jul. 1985.

[51]   S. Usui and I. Amidror, "Digital Low-Pass Differentiation for Biological Signal Processing," *IEEE Trans Biomed Eng.*, vol. 29, no. 10, pp. 686-693, 1982.

[52]   S. H. Kanoun, "A new digital signal processing technique for the estimation of motor unit action potential templates," Master's thesis, University of Waterloo, 1999.

[53]   J. Fang, G. C. Agarwal, and B. T. Shahani, "Decomposition of multiunit electromyographic signals," *IEEE Trans Biomed Eng.*, vol. 46, no. 6, pp. 685-697, Jun. 1999.

[54]   X. Ren, W. Zhizhong, and H. Xiao, "EMG signal decomposition based on wavelet transform and ICA method," *Journal of Data Acquisition & Processing*, vol. 21, no. 3, pp. 272-276, Sep. 2006.

[55]   X. Ren, X. Hu, Z. Wang, and Z. Yan, "MUAP extraction and classification based on wavelet transform and ICA for EMG decomposition," *Med Biol Eng Comput.*, vol. 44, no. 5, pp. 371-382, May. 2006.

[56]   X. M. Ren, Z. G. Yan, Z. Z. Wang, and X. Hu, "Noise reduction based on ICA decomposition and wavelet transform for the extraction of motor unit action potentials," *J Neurosci Methods.*, vol. 158, no. 2, pp. 313-322, 2006.

[57]   A. O. Andrade, S. Nasuto, P. Kyberd, C. M. Sweeney-Reed, and F. R. Van Kanijn, "EMG signal filtering based on Empirical Mode Decomposition," *Biomed Signal Process Control*, vol. 1, no. 1, pp. 44-55, Jan. 2006.

[58]   C. I. Christodoulou and C. S. Pattichis, "Unsupervised pattern recognition for the classification of EMG signals," *IEEE Trans Biomed Eng.*, vol. 46, no. 2, pp. 169-178, Feb. 1999.

[59]   D. Zennaro, P. Wellig, V. M. Koch, G. S. Moschytz, and T. Laubli, "A software package for the decomposition of long-term multichannel EMG signals using wavelet coefficients," *IEEE Trans Biomed Eng.*, vol. 50, no. 1, pp. 58-69, Jan. 2003.

[60]   Di Ge, "Unsupervised Bayesian Decomposition of Multiunit EMG Recordings Using Tabu Search," *IEEE Trans Biomed Eng.*, vol. 57, no. 3, pp. 561-571, Jan. 2010.

[61]   A. Gerber, R. M. Studer, R. J. P. de Figueiredo, and G. S. Moschytz, "A New Framework and Computer Program for Quantitative EMG Signal Analysis," *IEEE Trans Biomed Eng.*, vol. 31, no. 12, pp. 857-863, Dec. 1984.

[62]   D. Stashuk and H. De Bruin, "Automatic decomposition of selective needle-detected myoelectric signals," *IEEE Trans Biomed Eng.*, vol. 35, no. 1, pp. 1-10, Jan. 1988.

[63]   C. S. Pattichis, C. N. Schizas, and L. T. Middleton, "Neural network models in EMG diagnosis," *IEEE Trans Biomed Eng.*, vol. 42, no. 5, pp. 486-496, 1995.

[64]   E. Stålberg, B. Falck, M. Sonoo, S. Stålberg, and M. Åström, "Multi-MUP EMG analysis -- a two year experience in daily clinical work," *Electroencephalogr Clin Neurophysiol.*, vol. 97, no. 3, pp. 145-154, Jun. 1995.

[65]   G. Loudon, N. Jones, and A. Sehmi, "New signal processing techniques for the decomposition of EMG signals," *Med Biol Eng Comput.*, vol. 30, no. 6, pp. 591-599, Nov. 1992.

[66]   C. D. Katsis, Y. Goletsis, A. Likas, D. I. Fotiadis, and I. Sarmas, "A novel method for automated EMG decomposition and MUAP classification," *Artif Intell Med.*, vol. 37, no. 1, pp. 55-64, 2006.

[67]   C. D. Katsis, T. P. Exarchos, C. Papaloukas, Y. Goletsis, D. I. Fotiadis, and I. Sarmas, "A two-stage method for MUAP classification based on EMG decomposition," *Comput Biol Med.*, vol. 37, no. 9, pp. 1232-1240, 2007.

[68]   Z. Erim and Winsean Lin, "Decomposition of Intramuscular EMG Signals Using a Heuristic Fuzzy Expert System," *IEEE Trans Biomed Eng.*, vol. 55, no. 9, pp. 2180-2189, Sep. 2008.

[69]   M. Nikolic and C. Krarup, "EMGTools, an adaptive and versatile tool for detailed EMG analysis," *IEEE Trans Biomed Eng.*, Aug. 2010.

[70]   J. R. Florestal, P. A. Mathieu, and A. Malanda, "Automated Decomposition of Intramuscular Electromyographic Signals," *IEEE Trans Biomed Eng.*, vol. 53, no. 5, pp. 832-839, May. 2006.

[71]   E. Zarei, K. Maghooli, and S. M. P. Firoozabadi, "A New Approach for EMG Decomposition Based on Overlaps Solution," in *15th Intternational Conference on Digital Signal Processing*, 2007, pp. 119-122.

[72]   D. Stashuk and G. Paoli, "Robust supervised classification of motor unit action potentials," *Med Biol Eng Comput.*, vol. 36, no. 1, pp. 75-82, Jan. 1998.

[73]   D. W. Stashuk and R. K. Naphan, "Probabilistic inference-based classification applied to myoelectric signal decomposition," *IEEE Trans Biomed Eng.*, vol. 39, no. 4, pp. 346-355, Apr. 1992.

[74]   D. Stashuk and Y. Qu, "Adaptive motor unit action potential clustering using shape and temporal information," *Med Biol Eng Comput.*, vol. 34, no. 1, pp. 41-49, Jan. 1996.

[75]   K. C. McGill and L. J. Dorfman, "Automatic decomposition electromyography (ADEMG): validation and normative data in brachial biceps," *Electroencephalogr Clin Neurophysiol.*, vol. 61, no. 5, pp. 453-461, Nov. 1985.

[76]   S. Rasheed, D. Stashuk, and M. Kamel, "Adaptive certainty-based classification for decomposition of EMG signals," *Med Biol Eng Comput.*, vol. 44, no. 4, pp. 298-310, Apr. 2006.

[77]   S. Rasheed, D. Stashuk, and M. Kamel, "Adaptive fuzzy k-NN classifier for EMG signal decomposition," *Med Eng Phys.*, vol. 28, no. 7, pp. 694-709, Sep. 2006.

[78]   S. Rasheed, D. Stashuk, and M. Kamel, "A software package for interactive motor unit potential classification using fuzzy k-NN classifier," *Comput Methods Prog Biomed.*, vol. 89, no. 1, pp. 56-71, 2008.

[79]   S. Rasheed, D. Stashuk, and M. Kamel, "Fusion of multiple classifiers for motor unit potential sorting," *Biomedical Signal Processing and Control*, vol. 3, no. 3, pp. 229-243, Jul. 2008.

[80]   S. Rasheed, D. Stashuk, and M. Kamel, "An interactive environment for motor unit potential classification using certainty-based classifiers," *Simulation Modelling Practice and Theory*, vol. 16, no. 9, pp. 1293-1311, Oct. 2008.

[81] S. Rasheed and D. Stashuk, "Pattern Classification Techniques for EMG Signal Decomposition," in *Advanced Biosignal Processing*, Springer Berlin Heidelberg, 2009, pp. 267-289.

[82] S. Rasheed, D. W. Stashuk, and M. S. Kamel, "Diversity-based combination of non-parametric classifiers for EMG signal decomposition," *Pattern Anal Appl.*, vol. 11, no. 3-4, pp. 385-408, 2008.

[83] S. Rasheed, D. Stashuk, and M. Kamel, "Diversity-based combination of non-parametric classifiers for EMG signal decomposition," *Pattern Analysis & Applications*, vol. 11, no. 3, pp. 385-408, 2008.

[84] K. C. McGill and L. J. Dorfman, "High-Resolution Alignment of Sampled Waveforms," *IEEE Trans Biomed Eng.*, vol. 31, no. 6, pp. 462-468, 1984.

[85] R. E. Bellman, *Adaptive Control Processes: A Guided Tour*, First Edition ~ 1st Printing. Princeton University Press, 1961.

[86] M. H. Hassoun, Chuanming Wang, and A. R. Spitzer, "NNERVE: Neural Network Extraction of Repetitive Vectors for Electromyography. II. Performance analysis," *IEEE Trans Biomed Eng.*, vol. 41, no. 11, pp. 1053-1061, Nov. 1994.

[87] M. H. Hassoun, Chuanming Wang, and A. R. Spitzer, "NNERVE: Neural Network Extraction of Repetitive Vectors for Electromyography. I. Algorithm," *IEEE Transactions on Biomedical Engineering*, vol. 41, no. 11, pp. 1039-1052, Nov. 1994.

[88] R. Sarbast, "A multiclassifier approach to motor unit potential classification for EMG signal decomposition," PhD dissertation, University of Waterloo, 2006.

[89] S. Rasheed, "A Hybrid Classifier Fusion Approach for Motor Unit Potential Classification During EMG Signal Decomposition," *IEEE Trans Biomed Eng.*, vol. 54, no. 9, pp. 1715-1721, Jan. 2007.

[90] J. Fang, G. C. Agarwal, and B. T. Shahani, "Decomposition of EMG signal by wavelet spectrum matching," in *19th Ann. Int. Conf. Eng. in Med. Biol. Soc.*, 1997, vol. 3, pp. 1253-1256 vol.3.

[91] P. Wellig, G. S. Moschytz, and T. Liiubli, "Decomposition of EMG signals using time-frequency features," in *20th IEEE Eng Med Biol Soc.*, 1998, vol. 3, pp. 1497-1500 vol.3.

[92] H. Nakamura, K. Nagai, and M. Yoshida, "Application of Independent Component Analysis and Expansion Matching Filter for Automatic Detection of Motor Unit Action Potential Trains," in *27th IEEE Eng Med Biol Soc.*, 2005, pp. 5013-5016.

[93] P. Wellig and G. S. Moschytz, "Electromyogram decomposition using the single-lineage clustering algorithm and wavelets," in *IEEE International Conference on Electronics, Circuits and Systems (ICECS '99), 1999.*, 1999, vol. 1, pp. 537-540 vol.1.

[94] P. Wellig, G. S. Moschytz, and T. Laubli, "Decomposition of electromyogram long-term recordings," in *The First Joint BMES/EMBS Conference*, 1999, vol. 1, p. 578 vol.1.

[95] R. Yamada, J. Ushiba, Y. Tomita, and Y. Masakado, "Decomposition of electromyographic signal by principal component analysis of wavelet coefficients," in *IEEE Asian-Pacific Conf Biomed Eng.*, 2003, pp. 118-119.

[96] M. Reaz, M. Hussain, and F. Mohd-Yasin, "Techniques of EMG signal analysis: detection, processing, classification and applications," *Biological Procedures Online*, vol. 8, no. 1, pp. 11-35, Dec. 2006.

[97]   J. Florestal, P. Mathieu, and K. Mcgill, "Automatic decomposition of multichannel intramuscular EMG signals," *J Electromyogr Kinesiol.*, vol. 19, no. 1, pp. 1-9, Feb. 2009.

[98]   A. K. Jain, M. N. Murty, and P. J. Flynn, "Data Clustering: A Review," vol. 31, no. 3, pp. 264-323, 1999.

[99]   Rui Xu and D. Wunsch, "Survey of clustering algorithms," *IEEE Trans Neural Networks*, vol. 16, no. 3, pp. 645-678, 2005.

[100] P. Berkhin, "A Survey of Clustering Data Mining Techniques," in *Grouping Multidimensional Data*, J. Kogan, C. Nicholas, and M. Teboulle, Eds. Springer, 2006, pp. 25-71.

[101] A. K. Jain, "Data clustering: 50 years beyond K-means," *Pattern Recogn Lett.*, vol. 31, no. 8, pp. 651-666, Jun. 2010.

[102] D. Steinley, "K-means clustering: a half-century synthesis.," *Br J Math Stat Psychol*, vol. 59, no. 1, pp. 1-34, 2006.

[103] A. Baraldi and P. Blonda, "A survey of fuzzy clustering algorithms for pattern recognition. I," *IEEE Trans Sys Man Cyber*, vol. 29, no. 6, pp. 778-785, 1999.

[104] A. Baraldi and P. Blonda, "A survey of fuzzy clustering algorithms for pattern recognition. II," *IEEE Trans Sys Man Cyber*, vol. 29, no. 6, pp. 786-801, 1999.

[105] R. O. Duda, P. E. Hart, and D. G. Stork, *Pattern Classification*, 2nd ed. Wiley-Interscience, 2000.

[106] S. R. Kulkarni, G. Lugosi, and S. S. Venkatesh, "Learning pattern classification-a survey," *IEEE Trans Inform Theory*, vol. 44, no. 6, pp. 2178-2206, 1998.

[107] S. Kotsiantis, I. Zaharakis, and P. Pintelas, "Machine learning: a review of classification and combining techniques," *Artif Intell Rev.*, vol. 26, no. 3, pp. 159-190, Nov. 2006.

[108] B. Mambrito and C. J. De Luca, "A technique for the detection, decomposition and analysis of the EMG signal," *Electroencephalogr Clin Neurophysiol.*, vol. 58, no. 2, pp. 175-188, Aug. 1984.

[109] R. Gut and G. S. Moschytz, "High-precision EMG signal decomposition using communication techniques," *IEEE Trans Biomed Eng.*, vol. 48, no. 9, pp. 2487-2494, 2000.

[110] V. M. Koch and H.-A. Loeliger, "Decomposition of electromyographic signals by iterative message passing in a graphical model," in *26th IEEE Eng Med Biol Soc*, 2004, vol. 1, pp. 65-68.

[111] V. M. Koch and H.-A. Loeliger, "EMG signal decomposition by loopy belief propagation," in *IEEE Conf. Acoust, Speech, Signal Process*, 2005, vol. 5, p. v/397-v/400 Vol. 5.

[112] P. Guiheneuc and J. Calamel, "Automatic detection and pattern recognition of single motor unit potentials in needle EMG," in *Computer-Aided Electromyography and Expert System*, vol. 10, J. E. Desmedt, Ed. Karger, Basal, 1983, pp. 73–127.

[113] S. Rasheed, "A software package for interactive motor unit potential classification using fuzzy k-NN classifier," *Computer Methods and Programs in Biomedicine*, vol. 89, no. 1, pp. 56-71, Jan. 2008.

[114] D. B. Sanders and E. V. Stålberg, "AAEM minimonograph #25: Single-fiber electromyography," *Muscle Nerve*, vol. 19, no. 9, pp. 1069-1083, 1996.

[115] J. V. Trontelj, J. Jabre, and M. Mihelin, "Needle and Wire Detection Techniques," in *Electromyography*, P. P. Roberto Merletti, Ed. 2004, pp. 27-46.

[116] W. F. Haas, R. M. Studer, G. S. Moschytz, and M. Meyer, "Computer-aided electromyography," in *IEEE Symp Circuits and Systems*, 1988, pp. 2131-2134 vol.3.

[117] W. F. Haas and M. Meyer, "An automatic EMG decomposition systemfor routine clinical examination and clinical research-ARTMUP," in *Computer-Aided Electromyography and Expert Systems*, J. E. Desmedt, Ed. Holland: Elsevier, 1989, pp. 67–81.

[118] C. D. Katsis, D. I. Fotiadis, A. Likas, and I. Sarmas, "Automatic discovery of the number of MUAP clusters and superimposed MUAP decomposition in electromyograms," in . *4th IEEE International EMBS Conference; Special Topic on Information Technology Applications in Biomedicine*, 2003, pp. 177-180.

[119] D. Zennaro, P. Wellig, G. S. Moschytz, T. Laubli, and H. Krueger, "A decomposition software package for the decomposition of long-term multi-channel electromyrographic signals," in *25th IEEE Eng Med Biol Soc*, 2001, vol. 2, pp. 1070-1073 vol.2.

[120] D. Zennaro et al., "A method to test reliability and accuracy of the decomposition of multi-channel long-term intramuscular EMG signal recordings," *J Industrial Ergonomics*, vol. 30, no. 4-5, pp. 211-224, Oct. 2002.

[121] R. Kothari and D. Pitts, "On finding the number of clusters," *Pattern Recogn Lett.*, vol. 20, no. 4, pp. 405-416, 1999.

[122] S. H. Nawab, R. P. Wotiz, L. M. Hochstein, and C. J. De Luca, "Next-generation decomposition of multi-channel EMG signals," in *2nd IEEE EMBS/BMES joint. Conf.*, 2002, vol. 1, pp. 36-37 vol.1.

[123] S. H. Nawab, R. P. Wotiz, and C. J. De Luca, "Multi-Receiver Precision Decomposition of Intramuscular EMG Signals," in *28th IEEE Eng Med Biol Soc.*, New York, NY, 2006, pp. 1252-1255.

[124] Shey-Sheen Chang, C. J. De Luca, and S. H. Nawab, "Aliasing rejection in Precision Decomposition of EMG signals," in *30th IEEE Eng Med Biol Soc.*, 2008, pp. 4972-4975.

[125] S. Rasheed, D. Stashuk, and M. Kamel, "Multi-classification techniques applied to EMG signal decomposition," in *IEE Int Syst Man and Cyber.*, The Hague, Netherlands, 2004, pp. 1226-1231.

[126] S. H. Nawab and V. Lesser, "Integrated processing and understanding of signals," in *Symbolic and knowledge-based signal processing*, A. V. Oppenheim and S. H. Nawab, Eds. Prentice-Hall, Inc., 1992, pp. 251-285.

[127] V. L. Hamid, S. H. Nawab, and F. I. Klassner, "IPUS: An Architecture for the Integrated Processing and Understanding of Signals," *Artif Intell*, vol. 77, pp. 129-171, 1995.

[128] E. Chauvet, O. Fokapu, J. Hogrel, D. Gamet, and J. Duchêne, "Automatic identification of motor unit action potential trains from electromyographic signals using fuzzy techniques," *Med Biol Eng Comput.*, vol. 41, no. 6, pp. 646-653, Nov. 2003.

[129] L. Di Stefano and S. Mattoccia, "Fast template matching using bounded partial correlation," *Machine Vision and Applications*, vol. 13, no. 4, pp. 213-221, Feb. 2003.

[130] H. Etawil and D. Stashuk, "Resolving superimposed motor unit action potentials," *Med Biol Eng Comput.*, vol. 34, no. 1, pp. 33-40, Jan. 1996.

[131] R. De Figueiredo and A. Gerber, "Separation of superimposed signals by a cross-correlation method," in *IEEE Int. Conf. on Acoustics, Speech, and Signal Processing*, 1982, vol. 7, pp. 391-394.

[132] P. Bonato and Z. Erim, "Solving superposition of motor unit action potential waveforms through a cross-time-frequency based methodology," in *22nd IEEE Eng Med Biol Soc*, 2000, vol. 2, pp. 920-923 vol.2.

[133] P. Bonato, Z. Erim, and J. A. Gonzalez-Cueto, "Decomposition of superimposed waveforms using the cross time frequency transform," in *23rd IEEE Eng Med Biol Soc.*, 2001, vol. 2, pp. 1066-1069 vol.2.

[134] S. Hamid Nawab, R. Wotiz, and C. J. De Luca, "Improved resolution of pulse superpositions in a knowledge-based system EMG decomposition," in *26th IEEE Eng Med Biol Soc*, 2004, vol. 1, pp. 69-71.

[135] H. R. Marateb and K. C. McGill, "Resolving Superimposed MUAPs Using Particle Swarm Optimization," *IEEE Trans Biomed Eng.*, vol. 56, no. 3, pp. 916-919, Mar. 2009.

[136] K. C. McGill, "Optimal resolution of superimposed action potentials," *IEEE Trans Biomed Eng.*, vol. 49, no. 7, pp. 640-650, Jul. 2002.

[137] J. R. Florestal, P. A. Mathieu, and Ré. Plamondon, "A Genetic Algorithm for the Resolution of Superimposed Motor Unit Action Potentials," *IEEE Trans Biomed Eng.*, vol. 54, no. 12, pp. 2163-2171, Dec. 2007.

[138] R. De Figueiredo and A. Gerber, "Separation of superimposed signals by a cross-correlation method," *IEEE Trans Acoustics, Speech, and Signal Processing*, vol. 31, no. 5, pp. 1084-1089, 1983.

[139] Z. Xu and S. Xiao, "Estimation of motor unit firing statistics from surface EMG," in *20th IEEE Eng Med Biol Soc*, 1998, vol. 5, pp. 2639-2642 vol.5.

[140] D. W. Stashuk and Y. Qu, "Robust method for estimating motor unit firing-pattern statistics," *Med Biol Eng Comput.*, vol. 34, no. 1, pp. 50-57, Jan. 1996.

[141] S. D. Nandedkar, P. E. Barkhaus, and A. Charles, "Multi-motor unit action potential analysis (MMA)," *Muscle Nerve*, vol. 18, no. 10, pp. 1155-1166, 1995.

[142] S. Nandedkar and D. Sanders, "Median averaging of electromyographic motor unit action potentials: comparison with other techniques," *Med Biol Eng Comput.*, vol. 27, no. 6, pp. 566-571, Nov. 1989.

[143] D. W. Stashuk, "Mean, median and mode estimation of motor unit action potential templates," in *IEEE 18th IEEE Eng Med Biol Soc*, 1996, vol. 4, pp. 1498-1499 vol.4.

[144] E. Stålberg, S. Andreassen, B. Falck, H. Lang, A. Rosenfalck, and W. Trojaborg, "Quantitative analysis of individual motor unit potentials: a proposition for standardized terminology and criteria for measurement," *Clin Neurophysiol.*, vol. 3, no. 4, pp. 313-348, Oct. 1986.

[145] K. C. McGill, Z. C. Lateva, and M. E. Johanson, "Validation of a computer-aided EMG decomposition method," in *26th IEEE Eng Med Biol Soc.*, 2004, vol. 2, pp. 4744-4747.

[146] N. Sheikholeslami and D. Stashuk, "Supervised mutual-information based feature selection for motor unit action potential classification," *Med Biol Eng Comput.*, vol. 35, no. 6, pp. 661-670, Nov. 1997.

[147] M. Nikolic, J. A. Sorensen, K. Dahl, and C. Krarup, "Detailed analysis of motor unit activity," in *19th IEEE Eng Med Biol Soc.*, Chicago, IL, USA, 1997, pp. 1257-1260.

[148] V. M. Koch, H.-A. Loeliger, and K. C. McGill, "Resolution of superpositions in EMG signals using belief propagation: Results for the known constituent problem," *28th IEEE Eng Med Biol Soc*, pp. 1260-1263, 2006.

[149] C. J. De Luca, "Reflections on EMG signal decomposition," in *Computer-Aided Electromyography and Expert System*, J. E. Desmedt, Ed. Elsevier, 1989, pp. 33-37.

[150] D. Farina, R. Colombo, R. Merletti, and H. Baare Olsen, "Evaluation of intra-muscular EMG signal decomposition algorithms," *J Electromyogr Kinesiol.*, vol. 11, no. 3, pp. 175-187, Jun. 2001.

[151] D. W. Stashuk, "Simulation of electromyographic signals," *Journal of Electromyography and Kinesiology*, vol. 3, no. 3, pp. 157-173, Sep. 1993.

[152] D. Farina, A. Crosetti, and R. Merletti, "A model for the generation of synthetic intramuscular EMG signals to test decomposition algorithms," *IEEE Trans Biomed Eng.*, vol. 48, no. 1, pp. 66-77, 2001.

[153] A. Hamilton-Wright and D. W. Stashuk, "Physiologically based simulation of clinical EMG signals," *IEEE Trans Biomed Eng.*, vol. 52, no. 2, pp. 171-183, 2005.

[154] F. Jahanmiri Nezhad, "Motor unit firing pattern analysis for adaptive EMG signal decomposition," University of Waterloo, 2006.

[155] C. J. Luca and W. J. Forrest, "Some properties of motor unit action potential trains recorded during constant force isometric contractions in man," *Kybernetik*, vol. 12, no. 3, pp. 160-168, Mar. 1973.

[156] P. B. Matthews, "Relationship of firing intervals of human motor units to the trajectory of post-spike after-hyperpolarization and synaptic noise.," *J Physiol.*, vol. 492, no. 2, pp. 597-628, Apr. 1996.

[157] H. P. Clamann, "Statistical Analysis of Motor Unit Firing Patterns in a Human Skeletal Muscle," *Biophysical Journal*, vol. 9, no. 10, pp. 1233-1251, Oct. 1969.

[158] C. T. Moritz, B. K. Barry, M. A. Pascoe, and R. M. Enoka, "Discharge Rate Variability Influences the Variation in Force Fluctuations Across the Working Range of a Hand Muscle," *J Neurophysiol.*, vol. 93, no. 5, pp. 2449 -2459, May. 2005.

[159] H. Parsaei, F. Nezhad, D. Stashuk, and A. Hamilton-Wright, "Validating motor unit firing patterns extracted by EMG signal decomposition," *Med Biol Eng Comput.*, pp. 1-10, 2010.

[160] K. McGill and H. Marateb, "Rigorous A-Posteriori Assessment of Accuracy in EMG Decomposition," *IEEE Trans Neural Syst Rehabil Eng*, Jul. 2010.

[161] S. Yue and C. Y. Wang, "The null distribution of sample serial correlation coefficient," *Stochastic Environmental Research and Risk Assessment*, vol. 16, no. 1, pp. 77-100, Feb. 2002.

[162] J. Ekstedt, G. Nilsson, and E. Stålberg, "Calculation of the electromyographic jitter," *J Neurol Neurosurg Psychiatry*, vol. 37, no. 5, pp. 526-539, May. 1974.

[163] R. Fisher, "The use of multiple measurements in taxonomic problems," *Annals Eugen.*, vol. 7, pp. 179-188, 1936.

[164] Y. Wang and A. K. C. Wong, "From Association to Classification: Inference Using Weight of Evidence," *IEEE Trans Knowl Data Eng.*, vol. 15, no. 3, pp. 764–767, Mar. 2003.

[165] A.K.C. Wong and Yang Wang, "Pattern discovery: a data driven approach to decision support," *IEEE Trans Syst, Man, Cybern.*, vol. 33, no. 1, pp. 114-124, 2003.

[166] V. Vapnik, *The Nature of Statistical Learning Theory*, 2nd ed. Springer, 1999.

[167] V. N. Vapnik, *Statistical Learning Theory*. Wiley-Interscience, 1998.

[168] A. Hamilton-Wright, D. W. Stashuk, and H. R. Tizhoosh, "Fuzzy Classification Using Pattern Discovery," *IEEE Trans Fuzzy Syst.*, vol. 15, no. 5, pp. 772-783, 2007.

[169] J. Shawe-Taylor and N. Cristianini, *Kernel Methods for Pattern Analysis*, Illustrated edition. Cambridge University Press, 2004.

[170] M. Nikolic, "Detailed Analysis of Clinical Electromyography Signals EMG Decomposition, Findings and Firing Pattern Analysis in Controls and Patients with Myopathy and Amytrophic Lateral Sclerosis," University of Copenhage, 2001.

[171] P. Pudil, J. Novovičová, and J. Kittler, "Floating search methods in feature selection," *Pattern Recogn Lett.*, vol. 15, no. 11, pp. 1119-1125, 1994.

[172] G. Milligan and M. Cooper, "An examination of procedures for determining the number of clusters in a data set," *Psychometrika*, vol. 50, no. 2, pp. 159-179, 1985.

[173] A. D. Gordon, *Classification, 2nd Edition*, 2nd ed. Chapman & Hall/CRC, 1999.

[174] R. Tibshirani, G. Walther, and T. Hastie, "Estimating the number of clusters in a data set via the gap statistic," *Journal of the Royal Statistical Society: Series B (Statistical Methodology)*, vol. 63, no. 2, pp. 423, 411, 2001.

[175] R. Tibshirani and G. Walther, "Cluster Validation by Prediction Strength," *Journal of Computational and Graphical Statistics*, vol. 14, no. 3, pp. 511-528, Sep. 2005.

[176] C. A. Sugar, G. M. James, and M., "Finding the number of clusters in a data set: An information theoretic approach," *J Am Stat Assoc.*, vol. 98, p. 750--763, 2003.

[177] J. L. Semmlow, *Biosignal and biomedical image processing: MATLAB-based applications*. CRC Press, 2004.

[178] K. C. McGill, "[Online dataset R005, available at http://www.emglab.net]." .

[179] H. Parsaei, F. J. Nezhad, D. W. Stashuk, and A. Hamilton-Wright, "Validation of motor unit potential trains using motor unit firing pattern information," in *31st IEEE Eng Med Biol Soc.*, 2009, pp. 974-977.

[180] G. R. Davis, D. A. Ingram, W. F. Fincham, M. Swash, and M. S. Schwartz, "Jitter correction: A computer algorithm for reduction of the velocity recovery function artifact," *Muscle Nerve*, vol. 11, no. 6, pp. 534-539, 1988.

[181] J. Han and M. Kamber, *Data mining: concepts and techniques*. Morgan Kaufmann, 2006.

[182] H. Parsaei and D. W. Stashuk, "An SVM Classifier for detecting merged motor unit potential trains extracted by EMG signal decomposition using their MUP shape information," in *24th IEEE CCECE*, Niagara Falls, Canada, 2011.

[183] J. C. Platt, "Probabilistic outputs for support vector machines and comparisons to regularized likelihood methods," in *Advances in Large Margin Classiers*, A. J. Smola, P. Bartlett, B. Schölkopf, and D. Schuurmans, Eds. Cambridge, MIT Press, 1999, pp. 61-74.

[184] D. W. Hosmer and S. Lemeshow, *Applied logistic regression*, 2nd ed. Wiley-Interscience Publication, 2000.

[185] L. I. Kuncheva, *Combining pattern classifiers: methods and algorithms*. Wiley-IEEE, 2004.

[186] Wang Jeen-Shing and Chiang Jen-Chieh, "A Cluster Validity Measure With Outlier Detection for Support Vector Clustering," *IEEE Trans Systems, Man, and Cybernetics, Part B*, vol. 38, no. 1, pp. 78-89, 2008.

[187] L. Duan, L. Xu, Y. Liu, and J. Lee, "Cluster-based outlier detection," *Annals of Operations Research*, vol. 168, no. 1, pp. 151-168, Jun. 2008.

[188] M. B. Al-Zoubi, A. Al-Dahoud, and A. A. Yahya, "New outlier detection method based on fuzzy clustering," *WSEAS Trans Info Sci and App.*, vol. 7, no. 5, pp. 681–690, May. 2010.

[189] K. He, "Automated Measurement of Neuromuscular Jitter Based on EMG Signal Decomposition," Master's thesis, University of Waterloo, 2007.